UNIVERSIDADE FEDERAL DO CEARÁ
CENTRO DE TECNOLOGIA
DEPARTAMENTO DE ENGENHARIA QUÍMICA
PROGRAMA DE PÓS-GRADUAÇÃO EM ENGENHARIA QUÍMICA

EVANICE MEDEIROS DE PAIVA

BEYOND AN AGROINDUSTRIAL RESIDUE: VALORIZING CASHEW NUTSHELL THROUGH CIRCULAR ECONOMY STRATEGIES FOR PRODUCING BIOENERGY, BIO-BASED CHEMICALS, AND PARTICLEBOARDS

FORTALEZA

2024

EVANICE MEDEIROS DE PAIVA

BEYOND AN AGROINDUSTRIAL RESIDUE: VALORIZING CASHEW NUTSHELL THROUGH CIRCULAR ECONOMY STRATEGIES FOR PRODUCING BIOENERGY, BIO-BASED CHEMICALS, AND PARTICLEBOARDS

Thesis submitted to the Graduate Program in Chemical Engineering at the Federal University of Ceará to obtain the degree of Doctor of Chemical Engineering.

Advisor: Prof. Dr. Edy Sousa de Brito
Co-advisor: Prof. Dr. José Luiz Francisco Alves

FORTALEZA
2024

Dados Internacionais de Catalogação na Publicação
Universidade Federal do Ceará
Sistema de Bibliotecas
Gerada automaticamente pelo módulo Catalog, mediante os dados fornecidos pelo(a) autor(a)

P1b PAIVA, EVANICE MEDEIROS DE.
BEYOND AN AGROINDUSTRIAL RESIDUE: VALORIZING CASHEW NUTSHELL THROUGH CIRCULAR ECONOMY STRATEGIES FOR PRODUCING BIOENERGY, BIO-BASED CHEMICALS, AND PARTICLEBOARDS / EVANICE MEDEIROS DE PAIVA. – 2024.
190 f. : il. color.

Tese (doutorado) – Universidade Federal do Ceará, Centro de Tecnologia, Programa de Pós-Graduação em Engenharia Química, Fortaleza, 2024.
Orientação: Prof. Dr. Edy Sousa de Brito.
Coorientação: Prof. Dr. José Luiz Francisco Alves.

1. Cashew nutshell residues. 2. pyrolysis. 3. phenolic resin. 4. formaldehyde emission. 5. biodegradability. I. Título.

CDD 660

EVANICE MEDEIROS DE PAIVA

BEYOND AN AGROINDUSTRIAL RESIDUE: VALORIZING CASHEW NUTSHELL THROUGH CIRCULAR ECONOMY STRATEGIES FOR PRODUCING BIOENERGY, BIO-BASED CHEMICALS, AND PARTICLEBOARDS

Thesis submitted to the Graduate Program in Chemical Engineering at the Federal University of Ceará to obtain the degree of Doctor of Chemical Engineering.

Approved on August 5, 2024.

EXAMINING BOARD

Prof. ª Dr.ª Morsyleide de Freitas Rosa
Federal University of Ceará (UFC)

Prof. Dr. Men de Sá Moreira de Souza Filho
Embrapa Tropical Agroindustry

Prof. Dr. Flávio Luiz Honorato da Silva
Federal University of Paraiba (UFPB)

Prof. Dr. Maurício Alves da Motta Sobrinho
Federal University of Pernambuco (UFPE)

I dedicate this work to God, for its completion is a testimony to His constant presence by my side, strengthening me and granting me the wisdom necessary for its accomplishment.

ACKNOWLEDGMENTS

This work was carried out with the support of the Coordination for the Improvement of Higher Education Personnel – Brazil (CAPES) – Financing Code 00.

I would like to express my sincere thanks to friends, colleagues, professors, and institutions that have directly or indirectly contributed to the realization of this research.

Special thanks:

To God, for the opportunity, health, and courage to overcome all challenges.

To my parents, Inaldo Vidal de Paiva and Valdenice Medeiros de Paiva, for their constant support, valuable advice, and encouragement in pursuing my dreams.

To my housemates, for the friendship, companionship, and good times.

To coworkers at Embrapa-Fortaleza, for their support and collaboration towards the success of this research and for the moments of relaxation during free time.

To Prof. Dr. Alfredo Curbelo Garnica (*in memoriam*), for the encouragement and for writing my letter of recommendation to the PPGEQ-UFC, at the most difficult time of my life.

To my advisor, Prof. Dr. Edy Sousa de Brito, for the teachings, partnership, patience, guidance, and significant contribution to the development of this study.

To my co-advisor, Prof. Dr. José Luiz Francisco Alves, for the friendship, invaluable suggestions, and guidance that were crucial for improving the quality of this research.

To Dr. Adriano Lincoln, for the assistance and discussions during the development of this work.

To CAPES, UFC, and UFSC, which made this work possible.

To EMBRAPA, for providing the indispensable infrastructure for the research.

And to my late husband Milton Lucas Freitas Amancio, who, I am certain, has been watching over me.

"We never know how strong we are until being strong is the only choice."

Unknown

RESUMO

Este estudo foi motivado pela grande quantidade anual de cascas de castanha de caju produzidas globalmente, o que tem levantado preocupações ambientais quanto ao seu descarte adequado. Duas rotas tecnológicas foram propostas para a valorização desse resíduo lignocelulósico. A primeira consistiu no uso de técnicas de caracterização físico-química, análise cinética multicomponente, estudo termodinâmico e análise de produtos voláteis para avaliar o potencial das cascas de castanha de caju cruas (RCNS) e prensadas (PCNS) em reações de pirólise. Para isso, um analisador termogravimétrico e um pirolisador analítico acoplado a cromatografia gasosa-espectrometria de massa (Py-GC/MS) foram utilizados para realizar as reações de pirólise. O comportamento de pirólise de RCNS e PCNS foi modelado com precisão usando a função de deconvolução Asym2sig, que identificou cinco e quatro eventos de devolatilização paralelos, respectivamente. As energias de ativação médias para a pirólise de RCNS e PCNS situaram-se dentro das faixas de 63,8 a 249,3 e 91,1 a 167,4 kJ mol^{-1}, respectivamente, conforme determinado por quatro métodos isoconversionais (Friedman, Flynn-Wall-Ozawa, Kissinger-Akahira-Sunose e Starink). Fatores pré-exponenciais variando de $4{,}2\times10^{8}$ a $6{,}9\times10^{16}$ min^{-1} e de $4{,}8\times10^{8}$ a $3{,}2\times10^{11}$ min^{-1} foram estimados a partir do efeito de compensação cinética para a pirólise de RCNS e PCNS, respectivamente. O método de gráficos mestres na forma integral revelou que os modelos de reação mais prováveis envolvidos na pirólise de RCNS e PCNS pertencem aos mecanismos de crescimento por nucleação e reação de ordem *n*. A análise dos produtos voláteis revelou que os hidrocarbonetos alifáticos foram os componentes dominantes dos produtos voláteis condensáveis a 650 °C, enquanto as temperaturas de reação de 450 e 550 °C favoreceram a produção de compostos oxigenados. O estudo termodinâmico confirmou a viabilidade técnica de converter ambos os resíduos de casca de castanha de caju em bioenergia e produtos químicos renováveis devido à baixa barreira energética a ser superada. A segunda rota tecnológica envolveu a fabricação de painéis de partículas sustentáveis utilizando PCNS e resina fenólica ecologicamente correta obtida a partir da reação do líquido da casca de caju (LCC) residual com formaldeído em proporções mássica de LCC/formaldeído de 1:0,25, 1:0,5 e 1:0,75 em condições ácidas e a 105 °C. A resina foi caracterizada utilizando técnicas como Calorimetria Exploratória Diferencial (DSC), Espectroscopia no Infravermelho por Transformada de Fourier (FTIR), Cromatografia Líquida de Alta Eficiência (HPLC) e Ressonância Magnética Nuclear (NMR). Os painéis

de partículas foram submetidos a testes de tração e flexão e testes de absorção de água. Também foram avaliadas a emissão de formaldeído e o teor de biodegradabilidade dos painéis aglomerados. Entre as condições testadas, a utilização de adesivo com proporções de LCC/formaldeído de 1:0,25 e 1:0,50 resultou em painéis aglomerados de classe E1 (com menos de 8 mg/100 g de painel seco) em termos de emissões de formaldeído e melhorias significativas nas propriedades mecânicas. A biodegradabilidade dos painéis PB25, PB50 e PB75 foi de 30%, 21% e 20%, respectivamente, em 30 dias. Esses resultados demonstram o potencial da biomassa da casca de caju e da resina ambientalmente correta como adesivos na indústria de painéis de partículas. Ambas as rotas tecnológicas propostas se mostraram promissoras na valorização dos resíduos de casca de caju na produção de bioenergia, produtos químicos de base biológica e painéis de fibras de média densidade sustentáveis. Além disso, este estudo está alinhado com os Objetivos de Desenvolvimento Sustentável (ODS) e pode servir como base para futura implementação em larga escala. Isso tem o potencial de gerar empregos e promover a economia circular na indústria de beneficiamento de castanhas.

Palavras-chave: Resíduos de casca de caju, pirólise, resina fenólica, emissão de formaldeído, biodegradabilidade.

ABSTRACT

This study was motivated by the large annual amount of cashew nutshells produced globally, which has raised environmental concerns about their proper disposal. Two technological routes have been proposed for the valorization of this lignocellulosic residue. The first one consisted of using physical-chemical characterization techniques, multicomponent kinetic analysis, thermodynamic study, and volatile product analysis to evaluate the potential of raw (RCNS) and pressed (PCNS) cashew nutshells in pyrolysis reactions. For this purpose, a thermogravimetric analyzer and an analytical pyrolyzer coupled with gas chromatography-mass spectrometry (Py-GC/MS) were used to perform the pyrolysis reactions. The pyrolysis behavior of RCNS and PCNS was accurately modeled using the Asym2sig deconvolution function, which identified five and four parallel devolatilization events, respectively. The average activation energies for the pyrolysis of RCNS and PCNS fell within the ranges of 63.8−249.3 and 91.1−167.4 kJ mol^{-1}, respectively, as determined by four isoconversional methods (Friedman, Flynn–Wall–Ozawa, Kissinger–Akahira–Sunose, and Starink). Pre-exponential factors ranging from 4.2×10^{8} to 6.9×10^{16} min^{-1} and from 4.8×10^{8} to 3.2×10^{11} min^{-1} were estimated from the kinetic compensation effect for the pyrolysis of RCNS and PCNS, respectively. The method of master plots revealed that the most probable reaction models involved in the pyrolysis of RCNS and PCNS belong to the nucleation growth and nth-order reaction mechanisms. Analysis of the volatile products revealed that aliphatic hydrocarbons were the dominant components for condensable volatile products at 650 °C, while reaction temperatures of 450 and 550 °C favored the production of oxygenated compounds. The thermodynamic study confirmed the technical feasibility of converting both cashew nutshell residues into bioenergy and renewable chemicals due to the low energy barrier to overcome. The second technological route involved the production of sustainable particleboards using PCNS and eco-friendly phenolic resin obtained from the reaction of cashew nutshell liquid (CNSL) with formaldehyde at mass ratios of CNSL to formaldehyde of 1:0.25, 1:0.5, and 1:0.75 under acidic conditions and at 105 °C. The resin was characterized using techniques such as Differential Scanning Calorimetry (DSC), Fourier Transform Infrared Spectroscopy (FTIR), High-Performance Liquid Chromatography (HPLC), and Nuclear Magnetic Resonance (NMR). The particleboards were subjected to tensile and flexural tests, and water absorption tests. Formaldehyde emission and biodegradability content of the particleboards were also evaluated. Among the tested conditions, the use of adhesive with CNSL/formaldehyde ratios of 1:0.25 and

1:0.50 resulted in E1 grade particleboards (with less than 8 mg/100 g of dry panel) in terms of formaldehyde emissions and significant improvements in mechanical properties. The biodegradability of PB25, PB50, and PB75 panels was 30%, 21%, and 20%, respectively, in 30 days. These results demonstrate the potential of cashew nutshell biomass and eco-friendly resin as adhesives in the particleboard industry. Both proposed technological routes show promise in valorizing cashew nutshell residues in the production of bioenergy, bio-based chemicals, and sustainable medium-density fiberboards. Furthermore, this study is aligned with the Sustainable Development Goals (SDGs) and can serve as a foundation for future large-scale implementation. This has the potential to generate jobs and promote a circular economy in the nut processing industry.

Keywords: Cashew nutshell residues, pyrolysis, phenolic resin, formaldehyde emission, biodegradability.

CONCEPTUAL DIAGRAM

Why?

There is currently a high demand for sustainable products and practices of circular economy; Brazil is a major producer of cashew nuts, the extraction of which yields a considerable amount of cashew nutshells, rich in phenolic compounds and anacardic acid. Therefore, it is interesting to assess more suitable options for managing the waste from the cashew nut industry;
1) First technological route: The valorization of pressed cashew nutshells (PCSN) to produce bioenergy and biobased chemicals through pyrolysis has not yet been explored in the literature. Thus, the potential technological benefits of this route align academic and industrial interests;
2) Second technological route: Pressed cashew nutshell (PCNS) in particleboard production represents a gap in knowledge; Data on the production of phenolic resin from cashew nutshell liquid (CNSL) without the need for isolation of chemical compounds are limited; Moreover, the techno-economic analysis of particleboard production still needs to be explored;

Hypothesis

1) First technological route: - The pyrolysis of pressed cashew shells under specific conditions presents a kinetic and thermodynamic profile favorable to the production of bioenergy and renewable chemical products; - Multicomponent kinetic description is able to accurately predict kinetic data and help design and optimize pyrolysis; -The pyrolysis temperature has a significant impact on the distribution of volatile products resulting from the rapid pyrolysis of raw and pressed cashew nutshells.
2) Second technological route: - Particleboards produced from pressing cashew nutshells have the potential to offer a sustainable solution for the reuse of waste, due to their biodegradability and low formaldehyde emissions. - Ecological phenol-formaldehyde adhesives derived from CNSL can be used in the production of particleboards, resulting in good mechanical resistance for them. The techno-economic analysis indicates that scaling up particleboard production is viable.

Methodologies

Concepts of circular economy and green logistics applied to the valorization of cashew nutshells.
1)First technological route: Utilization of experimental data from pyrolysis and thermogravimetric analysis (TGA), combined with multicomponent kinetic modeling, to simulate the behavior of experimental pyrolysis; and calculation of thermodynamic parameters; Evaluation of volatile products through Py-GC/MS techniques, to assess the potential of bioenergy and renewable chemicals;
2) Second technological route: Production and characterization of phenolic resin derived from cashew nutshell liquid (CNSL) through DSC, FTIR, HPLC, and RMN techniques;
Conducting mechanical tests of tension, flexion, and water absorption on particleboards to assess their mechanical resistance; Experimental tests to evaluate the biodegradability and formaldehyde emission of particleboards; Scale-up simulation of particleboard production using SuperPro Designer software;

Responses

1) First technological route: Define a summative kinetic expression to represent the pyrolysis behavior of the residues; analyze thermodynamic parameters; Analyze the volatile products for utilization in biofuel production;
2) Second technological route: Define the chemical composition of the CNSL-formaldehyde adhesive and the possible chemical reaction; Determine the mass fractions of the particleboards to achieve a panel with mechanical strength, low formaldehyde emission, and biodegradable; Determine the minimum amount of residue required to make the production process viable.

THESIS METHODOLOGICAL SEQUENCE FLOWCHART

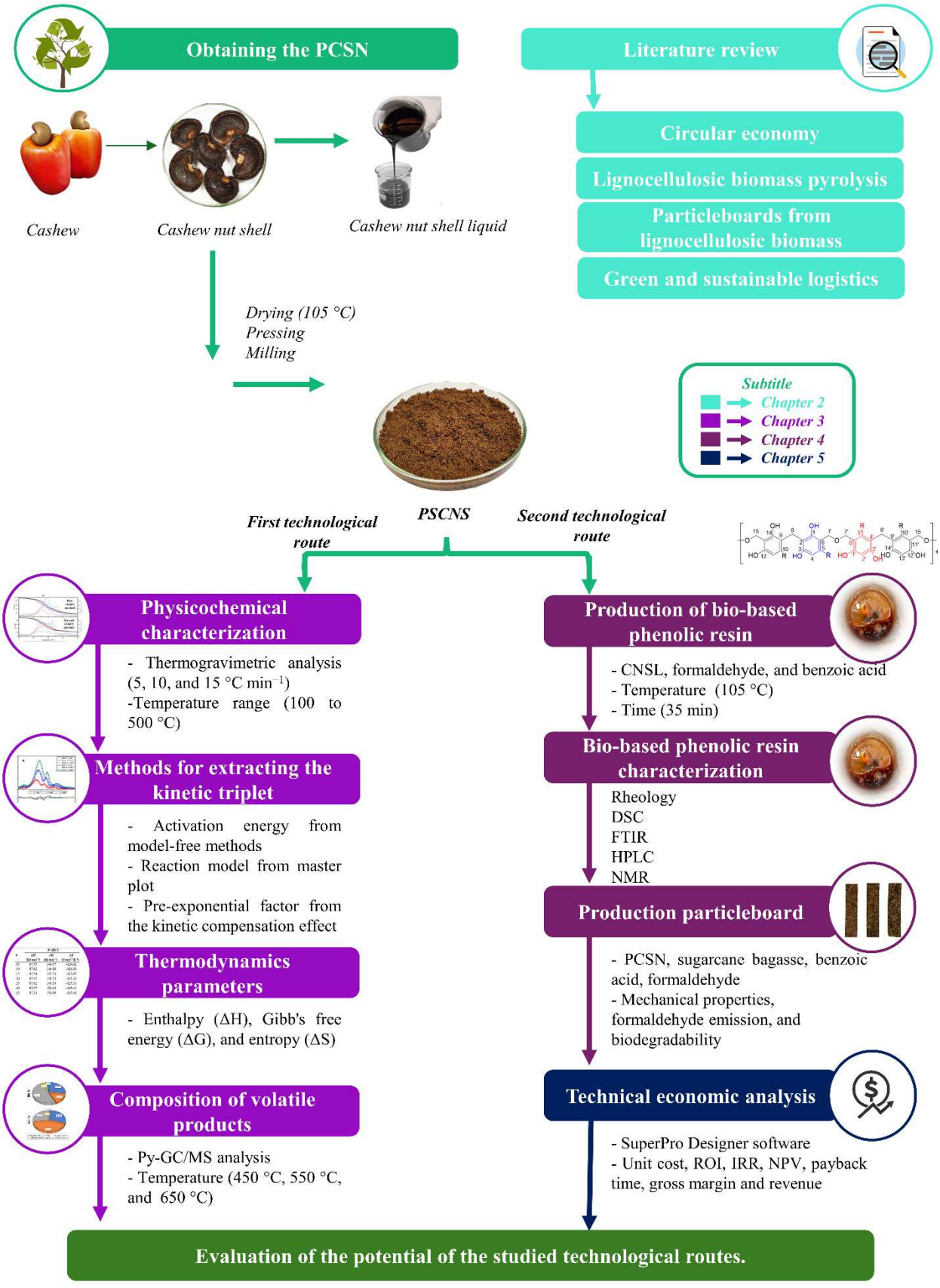

CNSL – Cashew nutshell liquid;

LIST OF FIGURES

LIST OF TABLES

LIST OF ABBREVIATIONS AND ACRONYMS

$(d\alpha/dt)_{average}$	Average value of the conversion rates (measured experimentally)
$(d\alpha/dT)_{dec}$	Conversion rates deconvoluted
$(d\alpha/dt)_{exp}$	Conversion rates (measured experimentally)
$(d\alpha/dT)_{exp}$	Experimental conversion rates
$(d\alpha/dt)_{sim}$	Conversion rates
$[(d\alpha/dt)_{exp}]_{max}$	Maximum value of the conversion rates (measured experimentally
A	Pre-exponential factor
A2	Avrami–Erofeev model
A3	Avrami–Erofeev reaction model
ASH	Inorganic matter
A-type	Avrami-erofeev
C	Carbon
c_i	Mass fraction of each pseudo-component i
C_i	Input of each individual
CNSL	Cashew nutshell liquid
CO_2	Carbon dioxide
DCF	Discounted cash flow
DMSO	Dimethyl sulfoxide
DTG	Differential thermogravimetric curve
D-type	Diffusion model
DETA	Diethylenetriamine
E_a	Activation energy
f(α)	Reaction models differential form
F1	First-order reaction model
F1	Phenolic resin in a mass ratio of 1:0.25 (CNSL: formaldehyde).
F2	Second-order reaction model
F2	Phenolic resin in a mass ratio of 1:0.50 (CNSL: formaldehyde).
F3	Phenolic resin in a mass ratio of 1:0.75 (CNSL: formaldehyde).
F9	Ninth order reaction
FAO	Food and Agriculture Organization of the United Nations
FC	Fixed carbon
Fit	Quality of agreement
FR	Friedman method

FTIR	Fourier transform infrared spectroscopy
F-type	Reaction order
FWO	Flynn–wall–ozawa method
g(α)	Reaction models integral form
gHMBC	Gradiente heteronuclear correlação múltipla quantum
gHSQC	Gradiente heteronuclear correlação única quantum
gHSQCAD	Gradient heteronuclear single quantum correlation with detection in multiple dimensions
H	Hydrogen
h	Plank constant (6.626×10−34 J s−1).
HD25	High-density particleboard manufactured with phenolic resin in a mass ratio of 1:0.25 (CNSL: formaldehyde)
HD50	High-density particleboard manufactured with phenolic resin in a mass ratio of 1:0.50 (CNSL: formaldehyde)
HD75	High-density particleboard manufactured with phenolic resin in a mass ratio of 1:0.75 (CNSL: formaldehyde)
HHV	Higher heating value
HPLC	Preparative reverse-phase high-performance liquid chromatography
ICTAC	International Confederation of Thermal Analysis and Calorimetry
IEA	International Energy Agency
IM	Inherent Moisture
IPDA	Isophorone diamine
IRR	Internal rate of return
k(T)	Reaction constant
KAS	Kissinger–akahira–sunose method
k_B	Boltzmann constant
KCE	Kinetic compensation effect
LHV	Lower heating value
ln A	Pre-exponential factor in its logarithmic form
M	Total points of experimental data
m	Mass of the resin
MOE	Modulus of Elasticity
MOR	Modulus of Rupture
N	Nitrogen

N	Total number of experimental determinations used during simulations
NaOH	Sodium hydroxide
NPV	Net Present Value
O	Oxygen
PB25	Low-density particleboard manufactured with phenolic resin in a mass ratio of 1:0.25 (CNSL: formaldehyde).
PB50	Low-density particleboard manufactured with phenolic resin in a mass ratio of 1:0.50 (CNSL: formaldehyde).
PB75	Low-density particleboard manufactured with phenolic resin in a mass ratio of 1:0.75 (CNSL: formaldehyde).
P-CL	Pseudo-cellulose
PCNS	Pressed cashew nutshells
P-EX	Pseudo-extractives
P-HC	Pseudo-hemicellulose
P-HC1	Primary pseudo-hemicellulose
P-HC2	Secondary pseudo-hemicellulose
P-LG	Pseudo-lignin
P-LG1	Primary pseudo-lignin
P-LG2	Secondary pseudo-lignin
P-type	Power-law
Py-GC/MS	Pyrolyzer coupled with gas chromatography-mass spectrometry
QOF	Quality of Fit
R	Gas constant (8.3145×10^{-3} kJ mol^{-1} K^{-1})
R^2	Coefficient of determination
RCNS	Raw cashew nutshells
REAch	Registration, Evaluation, Authorization, and Restriction of Chemicals
RMN	Nuclear magnetic resonance
ROI	Return on Investment
RSS	Residual sum of squares
R-type	Geometrical contraction
S	Sulfur
SCB	Sugarcane bagasse
STK	Starink method
t	Reaction time

TEA	Technical-economic analysis
T	Temperature
TG	Thermogravimetric curves
TGA	Thermogravimetric analysis
T_m	Maximum temperature peak
V	Volume of naoh solution used in the titration
VM	Volatile matter
Vo	Volume of naoh solution used in the blank test
w_1	Curve width
w_2; w_3	Two shape parameters
α	Conversion extent
β	Constant heating rate
ΔG	Variation in Gibbs free energy
ΔH	Variation in Enthalpy
ΔS	Variation in Entropy
ε	Error
θ	Maximum amplitude of the curve

SUMMARY

Chapter 1

INTRODUCTION AND OBJECTIVES

1 INTRODUCTION AND OBJECTIVES

1.1 Introduction

Cashew nut production is an agricultural activity of great importance in several regions of the world, predominantly concentrated in tropical countries such as India, Vietnam, Nigeria, Ivory Coast, and Brazil. According to data from the Food and Agriculture Organization of the United Nations (FAO), global production of cashew nuts with shells in 2023 was approximately 4.0 million tons (FAOSTAT, 2024). The cashew nut consists of its kernel, which represents approximately 28-30% of the total weight of the nut, the shell or kernel tegument, which accounts for about 3%, and the shell, which corresponds to 65-70% of the total weight of the nut after kernel extraction (MOHOD; KHANDETOD; POWAR, 2008).

The cashew nut kernel is widely consumed due to its nutritional constituents, which include proteins, fibers, vitamins, minerals, and unsaturated fats, beneficial to human health (AKOMOLAFE; OYELEYE; OBOH, 2022). In Brazil, the states of Ceará, Piauí, and Rio Grande do Norte stand out as the main producers of cashew nuts. The production of the kernel is carried out by both large factories, which hold significant market control and where the cashews are cooked in cashew nutshell liquid (CSNL), and small factories where the autoclaving and vaporization technique is adopted. In the state of Ceará, these small factories each produce approximately 180 tons of whole cashew nuts (with shell) annually. With around 70 factories in operation (EMBRAPA, 2024), this results in a total production of 7,000 to 9,000 tons of cashew nut shells (solid waste) per year. The extraction of the kernels generates large quantities of shells, which are typically stored in open silos and later sold for burning in industrial furnaces and/or brick kilns (ARAÚJO, 2013).

The incorrect disposal or burning of cashew nutshells has caused environmental pollution and health risks due to the presence of chemicals considered harmful. A study conducted by Josino *et al.* (2017) showed changes in all variables of the respiratory system mechanics of mice exposed to exhaust gases from the combustion of cashew nutshells (JOSINO et al., 2017). As the shell is burned, pollutants such as carbon dioxide, carbon monoxide, nitrogen dioxide, sulfur dioxide, and particulate matter are released (SERRA et al., 2021).

Law No. 12,305/2010, which establishes the Política Nacional de Resíduos Sólidos (PNRS) in Brazil, plays a fundamental role in defining guidelines for the management and proper disposal of these solid wastes. According to this legislation, cashew nutshells are officially recognized as waste (BRAZIL, 2010). PNRS classifies solid waste according to its hazardousness and specific characteristics, as established by Resolution CONAMA No. 313/2002. According to this classification, cashew nutshells generally fall into Class I – Hazardous (BRAZIL, 2002), due to the presence of CNSL, which is corrosive and flammable. In addition to classification, the PNRS also promotes the adoption of principles such as shared responsibility throughout the product lifecycle, economic valorization of waste, and prioritization of waste reduction, reuse, and recycling. In this context, the valorization of cashew nut shells as a low-cost raw material to produce bioenergy, renewable chemicals, and sustainable panels emerges as a promising alternative for sustainability and the circular economy.

The cashew harvest can vary depending on the region and specific climatic conditions. However, the common estimate is that it lasts about three months. In terms of logistics to maximize the reuse of this waste and to become competitive, it is essential to develop a comprehensive strategic plan that encompasses the collection and proper storage of the shells, taking into consideration their seasonality linked to the cashew harvest (ARAÚJO, 2013).

In recent years, there has been a growing demand for routes that enhance the value of cashew nutshells, contributing to the circular economy (MGAYA et al., 2019; DA SILVA; DE BRITO; FERREIRA, 2023). According to recent research described in the literature, cashew nutshells can be reused as raw material in the production of various products, such as activated carbon for water purification (KOUASSI et al., 2020), eco-friendly cement for construction (MANJUNATH et al., 2023), wood agglomerates (MARI; VILLENA, 2016), and biochar (TAPAS et al., 2023). These alternatives for enhancing the value of cashew nutshells can bring significant environmental and economic benefits, promoting a more sustainable and conscious approach to the development of new products.

On the other hand, the CNSL present in cashew nutshells has a chemical composition that varies according to the extraction method and temperature used. When extracted at low temperatures (below 180 °C), natural CNSL contains a higher amount of anacardic acid. Various extraction methods have been used to obtain natural CNSL,

including mechanical extraction at low temperatures, which results in a liquid containing around 70-80% anacardic acid, 13-20% cardol, and 1-10% cardanol (SOUZA et al., 2022). Additionally, extraction can be performed using solvents (such as water, hexane, and methanol) or supercritical fluids (using CO_2) (CRUZ REINA et al., 2023), and it is worth noting that the chosen method directly affects the chemical composition of natural CNSL. At high temperatures (above 180 °C), anacardic acid undergoes decarboxylation, leading to the formation of technical CNSL, in which cardanol is the main component, accounting for about 67-94%, while anacardic acid is reduced to 1-2%. In addition, technical CNSL contains 3-18% cardol and other substances present in low percentages (SOUZA et al., 2022; MGAYA, 2018). Due to the presence of these compounds, CNSL has potential to be used in a wide range of industrial applications, such as in the manufacture of varnishes (KYEI et al., 2022), adhesives (BRITO et al., 2023), and coatings/resins (RENAN et al., 2020). It is also used in the production of biodiesel (ADEKANBI; OLUGASA, 2022; BISCOFF; ENWEREMADU, 2023), and in the synthesis of nanostructured materials (ZAFAR et al., 2020).

Interest in research related to the production of bioenergy and bioproducts has significantly increased, driven by growing environmental concerns on a global scale (KUMAR et al., 2023). These studies aim primarily to find solutions to reduce greenhouse gas emissions and promote the transition to a greener and more sustainable economy (KUMAR et al., 2023). The use of biomass as a raw material has been an increasingly adopted strategy to develop sustainable technologies for bioenergy and bioproducts production (IFEANYI-NZE; OMIYALE, 2022). Among the various methods of producing bioenergy and bioproducts, pyrolysis is a thermal process that transforms biomass in the absence of oxygen into different products, such as bio-oil, gas, and biochar (OSMAN et al., 2023). The pyrolysis of cashew nut shells can become an important source of bioenergy, contributing to the reduction of dependence on fossil fuels and greenhouse gas emissions. It is important to note that the efficiency of the pyrolysis process and the quality of the product depend on both the biomass used and the process conditions (OSMAN et al., 2023). Therefore, evaluating the physicochemical characterization, triplet kinetic and thermodynamic parameters, and volatile products produced by the pyrolysis reaction attest to the viability of the lignocellulosic residuebeing converted into renewable bioenergy and chemicals products.

The use of biomass as a raw material to produce bioproducts, such as the manufacturing of lignocellulosic panels, is an alternative that favors environmental sustainability and contributes to the circular economy (LEE et al., 2022). The substitution of wood used in conventional panels with panels made from lignocellulosic residues offers several advantages, such as reducing deforestation of cultivated forests, lowering the risk of fluctuation of the wood market prices, and utilizing waste from different sources (forestry, agriculture, and construction) to reduce waste disposal in the environment. Recent studies indicate that lignocellulosic panels derived from various agricultural/agro-industrial residues, such as rice husk and coconut fiber (CHANDRAN et al., 2022), pine wood, bamboo, and yerba mate (RUSCH et al., 2023), and bean straw (FARIA et al., 2023) have been developed and find applications in different sectors, including construction, furniture, and packaging.

The use of pressed cashew nutshells in the production of lignocellulosic panels emerges as an advantageous alternative to add value to this waste. In addition to being readily available in cashew nut-producing regions, its utilization reduces its burning, thereby minimizing the emission of toxic gases into the environment. Additionally, the residual liquid present in the cashew nutshell can be utilized as a source of phenolic compounds to produce phenolic resin, used as an adhesive in panel manufacturing, resulting in improved mechanical strength. Therefore, the transformation of cashew nutshell waste into bioproducts and bioenergy is aligned with the Sustainable Development Goals (SDGs), promoting sustainable practices. This approach directly contributes to some SDG, encompassing areas such as clean and affordable energy (SDG 7), industry, innovation and infrastructure (SDG 9), sustainable cities and communities (SDG 11), responsible consumption and production (SDG 12), and climate action (SDG 13).

Finally, the motivation and novelty of this study include the investigation of two different routes for valorization of cashew nutshell, following the principles of circular economy. The first route of valorization concerns the study of the potential of raw cashew nutshell waste (RCNS) and pressed cashew nutshell waste (PCNS) to produce bioenergy and renewable chemicals through physicochemical characterization, multicomponent kinetic analysis, thermodynamic study, and volatile product analysis for pyrolysis reactions. The second route refers to the manufacturing of new lignocellulosic panels using pressed cashew nutshell, the evaluation of their chemical composition and

mechanical properties, as well as a study of their biodegradability and formaldehyde emission. Additionally, the study of phenolic resin involves the chemical characterization and rheological study with different formaldehyde concentrations.

1.2 Objectives

1.2.1 General objective

The overall aim of this study is to make scientific contributions toward the circular economy by valorizing pressed cashew nutshells to produce bioenergy and renewable chemicals through pyrolysis, and sustainable medium-density fiberboard using bio-based phenolic resin.

1.2.2 Specific objectives

a) Examining the possibility of valorizing cashew nutshell residues as feedstocks for producing bioenergy and renewable chemicals by conducting pyrolysis experiments using TGA and Py-GC/MS techniques. This will be achieved by investigating four critical aspects: (1) evaluating the physicochemical properties of the residues, (2) knowing the reaction by determining the kinetic triplets from a multi-component perspective, (3) estimating thermodynamic parameters, and (4) analyze the composition of volatile products.

b) Investigating the feasibility of utilizing cashew nutshell residue as feedstocks for producing lignocellulosic panels using bio-based phenolic resin. This investigation will address five crucial aspects: (1) characterization of the bio-based phenolic resin, (2) rheological study of the bio-based phenolic resin, (3) evaluation of the mechanical properties of the lignocellulosic panels, (4) analysis of the biodegradability and formaldehyde emission of the lignocellulosic panels, and (5) technical economic analysis of the production process.

1.3 Structure of the thesis

To facilitate understanding, this work is organized into six chapters. The first chapter consists of this introduction, while the second chapter provides an updated review of the literature on the topic of this thesis, highlighting the growing interest in the reuse

of cashew nutshells. The third chapter is based on the article already published in the Journal of Analytical and Applied Pyrolysis, and the fourth chapter was published in the journal Industrial Crops and Products. The fifth chapter is currently being prepared for submission to Industrial Crops and Products. The sixth and final chapter presents the conclusions of this study. Each chapter provides a detailed description of the experimental equipment, procedures employed, a review of relevant literature, and final observations. The content of each chapter is described below:

- Chapter 2: State of the Art
- Chapter 3: **Pyrolysis of cashew nutshell residues for bioenergy and renewable chemicals: kinetics, thermodynamics, and volatile products**

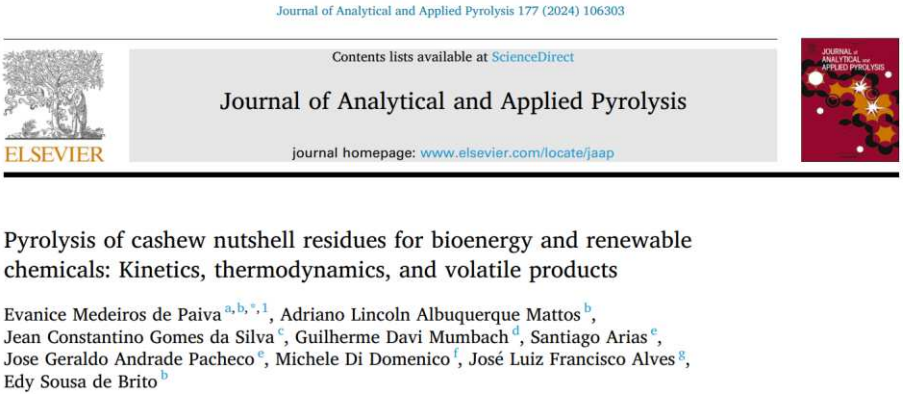

- Chapter 4: **Valorizing cashew nutshell residue for sustainable lignocellulosic panels using a bio-based phenolic resin as a circular economy solution**

- Chapter 5: Modeling of particleboard production from cashew nutshells using SuperPro Designer
- Chapter 6: Conclusion

References

ADEKANBI, M. L.; OLUGASA, T. T. Utilizing cashew nut shell liquid for the sustainable production of biodiesel: A comprehensive review. **Cleaner Chemical Engineering**, v. 4, n. August, p. 100085, 2022.

AKOMOLAFE, S. F.; OYELEYE, S. I.; OBOH, G. Effect of cashew (Anacardium occidentale L.) nut-supplemented diet on steroidogenic enzymes, hormonal and oxidative imbalances, and sperm parameters in cisplatin-induced reproductive toxicity in male rats. **Journal of Food Biochemistry**, v. 46, n. 7, 2 jul. 2022.

ARAÚJO, J. P. P. DE. **Agronegócio Caju: Práticas e Inovações**. 1ª ed. Brasília: Embrapa, 2013.

BISCOFF, R. K.; ENWEREMADU, C. C. Environmental Effects Cashew nutshell liquid : A potential inedible source of biodiesel for heavy duty vehicles in sub-Saharan Africa Cashew nutshell liquid : A potential inedible source of biodiesel for heavy duty vehicles in sub-Saharan Africa. **Energy Sources, Part A: Recovery, Utilization, and Environmental Effects**, v. 45, n. 1, p. 905–923, 2023.

BRAZIL. **National Council on the Environment, 2002**. Available at: <http://www.siam.mg.gov.br/sla/download.pdf?idNorma=263>. Accessed on: February 29, 2024.

BRAZIL. **Law No. 12,305, of August 2, 2010**. Available at: <https://www.planalto.gov.br/ccivil_03/_ato2007-2010/2010/lei/l12305.htm>. Accessed on: February 29, 2024.

BRITO, K. J. S. et al. Sustainable plasticizer from agroindustrial waste for natural rubber compounds: Influence on the curing system and compound properties. **Journal of Elastomers and Plastics**, v. 0, n. 0, p. 1–17, 2023.

CHANDRAN, A. et al. Particle board using rice husk and coconut fibre . Tablero de partículas con cáscara de arroz y fibra de coco. **Sustainability, Agri, Food and Environmental Research**, v. 11, n. 10, 2022.

CRUZ REINA, L. J. et al. Compressed fluids and Soxhlet extraction for the valorization of compounds from Colombian cashew (Anacardium occidentale) nut shells aimed at a cosmetic application. **Journal of Supercritical Fluids**, v. 192, n. July 2022,

2023.

DA SILVA, J.; DE BRITO, E. S.; FERREIRA, S. R. S. Biorefinery of Cashew By-Products: Recovery of Value-Added Compounds. **Food and Bioprocess Technology**, v. 16, n. 5, p. 944–960, 2023.

EMBRAPA. **Empresa Brasileira de Pesquisa Agropecuária (Embrapa)**. Available at: <https://www.embrapa.br/agroindustria-tropical>. Accessed on: February 2, 2024.

FAOSTAT : statistical Cahew nuts (crops production). Available at: <available: https://www.fao.org/faostat/en/#data/QV>. Accessed on: February 2, 2024.

FARIA, D. L. et al. Cardanol-based adhesive with reduced formaldehyde emission to produce particleboards with waste from bean crops. **Environmental Science and Pollution Research**, v. 30, n. 16, p. 48270–48287, 9 fev. 2023.

IFEANYI-NZE, F. O.; OMIYALE, C. O. Insights into the recent advances in the pretreatment of biomass for sustainable bioenergy and bio-products synthesis: Challenges and future directions. **European Journal of Sustainable Development Research**, v. 7, n. 1, p. em0209, 2022.

JOSINO, J. B. et al. Changes of respiratory system in mice exposed to PM4.0 or TSP from exhaust gases of combustion of cashew nut shell. **Environmental Toxicology and Pharmacology**, v. 56, n. August, p. 1–9, dez. 2017.

KOUASSI, B. G. et al. Preparation of Activated Carbon from Cashew Nut Shells for Water Purification. **Russian Journal of Non-Ferrous Metals**, v. 61, n. 1, p. 112–118, 29 jan. 2020.

KYEI, S. K. et al. Natural polyhydroxy resins in surface coatings : a review. **Journal of Coatings Technology and Research**, v. 19, n. 3, p. 775–794, 2022.

KUMAR, V. et al. Chemosphere Bioengineering of biowaste to recover bioproducts and bioenergy : A circular economy approach towards sustainable zero-waste environment. **Chemosphere**, v. 319, n. October 2022, p. 138005, 2023.

LEE, S. H. et al. Particleboard from agricultural biomass and recycled wood waste: a review. **Journal of Materials Research and Technology**, v. 20, p. 4630–4658, set. 2022.

MANJUNATH, B. et al. Potential utilization of regional cashew nutshell ash wastes as a cementitious replacement on the performance and environmental impact of eco-friendly mortar. **Journal of Building Engineering**, v. 66, n. October 2022, p. 105941, 2023.

MARI, E. L.; VILLENA, E. M. Properties of particleboard from wood wastesand cashew nut shell residue. **Philippine Journal of Science**, v. 145, n. 1, p. 1–8, 2016.

MGAYA, E. B. M. J. E. Chemical Valorization of Cashew Nut Shell Waste. **Topics in Current Chemistry**, v. 376, n. 2, p. 1–15, 2018.

MGAYA, J. et al. Cashew nut shell: A potential bio-resource for the production of bio-sourced chemicals, materials and fuels. **Green Chemistry**, v. 21, n. 6, p. 1186–1201, 2019.

MOHOD, A. G.; KHANDETOD, Y. P.; POWAR, A. G. Processed cashew shell waste as fuel supplement for heat generation. **Energy for Sustainable Development**, v. 12, n. 4, p. 73–76, 2008.

OSMAN, A. I. et al. **Materials, fuels, upgrading, economy, and life cycle assessment of the pyrolysis of algal and lignocellulosic biomass: a review**. [s.l.] Springer International Publishing, 2023.

RENAN, L. et al. Progress in Organic Coatings Development of BPA-free anticorrosive epoxy coatings from agroindustrial waste. **Progress in Organic Coatings**, v. 139, n. November 2019, p. 105449, 2020.

RUSCH, F. et al. Particleboard experimental production with bamboo, pine and mate for one product of new applications. **Maderas-Cienc Tecnol**, v. 25, n. SE-Article, p. 1–24, 2023.

SERRA, D. S. et al. Archives of Environmental & Occupational Health Lung injury caused by occupational exposure to particles from the industrial combustion of cashew nut shells : a mice model. **Archives of Environmental & Occupational Health**, v. 76, n. 1, p. 1–11, 2021.

SOUZA, N. DE O. et al. Cashew nut shell liquids: Antimicrobial compounds in prevention and control of the oral biofilms. **Archives of Oral Biology**, v. 133, n. July 2021, p. 0–9, 2022.

TAPAS, M. B. B. R. et al. Role of cashew shell biochar on EMI shielding behaviour of carbon fibre – epoxy nanocomposites in E , F , I and J band – microwave frequencies. **Biomass Conversion and Biorefinery**, p. 375–382, 2023.

ZAFAR, F. et al. Spectrochimica Acta Part A : Molecular and Biomolecular Application of FTIR-ATR spectroscopy to con fi rm the microwave assisted synthesis and curing of Cashew nut shell liquid derived nanostructured materials. **Spectrochimica Acta Part A: Molecular and Biomolecular Spectroscopy**, v. 228, p. 117732, 2020.

Chapter 2

LITERATURE REVIEW

2 LITERATURE REVIEW

2.1 Circular Economy: A Comprehensive Overview

The current model of organizing the production of goods and services in society follows mainly a linear approach: resources are extracted, go through a production process, are used by society, and then discarded, without considering external consequences. As a result, we are extracting more natural resources than the planet can sustain and wasting materials along the production chain, disregarding the embodied energy within them. Additionally, with the projected population growth until 2100, it is estimated that around 3 billion people will enter the middle class by 2030, becoming new consumers (DE OLIVEIRA; OLIVEIRA, 2023).

In this scenario, the concept of the circular economy emerges as a promising alternative to mitigate the negative effects of the current linear model, aiming to establish an economic system that is restorative and less harmful to the environment (STEPHENSON; DAMERELL, 2022). In contrast to the traditional linear model of "extract-produce-dispose," the circular economy seeks to keep products, materials, and resources in continuous use cycles. Therefore, the principles of the circular economy are increasingly seen as a viable solution to achieve sustainable development goals (WALKER, 2021).

Globally, several countries have been leading in the adoption of the circular economy. Government entities in Japan and South Korea are designing and implementing policies to facilitate the transition to a CE and achieve carbon neutrality (HERRADOR et al., 2022). Germany is known for its advanced regulations and practices. Japan is one of the most engaged countries in the circular economy, with efficient programs for selective collection and sorting (OGUNMAKINDE, 2019). The European Union is focused on the development and implementation of policies aimed at the use of renewable resources in both the energy sector and product development (D'ADAMO; GASTALDI; MORONE, 2022). China is increasingly directing its efforts towards the adoption of policies that promote the circular economy (LIU et al., 2021).

In Brazil, the circular economy is in the early stages of development but has been receiving increasing attention and importance in recent years. The country faces significant challenges related to waste management, resource efficiency, and

environmental sustainability. However, several initiatives and advancements are taking place in different sectors. Industries, especially multinational companies, are adopting the "Zero Waste to Landfill" policy, seeking alternatives for their waste, avoiding final disposal in landfills, and redistributing them in various production chains (MANCINI et al., 2021). Additionally, industries are committed to reducing their dependence on petrochemicals and petroleum-derived industrial components, aiming to replace them with sustainable alternatives based on biological resources, with the goal of mitigating the effects of global warming resulting from the indiscriminate production of greenhouse gases. Agro-industrial residues represents an abundant source of lignocellulosic biomass, a sustainable raw material that enables the development of a wide range of environmentally friendly bioproducts and bioenergy (ROJAS; ZAPATA; RUIZ-TIRADO, 2022; MUJTABA et al., 2023). Although Brazil still requires advancements in the field of circular economy, the prospects are promising and indicate a positive path for the adoption of these sustainable practices.

Research related to the utilization of agro-industrial waste for the development of the circular economy is constantly growing. In the scientific literature, studies exploring various agro-industrial residues can be found, such as the utilization of cassava waste for biogas production (CRUZ et al., 2021). Additionally, pineapple residues have been studied as an economical raw material to produce phenolic compounds and fibers, as well as a suitable substrate for fermentation aiming at ethanol and organic acid production (VIEIRA et al., 2022). Another potential source is cocoa pod husk, which is rich in methylxanthines such as caffeine and theobromine, and has high levels of indigestible fibers, suggesting its potential for bioethanol production (PORTO DE SOUZA VANDENBERGHE et al., 2022; YOGASWARA et al., 2021).

Another extensively studied agro-industrial waste example is cashew nutshell. Scientific studies have sought to explore its reuse aiming at promoting the circular economy and reducing waste generation during cashew processing. Among the applications, the shell use as a bioadsorbent for the removal of metal ions (Cu^{2+} and $Cr^{3+)}$ can be found (OLIVEIRA et al., 2021), conversion into activated carbon for dye adsorption, such as brilliant green (SAMIYAMMAL et al., 2022), liquid valorization of the shell through gasification for biochar production (DIEDHIOU et al., 2014; NGUYEN et al., 2021), particleboard manufacturing (MARI; VILLENA, 2016), a utilization of the shell for biofuel production (COULIBALY et al., 2022), concrete manufacturing using

cashew nutshell ash (MENDU; PANNEM, 2021), bio-oil production through pyrolysis (AMALIYAH; PUTRA, 2021), biomass briquette production (IFA et al., 2020), and its use as hybrid fillers to reinforce natural rubber composites (ABDUL-WAHAB ILAVBARE et al., 2018).

In addition to cashew nutshells, the valorization of cashew nutshell liquid (CNSL) has also been explored. CNSL has been the subject of study in the development of biofuels (OLUGASA; ADEKANBI; FASOGBON, 2022), hypercrosslinked polymers for the removal of volatile organic compounds (LIU et al., 2022), the development of drugs for Alzheimer's Disease (ULIASSI et al., 2021), the preparation of Partially Biobased Epoxy Resins and additives (MAKWANA et al., 2022; DINESHKUMAR J; JESUDAS T, 2023), lubricant as a renewable petrochemical product (SELVAMUTHUKUMAR et al., 2021), and biocomposites (UDHAYASANKAR; KATHIKEYAN, 2019).

Despite the promising applications of cashew nut shells, many of them are still limited to laboratory scale and involve complex processes, making practical implementation challenging. Overcoming these challenges requires in-depth research into the technical, economic, and environmental aspects of using cashew nut shells as a raw material. Additionally, it is essential to evaluate financial metrics such as Net Present Value (NPV), which is a crucial tool for assessing economic viability and efficiency, as well as Return on Investment (ROI) and payback period. These financial analyses are critical for making informed decisions and ensuring that investments are sustainable and profitable.

2.2 Residue utilization and sustainable development

The efficient utilization of agro-industrial waste plays a crucial role in the pursuit of sustainable development. In the specific context of cashew nut processing, this issue becomes even more relevant due to its economic importance and the large volume of waste generated during processing (ALMEIDA et al., 2013). Harnessing cashew nutshell waste for bioenergy and bioproducts production is aligned with the Sustainable Development Goals (SDGs) set by the United Nations, particularly (UNITED NATIONS, 2015):

a) SDG 7: Affordable and Clean Energy: Ensure access to affordable, reliable, sustainable, and modern energy for all.

b) SDG 9: Industry, Innovation, and Infrastructure: Build resilient infrastructure, promote inclusive and sustainable industrialization and foster innovation.
c) SGD 11: Sustainable Cities and Communities: Make cities and human settlements inclusive, safe, resilient, and sustainable.
d) SDG 12: Responsible Consumption and Production: Ensure sustainable consumption and production patterns.
e) SDG 13: Climate Action: Take urgent action to combat climate change and its impacts.

In Brazil, Law No. 12,305 implements the National Solid Waste Policy (PNRS) (BRAZIL, 2010), establishing comprehensive guidelines for proper waste management throughout the country. The PNRS aims not only to reduce the amount of waste generated but also to promote recycling, reuse, and ensure the proper final disposal of waste. Furthermore, Brazilian legislation addresses reverse logistics, a key strategy involving the collection and return of solid waste to the business sector for reuse or environmentally appropriate disposal. CONAMA Resolution No. 313 plays a fundamental role in defining technical criteria for classifying waste into three distinct classes: Class I (hazardous), Class II (non-inert), and Class III (inert) (BRAZIL, 2002). This classification is important for the proper management of each type of waste. This resolution complements the guidelines established by the PNRS, promoting an integrated and effective approach to sustainable solid waste management in Brazil.

The link between green logistics and the UN Sustainable Development Goals (SDGs) is fundamental to promoting sustainable practices on a global scale. Green logistics seeks to optimize the transport, storage, and distribution of waste, minimizing the environmental impact and maximizing the use of these resources (SEROKA-STOLKA,; OCIEPA-KUBICKA, 2019). Green logistics is an important tool for the development of the circular economy. Green logistics activities encompass reducing carbon emissions, efficiently using natural resources, reducing energy consumption in logistics activities, reducing waste, and managing its treatment (ALMEIDA et al., 2013).

Globally, society has been increasingly concerned with various aspects of ecological balance. This growth in ecological awareness has been accompanied by actions from companies and governments, either reactively or proactively, with varied strategic visions aimed at mitigating the most visible effects of various types of environmental impacts, thus protecting society and its interests. Currently, concerns regarding the triple

bottom line (**Figure 2.1**) have reshaped reality, with a growing focus on corporate responsibility and ethics, environmental stewardship, and social responsibility as fundamental to economic sustainability (LEITE, 2017).

Figure 2.1 − Triple bottom line.

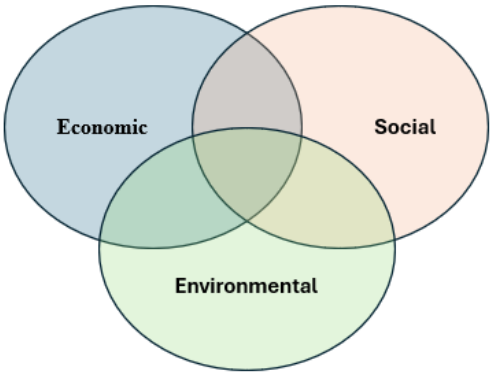

Source: (LEITE, 2017).

The implementation of green logistics practices, while beneficial for the environment and aligned with the Sustainable Development Goals (SDGs), faces several challenges. These challenges can range from high initial investment costs to technological limitations, especially in less developed regions (SEROKA-STOLKA, 2014).

2.3 Lignocellulosic biomass pyrolysis: state-of-the-art

Pyrolysis is a process that involves the thermal decomposition of organic materials in environments with absence of oxygen or low oxygen content (GALLEZOT, 2012). The pyrolysis of lignocellulosic biomass varies according to the characteristics of its individual pseudo-components, such as extractives, cellulose, hemicellulose, and lignin (RAVEENDRAN, 1996; ORFÃO; ANTUNES; FIGUEIREDO, 1999). These components thermally decompose efficiently, resulting in solid, liquid, and gaseous products. However, the proportions of the generated products are influenced by factors such as temperature, time, and specific process conditions (K N et al., 2022). The conversion mechanism of pyrolysis involves carbon formation, depolymerization, fragmentation, and other secondary reactions (K N et al., 2022).

There are two main pyrolysis technologies, differentiated by the heating rate and residence time, which affect the final product. Slow pyrolysis is characterized by low heating rates (10 °C.min^{-1}) and long residence times, while fast pyrolysis occurs at higher heating rates (102 °C.s^{-1}) and shorter residence times (PARK et al., 2014). Fast pyrolysis

tends to generate a higher proportion of gaseous products, such as pyrolysis gases and light hydrocarbons. Additionally, the rapid thermal decomposition of the material results in less char formation and higher production of bio-oils, which can be used as a renewable energy source or as feedstock to produce biofuels and chemicals (YUAN et al., 2020).

In the design and optimization of pyrolysis plants, it is essential to understand the kinetic and thermodynamic aspects involved in these processes (K N et al., 2022). When it comes to the pyrolysis of lignocellulosic biomass, a complex series of overlapping reactions occurs. Therefore, a single-step kinetic analysis is unable to fully represent the entire process with just one kinetic equation (DA SILVA et al., 2020a). On the other hand, the multicomponent kinetic approach interprets pyrolysis as a combination of independent parallel reactions, where each reaction has a distinct set of kinetic parameters such as activation energy, pre-exponential factor, and reaction model (DA SILVA et al., 2020; VYAZOVKIN et al., 2020). Previous studies suggest that the pyrolysis of lignocellulosic biomass can be divided into three or more parallel and independent devolatilization events, each with its own unique set of kinetic parameters (DA SILVA et al., 2020; MUMBACH et al., 2022b). Recently, the International Confederation of Thermal Analysis and Calorimetry (ICTAC) Kinetics Committee issued recommendations for the kinetic analysis of multi-step processes (VYAZOVKIN et al., 2020). However, there is a limited amount of research on the use of multicomponent kinetic analysis to describe the complex kinetics of pyrolysis in lignocellulosic biomass (DA SILVA et al., 2020; PINZI et al., 2020).

To accurately describe the behavior of pyrolysis, it is essential to have a comprehensive understanding of the triplet kinetic, which includes activation energy (*Ea*), pre-exponential factor (*A*), and reaction model (f(α)) (DA SILVA et al., 2020; MA et al., 2022). The dependence of activation energy on the degree of conversion from thermal decomposition rate data (DTG) can be determined using different available isoconversional methods. These methods include Friedman (FR), Flynn-Wall-Ozawa (FWO), Kissinger-Akahira-Sunose (KAS), and Starink (STK), which are applied in a linearized form (GUPTA; GUPTA; MONDAL, 2022). Activation energy is an energy barrier that needs to be overcome for a chemical reaction to occur, therefore, the lower the value of activation energy, the more economically viable the process will be (GUPTA; MONDAL, 2019).

To estimate the frequency factor (A), the kinetic compensation effect (KCE) can be utilized, which establishes a linear relationship between the Arrhenius parameters (E_a and A) in thermally induced solid-state reactions, such as biomass pyrolysis (DA SILVA et al., 2020a). The factor A represents the fraction of collisions resulting in a chemical reaction, that is, the probability of a chemical reaction occurring relative to the total number of collisions (CAI; LIU, 2008). Furthermore, to characterize the kinetics of the thermal decomposition reaction, different reaction models, both in differential and integral forms (Appendix A), have been applied to establish relationships between thermodynamic and kinetic parameters, contributing to a more comprehensive understanding of the thermal decomposition process (KHAWAM; FLANAGAN, 2006).

Reaction models f(α) can be confirmed through the master-plot method, which is a widely used approach in kinetic analysis (BAUER, 2014). This method involves representing experimental reaction rate data under different temperature and concentration conditions on a single graph, using a modified time scale. After testing various models, the master-plot method identifies the most plausible one, validating the choice of the reaction model based on the fit to the experimental data (PINZI et al., 2020).

Thermodynamic parameters (ΔH, ΔG e ΔS) make essential roles in pyrolysis studies. Enthalpy (ΔH) is related to the amount of thermal energy involved in the pyrolysis reaction. It provides information about the energy required to break the chemical bonds of organic materials and form the resulting products, such as gases, bio-oil, and biochar (DONG et al., 2022). A lower enthalpy indicates a more energetically favorable reaction, which can have positive implications for the energy efficiency of the process. Entropy (ΔS) is associated with the degree of disorder in a pyrolysis reaction. Gibbs free energy (ΔG) is a measure of the thermodynamic feasibility of pyrolysis and allows determining whether the reaction will occur spontaneously under certain temperature and pressure conditions (DONG et al., 2022).

In **Table 2.1**, the values of the kinetic triplet (Ea, A, and $f(\alpha)$) and thermodynamic parameters (ΔH, ΔG e ΔS) for biomass pyrolysis obtained from a multicomponent perspective reported in the literature are presented.

Table 2.1 − State-of-the-art of kinetic triplet and thermodynamic parameters for lignocellulosic biomass pyrolysis acquired under a multi-component perspective.

Feedstock	E_a (kJ mol^{-1})	A (min^{-1})	$f(\alpha)$	ΔH (kJ mol^{-1})	ΔG (kJ mol^{-1})	ΔS (J mol^{-1} K^{-1})	Reference
Cenchrus echinatus	158.28 for P-HC, 178.98 for P-CL, 337.53 for P-LG	1.08×10^{15} for P-HC, 1.46×10^{15} for P-CL, 1.36×10^{31} for P-LG	F3 model for P-HC, R3 model for P-CL, F7 model for P-LG	154.28 for P-HC, 174.25 for P-CL, 245.05 for P-LG	155.94 for P-HC, 175.57 for P-CL, 166.55 for P-LG	−3.42 for P-HC, −2.32 for P-CL, 139.44 for P-LG	Ref. (ALVES et al., 2023a)
Eleusine indica	98.89 for P-HC, 114.19 for P-CL, 206.21 for P-LG	1.73×10^{9} for P-HC, 6.06×10^{9} for P-CL, 1.16×10^{19} for P-LG	F2 model for P-HC, A2 model for P-CL, F6 model for P-LG	94.58 for P-HC, 109.32 for P-CL, 149.76 for P-LG	154.19 for P-HC, 171.16 for P-CL, 167.60 for P-LG	−115.02 for P-HC, −105.61 for P-CL, −28.39 for P-LG	Ref. (ALVES et al., 2022a)
Ponkan peel	84.47 for P-HC, 161.01 for P-CL, 391.29 for P-LG	2.51×10^{8} for P-HC, 4.93×10^{13} for P-CL, 2.86×10^{33} for P-LG	R3 model for P-HC, R3 model for P-CL, F8 model for P-LG	– – –	– – –	– – –	Ref. (DA SILVA et al., 2020c)
Açaí seed	103.95 for P-HC, 135.01 for P-CL, 346.24 for P-LG	1.89×10^{9} for P-HC, 1.98×10^{9} for P-CL, 8.41×10^{23} for P-LG	F1 model for P-HC, F3 model for P-CL, F8 model for P-LG	99.13 for P-HC, 129.38 for P-CL, 338.54 for P-LG	164.27 for P-HC, 180.27 for P-CL, 199.75 for P-LG	−115.00 for P-HC, −77.55 for P-CL, 162.02 for P-LG	Ref. (ALVES et al., 2021)
Catole coconut	124.70 for P-HC, 160.31 for P-CL, 152.12 for P-LG	3.59×10^{11} for P-HC, 2.78×10^{13} for P-CL, 5.37×10^{14} for P-LG	F1 model for P-HC, A2 model for P-CL, F8 model for P-LG	120.26 for P-HC, 155.28 for P-CL, 147.74 for P-LG	158.06 for P-HC, 176.94 for P-CL, 153.05 for P-LG	−70.88 for P-HC, −35.78 for P-CL, −9.95 for P-LG	Ref. (ALVES et al., 2022b)
Pecan nutshell	100.73b for P-HC, 124.82 for P-CL, 363.48 for P-LG	5.50×10^{8} for P-HC, 1.32×10^{9} for P-CL, 4.86×10^{18} for P-LG	F2 model for P-HC, R3 model for P-CL, F11 model for P-LG	95.86 for P-HC, 119.31 for P-CL, 244.05 for P-LG	169.42 for P-HC, 198.33 for P-CL, 189.80 for P-LG	−125.54 for P-HC, −119.29 for P-CL, 69.69 for P-LG	Ref. (MUMBACH et al., 2022b)
Macauba	90.63 for P-HC, 114.10 for P-CL, 153.60 for P-LG	5.86×10^{7} for P-HC, 3.28×10^{8} for P-CL, 2.31×10^{13} for P-LG	R3 model for P-HC, R2 model for P-CL, F8 model for P-LG	86.19 for P-HC, 107.18 for P-CL, 148.90 for P-LG	162.85 for P-HC, 184.19 for P-CL, 169.69 for P-LG	−143.41 for P-HC, −130.07 for P-CL, −36.66 for P-LG	Ref. (ALVES et al., 2022c)

Continued

Feedstock	E_a (kJ mol^{-1})	A (min^{-1})	$f(\alpha)$	ΔH (kJ mol^{-1})	ΔG (kJ mol^{-1})	ΔS (J mol^{-1} K^{-1})	Reference
Mango	114.17 for P-EX, 150.47 for P-HC, 190.57 for P-Cl, 173.15 for P-LG	3.73×10^{11} for P-EX, 2.57×10^{13} for P-HC, 5.56×10^{14} for P-CL, 2.62×10^{15} for P-LG	F3 model for P-EX, F2 model for P-HC, A2 model for P-CL, F7 model for P-LG	109.89 for P-EX, 145.51 for P-HC, 183.05 for P-CL, 167.84 for P-LG	146.13 for P-EX, 167.22 for P-HC, 190.87 for P-CL, 166.88 for P-LG	−70.28 for P-EX, −36.33 for P-HC, −11.70 for P-CL, 1.62 for P-LG	Ref. (ALVES et al., 2022c, 2023b)
Sugarcane bagasse	130.80 for P-EX, 129.10 for P-HC, 136.40 for P-CL, 170.70 for P-LG	4.00×10^{13} for P-EX, 5.48×10^{11} for P-HC, 5.32×10^{10} for P-CL, 5.41×10^{13} for P-LG	F2 model for P-EX, F2 model for P-HC, R3 model for P-CL, F4 model for P-LG	– – – –	– – – –	– – – –	Ref. (DA SILVA et al., 2020b)
Cocoa shell	104.56 for P-EX, 152.41 for P-HC1, 139.48 for P-HC2, 144.90 for P-CL, 201.42 for P-LG	2.55×10^{11} for P-EX, 5.55×10^{15} for P-HC1, 1.60×10^{13} for P-HC2, 1.97×10^{12} for P-CL, 8.65×10^{16} for P-LG	F1 model for P-EX, F2 model for P-HC1, F1 model for P-HC2, R2 model for P-CL, F8 model for P-LG	100.64 for P-EX, 148.12 for P-HC1, 134.93 for P-HC2, 139.98 for P-CL, 196.10 for P-LG	134.95 for P-EX, 143.19 for P-HC1, 156.54 for P-HC2, 174.03 for P-CL, 176.54 for P-LG	−72.70 for P-EX, 9.60 for P-HC1, −39.51 for P-HC2, −57.59 for P-CL, 30.69 for P-LG	Ref.(MUMBACH et al., 2022a)
Cupuassu shell	103.36 for first pyrolysis stage, 177.37 for second pyrolysis stage	1.64×10^{8} for first pyrolysis stage, 3.19×10^{10} for second pyrolysis stage	D2 model for first pyrolysis stage, F4 model for second pyrolysis stage	98.47 for first pyrolysis stage, 125.27 for second pyrolysis stage	178.28 for first pyrolysis stage, 196.69 for second pyrolysis stage	−135.66 for first pyrolysis stage, −93.94 for second pyrolysis stage	Ref. (ALVES et al., 2022d)
Butia	111.94 for P-EX, 138.25 for P-HC, 132.70 for P-CL, 174.00 for P-LG	2.58×10^{11} for P-EX, 1.80×10^{12} for P-HC, 1.15×10^{10} for P-CL, 2.89×10^{14} for P-LG	F3 model for P-EX, F2 model for P-HC, R2 model for P-CL, F6 model for P-LG	107.67 for P-EX, 133.40 for P-HC, 125.55 for P-CL, 167.88 for P-LG	145.34 for P-EX, 167.42 for P-HC, 190.47 for P-CL, 201.75 for P-LG	−73.32 for P-EX, −58.22 for P-HC, −101. 06 for P-CL, −45.87 for P-LG	Ref.(MUMBACH et al., 2022c)
Royal palm tree	75.77 for P-EX, 104.44 for P-HC, 127.64 for P-CL, 146.76 for P-LG	9.54×10^{7} for P-EX, 5.72×10^{9} for P-HC, 7.05×10^{10} for P-CL, 1.16×10^{13} for P-LG	A2 model for P-EX, F1 model for P-HC, A2 model for P-CL, F7 model for P-LG	71.79 for P-EX, 99.88 for P-HC, 121.27 for P-CL, 144.28 for P-LG	138.01 for P-EX, 157.78 for P-HC, 172.79 for P-CL, 173.17 for P-LG	−138.44 for P-EX, −105.53 for P-HC, −85.45 for P-CL, −43.67 for P-LG	Ref. (ALVES et al., 2023c)

Continued

Feedstock	E_a (kJ mol^{-1})	A (min^{-1})	$f(\alpha)$	ΔH (kJ mol^{-1})	ΔG (kJ mol^{-1})	ΔS (J mol^{-1} K^{-1})	Reference
Pequi seeds	88.50 for P-EX, 102.01 for P-HC, 124.01 for P-CL, 151.38 for P-LG	1.25×10^{7} for P-EX, 1.97×10^{8} for P-HC, 9.41×10^{8} for P-CL, 3.02×10^{8} for P-LG	D3 model for P-EX, A3 model for P-HC, R2 model for P-CL, F6 model for P-LG	110.51 for P-EX, 142.78 for P-HC, 156.50 for P-CL, 263.53 for P-LG	146.53 for P-EX, 167.69 for P-HC, 176.09 for P-CL, 77.46 for P-LG	−70.90 for P-EX, −42.58 for P-HC, −31.91 for P-CL, 250.56 for P-LG	Ref.(MUMBACH et al., 2024)
Pequi peel	114.73 for P-EX, 147.64 for P-HC, 162.68 for P-CL, 305.58 for P-LG	3.61×10^{11} for P-EX, 1.80×10^{13} for P-HC, 4.49×10^{13} for P-CL, 2.39×10^{30} for P-LG	F2 model for P-EX, F3 model for P-HC, A3 model for P-CL, F11 model for P-LG	83.83 for P-EX, 96.86 for P-HC, 116.57 for P-CL, 145.61 for P-LG	166.53 for P-EX, 180.24 for P-HC, 199.74 for P-CL, 193.98 for P-LG	−147.29 for P-EX, −134.55 for P-HC, −122.33 for P-CL, −69.61 for P-LG	Ref.(MUMBACH et al., 2024)
Sesame stalk	125.11 for first pyrolysis stage, 145.60 for second pyrolysis stage	1.64×10^{8} for first pyrolysis stage, 3.19×10^{10} for second pyrolysis stage	D2 model for first pyrolysis stage, F4 model for second pyrolysis stage	120.52 for first pyrolysis stage, 139.94 for second pyrolysis stage	170.63 for first pyrolysis stage, 214.70 for second pyrolysis stage	−86.33 for first pyrolysis stage, −99.00 for second pyrolysis stage	Ref. (HUANG; WANG; REN, 2024)

Abbreviations: P−EX, pseudo-extractives; P−HC, pseudo-hemicellulose; P−HC1, primary pseudo-hemicellulose; P−HC2, secondary pseudo-hemicellulose; P−CL, pseudo-cellulose; and P−LG, pseudo-lignin.

Source: Elaborated by the author

Based on extensive research in the literature (**Table 2.1**), it is found that there are only a few studies addressing the combination of multicomponent kinetic modeling and the estimation of thermodynamic parameters for biomass. However, specifically regarding cashew nutshell waste, both in its raw form and as oil-extracted cake, this knowledge gap becomes even more apparent. Furthermore, the analysis of volatile products is still limited in these studies.

Accurate separation and identification of pyrolysis products facilitate qualitative and quantitative analyses under varied operating conditions (HUANG et al., 2023). Characterizing volatile products is crucial during a pyrolysis reaction due to the wide variety of compounds that can be generated, including hydrocarbons, organic acids, aldehydes, and ketones. These data can be used to adjust operational parameters such as temperature, reaction time, and heating rate, aiming to maximize the production of desired compounds or minimize the formation of unwanted byproducts (FORTES; BAUGH, 2004). Understanding volatile products enables the development of more efficient and sustainable strategies for valorizing lignocellulosic waste, such as cashew nutshells.

This study represents a contribution in evaluating the potential of cashew nutshell waste, both in its raw and pressed form, for pyrolysis using combinations of volatile product characterization analysis, kinetic analysis, and multicomponent thermodynamic study. This approach provides valuable insights for the sustainable utilization of these waste materials and the generation of bioproducts and bioenergy, while also providing a solid foundation for designing pyrolytic reactors.

2.4 Particleboards from lignocellulosic biomass

The use of alternative raw materials in the production of particleboards emerges as an innovative strategy to replace conventional wood, as well as enable the reuse of agro-industrial waste. The growing awareness of the importance of sustainability has driven the search for solutions that promote circular economy and reduce environmental impact (LEE et al., 2022).

Particleboard, also known as particleboard or chipboard, is a material composed of small wood particles bonded with synthetic resins. This type of panel is widely used as a more economical and sustainable alternative to solid wood in various applications, such as furniture manufacturing, flooring, partitions, and wall coverings (GU et al., 2019).

The cost of materials used in the production of particleboard, such as resin and wood chips, represents the largest portion of the total costs of particleboard panels. These materials account for approximately 40% to 60% of the total production costs. Studies indicate that the cost of resin represents approx. 30% – 50% of the total cost of materials used in the production of particleboards (SOLT et al., 2019). In addition to bringing environmental benefits, replacing wood chips with agro-industrial waste can result in significant cost savings.

The production of particleboard is influenced by a variety of properties that play a fundamental role in determining the quality and performance of the material. The main properties that have a significant influence include particle size and distribution, moisture content, choice and quantity of adhesives used, panel density, and the pressure and temperature applied during the pressing process (ISLAM; ALAM; HANNAN, 2012; SHI et al., 2006). Proper consideration of these properties is crucial to ensure the production of particleboard panels with desired characteristics such as strength, dimensional stability, and durability, according to specific material applications.

Currently, there is a growing interest and research in the sustainable production of particleboard using agro-industrial waste as raw materials. In **Table 2.2**, a state-of-the-art can be found, presenting a comprehensive overview of the main agro-industrial wastes employed in the manufacturing of particleboard, as well as the main variables studied.

Table 2.2− Current production of particleboards using various agricultural residues as raw materials, along with the key variables employed in the manufacturing process.

Feedstock	*Density* (kg m^{-3})	*Adhesive*	*Specific pressing (MPa)*	*Temperature (°C); press time (min)*	*MOR (MPa);*	*MOE (MPa)*	Reference
Coconut Husk	650.0	Urea–formaldehyde	3.92	160 °C; 8 min	15.10 – 19.90	2016.0 – 2850.0	Ref. (NARCISO et al., 2021)
Rice Husk	594.0 – 618.0	Tamarind with formalin and tamarind with boric acid	5.00	160 – 170 °C; 15 – 20 min	9.87 –16.80	-	Ref. (BUDDI; VALLI; SAXENA, 2022)
Bean straw	640.0	Cardanol-formaldehyde Urea-formaldehyde	4.00 4.00	160 °C; 13 min 160 ºC; 8 min	4.39 2.45	1172.0 764.0	Ref. (FARIA et al., 2023)
Sugarcane bagasse, maize stock, and rice husks	604.0 – 611.0	Cassava-starch mix with borax	6.50	30 °C	13.55 – 14.83	2364.2 – 3329.93	Ref. (KARIUKI et al., 2019)
Green coconut and sugarcane bagasse fibers	500.0 700.0	Castor oil polyurethane resin	5.00	100 °C; 10 min	5.89 16.20	650.0 1879.0	Ref. (FIORELLI; BUENO; CABRAL, 2019)
Cotton stalks and poplar wood	650.0	Urea-formaldehyde resin and melamine-formaldehyde resin	−	10 min;	17.09 – 24.50	2432.0 – 4783.0	Ref. (NAZERIAN et al., 2018)
Bamboo, pine and mate	880.0 – 940.0	Melamine-urea-formaldehyde (MUF)	5.88	120 °C; 10 min	12.00 – 19.80	1550.0 – 2489.0	Ref. (RUSCH et al., 2023)
Sugarcane bagasse	750.0 – 1060.0	Polyurethane resins Urea-formaldehyde	3.00	100 °C; 3 − 7 min 130 °C; 3 − 7 min	3.44 – 35.00	486.0 – 3555.0	Ref.(BUZO et al., 2020)
Oil palm empty fruit bunch	800.0	Natural binder wheat Tapioca Corn starch	12.00	180 °C; 20 min	15.30 14.40 14.20 12.60	2078.0 1823.0 1771.0 1335.0	Ref. (NADHARI et al., 2020a)

Continued

Feedstock	*Density* (kg m^{-3})	*Adhesive*	*Specific pressing (MPa)*	*Temperature (°C); press time (min)*	*MOR (MPa);*	*MOE (MPa)*	Reference
Coconut Shell	400.0 – 900.0 > 900.0	Epoxidized natural latex and gelatinized tapioca starch	5.00	170 °C; 5 min	7.00 – 22.00	2000.0 – 5800.0	Ref. (WATCHARAWITTHAYA; SRISAWAT; CHIARAKORN, 2024)
Sugarcane bagasse	651.0 – 800.0	Benzoxazine derived from bio-oil	5.00	180 °C; 10 min	10.00 – 14.00	940.0 – 509.0	(LINCOLN et al., 2023)
Doum Palm and Balanite shells	900.0 – 1200.0	Polyester	1.00	150 °C; 5 min	1.10 – 4.30	115.0 – 1416.0	(BETENÉ et al., 2023)
Oil palm mesocarp fiber and palm kernel shell	1000.0	Phenol formaldehyde	4.00	160 °C; 6 min	19.50 – 20.90	1187.0 – 2456.0	Ref. (BOONSOMBUTI et al., 2023)
Rapeseed stalks and palm waste	700.0	-	8.00 – 14.00	230 °C; 60 min	10.40 – 26.00	950.0 – 3340.0	Ref. (NAJAHI et al., 2023)
Wheat straw and distiller's dried grain with solubles	600.0	Phenol formaldehyde	3.80	195 °C; 12 min	1.00 – 5.00	300.0 – 1000.0	Ref. (REGMI et al., 2022)
Palm sugar fiber and cassava bagasse	320.0 – 610.0	Mycelium of Ganoderma lucidum	–	Cool pressed; 10 min	0.48 – 3.08	23.8 – 411.5	Ref. (AGUSTINA et al., 2019)
Sorghum (Sorghum bicolor)	800.0	Maleic acid, citric acid and phenol-formaldehyde	6.50	200 °C; 12 min	11.90 – 25.70	3020.0 – 3570.0	Ref. (SUTIAWAN et al., 2022)
Macadamia nut carpel, coffee husk and papaya stem	700.0	Urea-formaldehyde or tannin-urea-formaldehyde	3.90	160 °C; 10 min	4.80 – 10.60	686.5 – 1452.0	Ref. (MARTINS et al., 2021)

Continued

Feedstock	*Density* (kg m^{-3})	*Adhesive*	*Specific pressing (MPa)*	*Temperature (°C); press time (min)*	*MOR (MPa);*	*MOE (MPa)*	Reference
Tea oil camellia (Camellia oleifera Abel.) shells	720.0	Polymeric diphenylmethane diisocyanate	3.50 – 4.00	180 – 200 °C; 3 – 5 min	4.18 – 6.68	692.0 – 1095.0	Ref. (CHAYDARREH et al., 2021)
Rice husk	510.0 – 610.0	Fevicol, Ponal and woodfix	10.00	Cool pressed; 7 days	1.00 – 2.50	15.0 – 27.0	Ref. (OLUPOT et al., 2022)
Sugarcane bagasse	800.0	–	12.00	180 °C; 10 – 40 min	15.20	1710.0	Ref. (NADHARI et al., 2020b)
Sugarcane bagasse and bamboo culm particles	650.0	UF-based adhesive with the catalyst (ammonium sulphate, 5% solids in the adhesive)	3.40	180 °C; 10 min	9.20	1031.3	Ref. (BRITO et al., 2020)
Rice husk and soy proteins	900.0 – 1000.0	Soybean protein concentrate; Tung oil	5.00	140 °C; 25 min	14.50 – 23.50	2400.0 – 2780.0	Ref. (CHALAPUD et al., 2020)
Wheat straw and rapeseed straw	490.0	Urea-formaldehyde	9.00	55 °C; 2.5 min	–	1154.0 – 1347.0	Ref. (HÝSKOVÁ et al., 2020)

Source: Elaborated by the author

In the context of particleboard manufacturing, the largest consumption of phenol-formaldehyde resin occurs in the wood derivatives industry, where it is widely used as an adhesive in the production of particleboards, plywood, fiberboards, MDF panels, and other products (SARIKA et al., 2020). CNSL can be promising source of phenol to produce sustainable phenolic resins. Studies have explored the use of CNSL-based binders/adhesives for particleboard production (AKARANTA, 2000; LUBI; THACHIL, 2007, 2000). However, it is relevant to note that the utilization of technical CNSL for phenolic resin manufacturing requires the extraction of phenolic compounds by solvents, resulting in additional costs in the production process. This information is supported by the following studies: Rahmawati *et al.* (2019) developed a phenolic resin by isolating cardanol from technical CNSL using liquid-liquid extraction method, which involves the use of solvents (RAHMAWATI et al., 2019). Da Silva *et al.* (2023) developed and characterized novolac type phenolic resins from technical CNSL using column chromatography technique to obtain cardanol (DA SILVA et al., 2023). Marliyana *et al.* (2022) synthesized acetaldehyde novolac resin based on cardanol derived from technical CNSL, using liquid-liquid extraction method with acetone as a solvent to isolate cardanol from CNSL (MARLIYANA; WAHYUNINGSIH; HAYATI, 2022). Makwana *et al.* produced an epoxy resin, using silica gel column chromatography to separate cardanol and cardol from technical CNSL, and employed two hardeners, isophorone diamine (IPDA) and diethylenetriamine (DETA), for resin curing (MAKWANA et al., 2022b).

The adoption of particleboard manufacturing processes using natural CNSL (obtained by pressing at room temperature) emerges as a feasible alternative in small-scale factories, which are common in northeastern Brazil. This simplified extraction method eliminates the need to isolate the chemical compounds present in CNSL. However, it is important to note that the feasibility of experimental particleboard production using cashew nutshell residue, in conjunction with a phenolic resin derived from residual CNSL, remains unexplored in the existing literature. This knowledge gap represents an opportunity for the experimental implementation of this study, followed by the modeling of the production process using Super Pro Design software. This approach will allow for a comprehensive economic evaluation of the developed process, contributing not only to scientific and technological advancement but also to the promotion of sustainability in the particleboard manufacturing industry.

2.5 References

ABDUL-WAHAB ILAVBARE, O. et al. Hybridisation of Carbon Black: Cashew Nut Shell Powder as Fillers on the Mechanical Properties of Natural Rubber Composites. **Composite Materials**, v. 2, n. 2, p. 49–54, 2018.

AGUSTINA, W. et al. Physical and mechanical properties of composite boards from the mixture of palm sugar fiber and cassava bagasse using mycelium of Ganoderma lucidum as a biological adhesive. **IOP Conference Series: Earth and Environmental Science**, v. 374, n. 1, p. 012012, 5 nov. 2019.

AKARANTA, O. Production of particle boards from bioresources. **Bioresource Technology**, v. 75, n. 1, p. 87–89, 2000.

ALMEIDA, F. A. S. DE et al. **Gestão da Informação, Inovação e Logistica**. [s.l: s.n.].

ALVES, J. L. F. et al. Exploring Açaí Seed (Euterpe oleracea) Pyrolysis Using Multi-component Kinetics and Thermodynamics Assessment Towards Its Bioenergy Potential. **BioEnergy Research**, v. 14, n. 1, p. 209–225, 6 mar. 2021.

ALVES, J. L. F. et al. Kinetic triplet and thermodynamic parameters of the pyrolysis reaction of invasive grass Eleusine indica biomass: a new low-cost feedstock for bioenergy production. **Biomass Conversion and Biorefinery**, 2022a.

ALVES, J. L. F. et al. Prospection of catole coconut (Syagrus cearensis) as a new bioenergy feedstock: Insights from physicochemical characterization, pyrolysis kinetics, and thermodynamics parameters. **Renewable Energy**, v. 181, p. 207–218, 2022b.

ALVES, J. L. F. et al. Potential of macauba endocarp (Acrocomia aculeate) for bioenergy production: Multi-component kinetic study and estimation of thermodynamic parameters of activation. **Thermochimica Acta**, v. 708, p. 179134, fev. 2022c.

ALVES, J. L. F. et al. Evaluating the bioenergy potential of cupuassu shell through pyrolysis kinetics, thermodynamic parameters of activation, and evolved gas analysis with TG/FTIR technique. **Thermochimica Acta**, v. 711, n. February, p. 179187, maio 2022d.

ALVES, J. L. F. et al. Assessing the potential of the invasive grass Cenchrus echinatus for bioenergy production: A study of its physicochemical properties, pyrolysis

kinetics and thermodynamics. **Thermochimica Acta**, v. 724, n. April, p. 179500, jun. 2023a.

ALVES, J. L. F. et al. Physicochemical properties, pyrolysis kinetics, thermodynamic parameters of activation, and evolved volatiles of mango seed waste as a bioenergy feedstock: A potential exploration. **Thermochimica Acta**, v. 725, n. April, p. 179519, jul. 2023b.

ALVES, J. L. F. et al. Valorization of royal palm tree agroindustrial waste via pyrolysis with a focus on physicochemical properties, kinetic triplet, thermodynamic parameters, and volatile products. **Biomass and Bioenergy**, v. 177, n. July, p. 106937, out. 2023c.

AMALIYAH, N.; PUTRA, A. E. E. Microwave-Assisted Pyrolysis of Cashew Nut Shell. **International Journal of Design & Nature and Ecodynamics**, v. 16, n. 2, p. 227–232, 30 abr. 2021.

BAUER, M. Plot, Master-Plot, and related Matters. **Zeitschrift für Literaturwissenschaft und Linguistik**, v. 44, n. 4, p. 31–50, 23 dez. 2014.

BETENÉ, A. D. O. et al. Processing of tropical agro-industrial waste for particleboard manufacture: Dimensional stability and mechanical performance. **Journal of Building Engineering**, v. 76, n. April, p. 107369, out. 2023.

BOONSOMBUTI, A. et al. The use of lignin from palm kernel shell (PKS) to fabricate oil palm mesocarp fiber (OPMF) particleboards. **International Journal of Adhesion and Adhesives**, v. 125, n. June, p. 103425, jul. 2023.

BRAZIL. **National Council on the Environment**. Available at: <http://www.siam.mg.gov.br/sla/download.pdf?idNorma=263>. Accessed on: February 29, 2024.

BRAZIL. **Law No. 12,305, of August 2, 2010**. Available at: <https://www.planalto.gov.br/ccivil_03/_ato2007-2010/2010/lei/l12305.htm>. Accessed on: February 2, 2024.

BRITO, F. M. S. et al. Technological characterization of particleboards made with sugarcane bagasse and bamboo culm particles. **Construction and Building Materials**, v. 262, p. 120501, nov. 2020.

BUDDI, T.; VALLI, S.; SAXENA, K. K. Manufacturing and Evaluation of Mechanical Properties for Rice Husk Particle Board Using IoT. **Indian Journal of Engineering & Materials Sciences**, v. 29, n. December, p. 750–754, 2022.

BUZO, A. L. S. C. et al. Addition of sugarcane bagasse for the production of particleboards bonded with urea-formaldehyde and polyurethane resins. **Wood Research**, v. 65, n. 5, p. 727–736, 7 nov. 2020.

CAI, J.; LIU, R. Dependence of the frequency factor on the temperature: a new integral method of nonisothermal kinetic analysis. **Journal of Mathematical Chemistry**, v. 43, n. 2, p. 637–646, 8 fev. 2008.

CHALAPUD, M. C. et al. Biobased particleboards based on rice husk and soy proteins: Effect of the impregnation with tung oil on the physical and mechanical behavior. **Construction and Building Materials**, v. 230, p. 116996, jan. 2020.

CHAYDARREH, K. C. et al. Utilization of tea oil camellia (Camellia oleifera Abel.) shells as alternative raw materials for manufacturing particleboard. **Industrial Crops and Products**, v. 161, p. 113221, mar. 2021.

COULIBALY, A. et al. Valuation of cashew nut shell for the production of biofuel. **Energy Reports**, v. 8, n. May, p. 691–707, nov. 2022.

CRUZ, I. A. et al. Valorization of cassava residues for biogas production in Brazil based on the circular economy: An updated and comprehensive review. **Cleaner Engineering and Technology**, v. 4, n. December 2020, p. 100196, out. 2021.

D'ADAMO, I.; GASTALDI, M.; MORONE, P. Economic sustainable development goals: Assessments and perspectives in Europe. **Journal of Cleaner Production**, v. 354, n. April, p. 131730, jun. 2022.

DA SILVA, J. C. G. et al. Single-step and multi-step thermokinetic study – Deconvolution method as a simple pathway for describe properly the biomass pyrolysis for energy conversion. **Energy Conversion and Management**, v. 209, n. March, p. 112653, 2020a.

DA SILVA, J. C. G. et al. Single-step and multi-step thermokinetic study – Deconvolution method as a simple pathway for describe properly the biomass pyrolysis for energy conversion. **Energy Conversion and Management**, v. 209, n. February, p.

112653, 2020b.

DA SILVA, J. C. G. et al. Torrefaction of ponkan peel waste in tubular fixed-bed reactor: In-depth bioenergetic evaluation of torrefaction products. **Energy**, v. 210, p. 118569, nov. 2020c.

DA SILVA, K. T. et al. Bio-based novolac resins from cashew nut processing waste: Alternative resource for the development of high-value sustainable products. **Journal of Applied Polymer Science**, v. 140, n. 13, 5 abr. 2023.

DE OLIVEIRA, C. T.; OLIVEIRA, G. G. A. What Circular economy indicators really measure? An overview of circular economy principles and sustainable development goals. **Resources, Conservation and Recycling**, v. 190, n. September 2022, p. 106850, mar. 2023.

DIEDHIOU, A. et al. Study of cashew nut shells Valorisation by gasification. **Chemical Engineering Transactions**, v. 39, n. Special Issue, p. 1171–1176, 2014.

DINESHKUMAR J; JESUDAS T. Hybrid polymer matrix development using cashew nut shell liquid as an additive into epoxy resin. **Journal of the Chinese Institute of Engineers**, v. 46, n. 4, p. 380–388, 19 maio 2023.

DONG, R. et al. A comprehensive evaluation on pyrolysis kinetics, thermodynamics, product properties and formation pathways of jatropha oil for high-value utilization. **Fuel**, v. 313, n. December 2021, p. 122982, abr. 2022.

FARIA, D. L. et al. Cardanol-based adhesive with reduced formaldehyde emission to produce particleboards with waste from bean crops. **Environmental Science and Pollution Research**, v. 30, n. 16, p. 48270–48287, 9 fev. 2023.

FIORELLI, J.; BUENO, S. B.; CABRAL, M. R. Assessment of multilayer particleboards produced with green coconut and sugarcane bagasse fibers. **Construction and Building Materials**, v. 205, p. 1–9, abr. 2019.

FORTES, I. C. P.; BAUGH, P. J. Pyrolysis-GC/MS studies of vegetable oils from Macauba fruit. **Journal of Analytical and Applied Pyrolysis**, v. 72, n. 1, p. 103–111, 2004.

GALLEZOT, P. Conversion of biomass to selected chemical products. **Chemical Society Reviews**, v. 41, n. 4, p. 1538–1558, 2012.

GU, Y. et al. International Journal of Biological Macromolecules Preparation , characterization and properties of starch-based adhesive for wood-based panels. **International Journal of Biological Macromolecules**, v. 134, p. 247–254, 2019.

GUPTA, G. K.; MONDAL, M. K. Kinetics and thermodynamic analysis of maize cob pyrolysis for its bioenergy potential using thermogravimetric analyzer. **Journal of Thermal Analysis and Calorimetry**, v. 137, n. 4, p. 1431–1441, 2019.

GUPTA, S.; GUPTA, G. K.; MONDAL, M. K. Thermal degradation characteristics, kinetics, thermodynamic, and reaction mechanism analysis of pistachio shell pyrolysis for its bioenergy potential. **Biomass Conversion and Biorefinery**, v. 12, n. 11, p. 4847–4861, 2022.

HERRADOR, M. et al. Circular economy and zero-carbon strategies between Japan and South Korea: A comparative study. **Science of The Total Environment**, v. 820, p. 153274, maio 2022.

HUANG, Y. et al. Fast pyrolysis behaviors of biomass with high contents of ash and nitrogen using TG-FTIR and Py-GC/MS. **Journal of Analytical and Applied Pyrolysis**, v. 170, n. October 2022, p. 105922, 2023.

HUANG, Z.; WANG, X.; REN, X. Kinetic study of sesame stalk pyrolysis by thermogravimetric analysis. **Renewable Energy**, v. 222, n. December 2023, p. 119878, fev. 2024.

HÝSKOVÁ, P. et al. Utilization of agricultural rests: Straw-based composite panels made from enzymatic modified wheat and rapeseed straw. **Industrial Crops and Products**, v. 144, n. February 2019, p. 112067, fev. 2020.

IFA, L. et al. Techno-economic analysis of bio-briquette from cashew nut shell waste. **Heliyon**, v. 6, n. 9, p. e05009, 2020.

ISLAM, A.; ALAM, R.; HANNAN, O. Composites : Part B Multiresponse optimization based on statistical response surface methodology and desirability function for the production of particleboard. **Composites: Part B**, v. 43, n. 3, p. 861–868, 2012.

K N, Y. et al. Lignocellulosic biomass-based pyrolysis: A comprehensive review. **Chemosphere**, v. 286, n. P2, p. 131824, 2022.

KARIUKI, S. W. et al. Characterization of Prototype Formulated Particleboards

from Agroindustrial Lignocellulose Biomass Bonded with Chemically Modified Cassava Peel Starch. **Advances in Materials Science and Engineering**, v. 2019, p. 1–15, 11 nov. 2019.

KHAWAM, A.; FLANAGAN, D. R. Solid-State Kinetic Models: Basics and Mathematical Fundamentals. **The Journal of Physical Chemistry B**, v. 110, n. 35, p. 17315–17328, set. 2006.

LEE, S. H. et al. Particleboard from agricultural biomass and recycled wood waste: a review. **Journal of Materials Research and Technology**, v. 20, p. 4630–4658, set. 2022.

LEITE, P. R. **Logística Reversa Sustentabilidade e competitividade**. 1ª ed. São Paulo: [s.n.].

LINCOLN, A. et al. Resins and fibers from sugarcane bagasse to produce medium - density fiberboard. **Biomass Conversion and Biorefinery**, n. 0123456789, 2023.

LIU, Y. et al. Review of waste biorefinery development towards a circular economy: From the perspective of a life cycle assessment. **Renewable and Sustainable Energy Reviews**, v. 139, n. April 2020, p. 110716, abr. 2021.

LIU, Z. et al. Preparation of hypercrosslinked polymers with cashew nut shell liquid for removal of volatile organic compounds. **Polymer Engineering & Science**, v. 62, n. 6, p. 1823–1832, 30 jun. 2022.

LUBI, C. M.; THACHIL, E. T. Particleboard from cashew nut shell liquid. **Polymer - Plastics Technology and Engineering**, v. 46, n. 4, p. 393–400, 2007.

LUBI, M. C.; THACHIL, E. T. Cashew nut shell liquid (CNSL) - A versatile monomer for polymer synthesis. **Designed Monomers and Polymers**, v. 3, n. 2, p. 123–153, 2000.

MA, C. et al. Thermogravimetric pyrolysis kinetics study of tobacco stem via multicomponent kinetic modeling, Asym2sig deconvolution and combined kinetics. **Bioresource Technology**, v. 360, n. June, p. 127539, 2022.

MAKWANA, K. et al. Cardol: Cashew nut shell liquid (CNSL) - derived starting material for the preparation of partially bio-based epoxy resins. **European Polymer Journal**, v. 166, n. December 2021, p. 111029, mar. 2022a.

MAKWANA, K. et al. Cardol: Cashew nut shell liquid (CNSL) - derived starting material for the preparation of partially bio-based epoxy resins. **European Polymer Journal**, v. 166, n. December 2021, p. 111029, mar. 2022b.

MANCINI, S. D. et al. Circular Economy and Solid Waste Management: Challenges and Opportunities in Brazil. **Circular Economy and Sustainability**, v. 1, n. 1, p. 261–282, 26 jun. 2021.

MARI, E. L.; VILLENA, E. M. Properties of particleboard from wood wastesand cashew nut shell residue. **Philippine Journal of Science**, v. 145, n. 1, p. 1–8, 2016.

MARLIYANA, S. D.; WAHYUNINGSIH, S.; HAYATI, N. N. Synthesis of Cardanol-Based Acetaldehyde Novolac Resin from Cashew Nut Shell Liquid (CNSL). **Jurnal Kimia Sains dan Aplikasi**, v. 25, n. 9, p. 316–321, 23 dez. 2022.

MARTINS, R. S. F. et al. Investigation of agro-industrial lignocellulosic wastes in fabrication of particleboard for construction use. **Journal of Building Engineering**, v. 43, n. March, p. 102903, nov. 2021.

MENDU, J. K.; PANNEM, R. M. R. Assessment of mechanical properties of cashew nut shell ash blended concrete. **Innovative Infrastructure Solutions**, v. 6, n. 4, p. 227, 28 dez. 2021.

MUJTABA, M. et al. Lignocellulosic biomass from agricultural waste to the circular economy: a review with focus on biofuels, biocomposites and bioplastics. **Journal of Cleaner Production**, v. 402, n. November 2022, p. 136815, maio 2023.

MUMBACH, G. D. et al. Pyrolysis of cocoa shell and its bioenergy potential: evaluating the kinetic triplet, thermodynamic parameters, and evolved gas analysis using TGA-FTIR. **Biomass Conversion and Biorefinery**, v. 12, n. 3, p. 723–739, 2022a.

MUMBACH, G. D. et al. Prospecting pecan nutshell pyrolysis as a source of bioenergy and bio-based chemicals using multicomponent kinetic modeling, thermodynamic parameters estimation, and Py-GC/MS analysis. **Renewable and Sustainable Energy Reviews**, v. 153, n. January 2022, p. 111753, jan. 2022b.

MUMBACH, G. D. et al. Investigation on prospective bioenergy from pyrolysis of butia seed waste using TGA-FTIR: Assessment of kinetic triplet, thermodynamic parameters and evolved volatiles. **Renewable Energy**, v. 191, p. 238–250, maio 2022c.

MUMBACH, G. D. et al. Unlocking the potential of pequi (Caryocar brasiliense) residues for bioenergy and renewable chemicals: Multicomponent kinetic modeling, thermodynamic parameter estimation, and characterization of volatile products through TGA and Py-GC/MS experiments. **Industrial Crops and Products**, v. 209, n. July 2023, p. 117928, mar. 2024.

NADHARI, W. N. A. W. et al. Mechanical and physical properties of binderless particleboard made from oil palm empty fruit bunch (OPEFB) with addition of natural binder. **Materials Today: Proceedings**, v. 31, p. 287–291, 2020a.

NADHARI, W. N. A. W. et al. Sugarcane (Saccharum officinarium L.) bagasse binderless particleboard: Effect of hot pressing time study. **Materials Today: Proceedings**, v. 31, p. 313–317, 2020b.

NAJAHI, A. et al. Harvesting value from agricultural waste: Dimensionally stable fiberboards and particleboards with enhanced mechanical performance and fire retardancy through the use of lignocellulosic nanofibers. **Industrial Crops and Products**, v. 204, n. August, p. 117336, nov. 2023.

NARCISO, C. R. P. et al. Potential for the Use of Coconut Husk in the Production of Medium Density Particleboard. **Waste and Biomass Valorization**, v. 12, n. 3, p. 1647–1658, 2021.

NAZERIAN, M. et al. Application of response surface methodology for evaluating particleboard properties made from cotton stalk particles. **Wood Material Science and Engineering**, v. 13, n. 2, p. 73–80, 2018.

NGUYEN, H. N. et al. Kinetic and structural changes during gasification of cashew nut shell char particles. **Environmental Progress & Sustainable Energy**, v. 40, n. 3, 30 maio 2021.

OGUNMAKINDE. A Review of Circular Economy Development Models in China, Germany and Japan. **Recycling**, v. 4, n. 3, p. 27, 3 jul. 2019.

OLIVEIRA, K. F. S. DE et al. Cashew nut shell (Anarcadium accidentale L) charcoal as bioadsorbent to remove Cu2+ and Cr3+. **Research, Society and Development**, v. 10, n. 2, p. e0510212238, 1 fev. 2021.

OLUGASA, T. T.; ADEKANBI, M. L.; FASOGBON, S. K. Performance and

Emission Characteristics of Compression Ignition Engine Running on a Blend of Cashew Nut Shell Liquid and Biodiesel Produced from Orange Peel. **European Journal of Sustainable Development Research**, v. 6, n. 4, p. em0197, 15 jul. 2022.

OLUPOT, P. W. et al. Effects of sawdust and adhesive type on the properties of rice husk particleboards. **Results in Engineering**, v. 16, n. November, p. 100775, dez. 2022.

ORFÃO, J. J. M.; ANTUNES, F. J. A.; FIGUEIREDO, J. L. Pyrolysis kinetics of lignocellulosic materials—three independent reactions model. **Fuel**, v. 78, n. 3, p. 349–358, fev. 1999.

PARK, J. et al. Slow pyrolysis of rice straw: Analysis of products properties, carbon and energy yields. **Bioresource Technology**, v. 155, p. 63–70, mar. 2014.

PINZI, S. et al. A simplified method for kinetic modeling of coffee silver skin pyrolysis by coupling pseudo-components peaks deconvolution analysis and model free-isoconversional methods. **Fuel**, v. 278, n. February, p. 118260, out. 2020.

PORTO DE SOUZA VANDENBERGHE, L. et al. Added-value biomolecules' production from cocoa pod husks: A review. **Bioresource Technology**, v. 344, n. October 2021, p. 126252, jan. 2022.

RAHMAWATI, P. et al. Synthesis of Cardanol-Based Novolac Resin from Cashew Nut Shell Liquid. **Journal of Engineering Science**, v. 15, p. 23–33, 31 maio 2019.

RAVEENDRAN, K. Pyrolysis characteristics of biomass and biomass components. **Fuel**, v. 75, n. 8, p. 987–998, jun. 1996.

REGMI, S. et al. High fiber fraction DDGS – A functional filler for manufacturing low-density particleboards. **Industrial Crops and Products**, v. 181, n. January, p. 114793, jul. 2022.

ROJAS, L. F.; ZAPATA, P.; RUIZ-TIRADO, L. Agro-industrial waste enzymes: Perspectives in circular economy. **Current Opinion in Green and Sustainable Chemistry**, v. 34, p. 100585, abr. 2022.

RUSCH, F. et al. Particleboard experimental production with bamboo, pine and mate for one product of new applications. **Maderas-Cienc Tecnol**, v. 25, n. SE-Article, p. 1–24, 2023.

SAMIYAMMAL, P. et al. Adsorption of brilliant green dye onto activated carbon prepared from cashew nut shell by KOH activation: Studies on equilibrium isotherm. **Environmental Research**, v. 212, n. PD, p. 113497, 2022.

SARIKA, P. R. et al. Bio-based alternatives to phenol and formaldehyde for the production of resins. **Polymers**, v. 12, n. 10, p. 1–24, 2020.

SEROKA-STOLKA, O.; OCIEPA-KUBICKA, A. Green logistics and circular economy. **Transportation Research Procedia**, v. 39, n. 2018, p. 471–479, 2019.

SELVAMUTHUKUMAR, M. et al. Investigation on the lubricating behavior of cashew nut shell liquid oil as a renewable and reliable petrochemical product. **Materials Today: Proceedings**, v. 44, p. 3583–3588, 2021.

SHI, J. et al. Preparation and properties of waste tea leaves particleboard. **Forestry Studies in China**, v. 8, n. 1, p. 41–45, 2006.

SOLT, P. et al. Technological performance of formaldehyde-free adhesive alternatives for particleboard industry. **International Journal of Adhesion and Adhesives**, v. 94, n. May, p. 99–131, 2019.

STEPHENSON, P. J.; DAMERELL, A. Bioeconomy and Circular Economy Approaches Need to Enhance the Focus on Biodiversity to Achieve Sustainability. **Sustainability**, v. 14, n. 17, p. 10643, 26 ago. 2022.

SUTIAWAN, J. et al. The properties of particleboard composites made from three sorghum (Sorghum bicolor) accessions using maleic acid adhesive. **Chemosphere**, v. 290, n. November 2021, p. 133163, mar. 2022.

UDHAYASANKAR, R.; KATHIKEYAN, B. PREPARATION AND PROPERTIES OF CASHEW NUT SHELL LIQUID-BASED COMPOSITE REINFORCED BY COCONUT SHELL PARTICLES. **Surface Review and Letters**, v. 26, n. 04, p. 1850174, 21 maio 2019.

ULIASSI, E. et al. Cashew Nut Shell Liquid (CNSL) as a Source of Drugs for Alzheimer's Disease. **Molecules**, v. 26, n. 18, p. 5441, 7 set. 2021.

UNITED NATIONS. **Sustainable Development Goals**. Available at: <https://www.undp.org/sustainable-development-goals?utm_source=EN&utm_medium=GSR&utm_content=US_UNDP_PaidSearch_Br

and_English&utm_campaign=CENTRAL&c_src=CENTRAL&c_src2=GSR&gclid=CjwKCAiAheacBhB8EiwAItVO25DuoyH1lxaCvq7E9rRzGOAVENA4-QTC98fo538m7CcY_5XHRyIH0B>. Accessed on: March 3, 2023.

VIEIRA, I. M. M. et al. Valorization of Pineapple Waste: a Review on How the Fruit's Potential Can Reduce Residue Generation. **BioEnergy Research**, v. 15, n. 2, p. 924–934, 11 jun. 2022.

VYAZOVKIN, S. et al. Thermochimica Acta ICTAC Kinetics Committee recommendations for analysis of multi-step kinetics. **Thermochimica Acta**, v. 689, n. March, p. 178597, 2020.

WALKER, T. R. (Micro)plastics and the UN Sustainable Development Goals. **Current Opinion in Green and Sustainable Chemistry**, v. 30, p. 100497, ago. 2021.

WATCHARAWITTHAYA, A.; SRISAWAT, N.; CHIARAKORN, S. Wood Substitute Material from Coconut Shell Waste and Green Adhesive. **Environment and Natural Resources Journal**, v. 22, n. 1, p. 1–11, 1 jan. 2024.

Y OGASWARA, R. R. et al. A Kinetic Study in Fermentation of Cocoa Pod Husk using Zymomonas Mobilis. **IOP Conference Series: Materials Science and Engineering**, v. 1125, n. 1, p. 012093, 1 maio 2021.

YUAN, T. et al. Comparison of bio-chars formation derived from fast and slow pyrolysis of walnut shell. **Fuel**, v. 261, n. August 2019, p. 116450, 2020.

Chapter 3

Pyrolysis of cashew nutshell residues for bioenergy and renewable chemicals: kinetics, thermodynamics, and volatile products

3 PYROLYSIS OF CASHEW NUTSHELL RESIDUES FOR BIOENERGY AND RENEWABLE CHEMICALS: KINETICS, THERMODYNAMICS, AND VOLATILE PRODUCTS

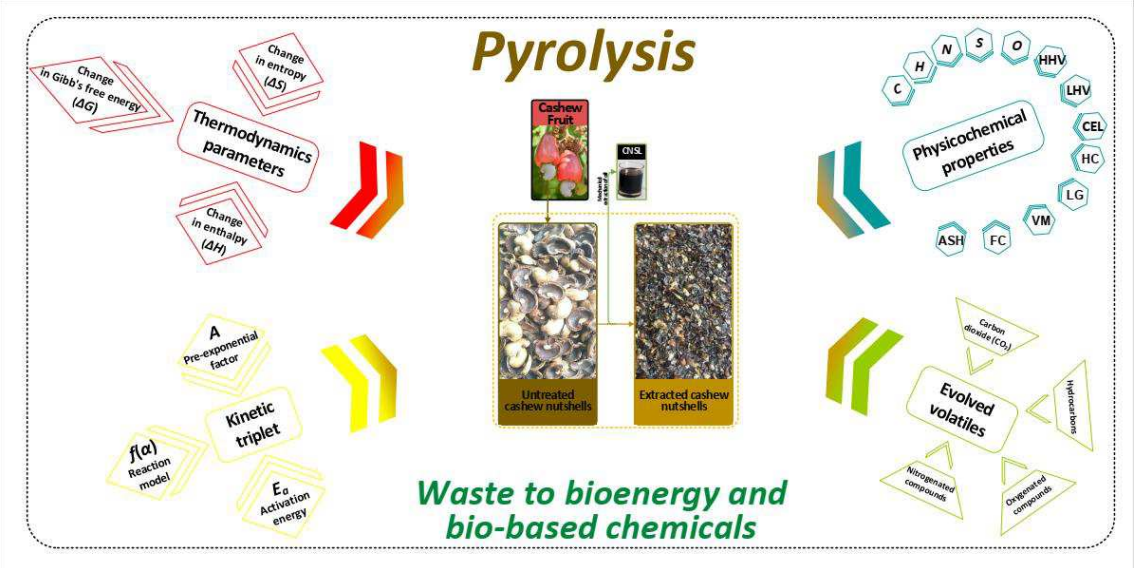

3.1 Abstract

The present study's motivation and novelty are related to the potential of raw (RCNS) and pressed (PCNS) cashew nutshell residues for producing bioenergy and renewable chemicals through their physicochemical characterization and pyrolysis processing (multicomponent kinetic analysis, thermodynamic study, and volatile product analysis). A thermogravimetric analyzer and an analytical pyrolyzer coupled with gas chromatography–mass spectrometry (Py–GC/MS) were used to perform the pyrolysis reactions. The pyrolysis behavior of RCNS and PCNS was accurately modeled with the help of the Asym2sig deconvolution function through five and four parallel devolatilization events, respectively. The average activation energies for the pyrolysis of RCNS and PCNS fell in the ranges of 63.8−249.3 and 91.1−167.4 kJ mol^{-1}, respectively, as determined by four isoconversional methods (Friedman, Flynn–Wall–Ozawa, Kissinger–Akahira–Sunose, and Starink). Pre-exponential factors ranging from 4.2×10^{8} to 6.9×10^{16} min^{-1} (RCNS) and 4.8×10^{8} to 3.2×10^{11} min^{-1} (PCNS) were estimated from the kinetic compensation effect. The master plots method evidenced that the most likely reaction models involved in the pyrolysis pertain to the nucleation-growth and *n*-order reaction mechanisms. Based on the multiple kinetic triplets acquired, the verification step of the summative rate expressions indicated excellent agreement between the simulated behavior and the experimental data, with a minimum quality of fit of 93.1%. The pyrolysis

route can valorize both cashew nutshell residues to obtain renewable chemicals promoting the circular economy, as verified by Py-GC/MS analysis. Aliphatic hydrocarbons were the dominant components of the condensable volatile products at 650 °C, while reaction temperatures of 450 and 550 °C favored the production of oxygenated compounds. Due to the low potential energy barrier, the thermodynamic study attests to the viability of converting the studied residues into valuable products. The present results play an essential role in the utility of both cashew nutshell residues as inexpensive feedstocks for pyrolysis, possibly leading to bioenergy and biobased chemicals, which fall under the principle of valorization of lignocellulosic residues.

Keywords: Cashew nutshell residues, bioenergy potential, multicomponent kinetics, thermodynamic study, Py–GC/MS analysis.

3.2 Introduction

Presently, the high energy consumption derived from nonrenewable sources has caused environmental concerns since these sources promote negative ecological impacts and increase pollution (LIBORIO et al., 2023). The world's primary energy consumption is concentrated in oil (30%), coal (25%), natural gas (25%), renewable energy (15%), and nuclear energy (5%), according to data from the International Energy Agency (IEA) regarding 2020 (AGENCY, [s.d.]). The production of bioenergy exploring the potential of biowaste has become attractive as an alternative energy source, which generates few pollutants, has fewer environmental risks, and has a greater capacity for reuse (HU et al., 2022). Biomass, being cost-effective and readily accessible, can be regarded as a primary option in pursuing enhanced energy matrix diversification, aiming to mitigate reliance on fossil fuels (COSTA et al., 2022).

Pyrolysis, combustion, and gasification processes are recognized thermochemical routes for converting biomass into usable forms of energy (HUANG et al., 2021). Pyrolysis, when compared to combustion, offers a simple operation, lower polluting gas emissions, and a reasonable cost, which are great merits of this conversion-based technology (YAO et al., 2020b). The successful design and operational practice of large-scale biomass pyrolysis reactors requires in-depth research to establish fundamental variables such as the kinetic triplet, thermodynamic parameters, and volatile products (MA et al., 2022; XU et al., 2020). Thermogravimetric analysis (TGA) is a valuable thermoanalytical technique that records pyrolysis behaviors in the form of mass loss and the rate of mass loss profiles with respect to temperature (SANGARÉ et al., 2021). It provides high repeatale reference data for determining the kinetic triplet and thermodynamic

parameters of lignocellulosic biomass pyrolysis (VYAZOVKIN et al., 2014). Advanced thermoanalytical techniques, particularly pyrolysis techniques hyphenated to GC/MS, effectively characterize volatile pyrolysis products online (MARTINS MAYER et al., 2018). Because of the high heating rate that can be applied to a sample and accurate temperature reproducibility, Py-GC/MS is frequently used to investigate the effect of temperature on the distribution of volatile products under fast pyrolysis conditions (MA et al., 2019; MUMBACH et al., 2022a; QIAO et al., 2019).

The cashew tree (*Anacardium occidentale*) is native to the northeast region of Brazil and has high socioeconomic importance, especially in the semiarid region, as it generates employment and income in the driest time of the year. According to the Food and Agriculture Organization of the United Nations (FAO), Sri Lanka, Mali, and Mozambique had the highest production of cashew nuts in the world in 2020, with approximately 666 thousand tons. Brazil is ranked fourth in the world production of cashew nuts ("Food and Agriculture Organization of the United Nations Statistics", 2022). The shell of the cashew nut, generated in the extraction of the fruit, represents approximately 65% to 70% of its mass and contains spongy cavities that hold approximately 20% to 25% of an oil called cashew nutshell liquid (CNSL) (KUMAR et al., 2002). Obtaining CNSL generates a high amount of pressed nutshell, which constitutes a major environmental problem. This residue, rich in phenolic compounds, is not recommended for disposal in landfills or burning in boilers due to the production of acidic vapors (high concentrations of CO, NO_x, and CH_4) (SANTOS et al., 2022). It was hypothesized that cashew nutshell residues (the raw biomass and the pressed biomass post extraction of cashew nutshell liquid) could be valorized as new feedstocks for the pyrolysis process, thereby offering a potential solution for reducing environmental impacts associated with their improper disposal. This approach involves converting these lignocellulosic agro-industrial residues into renewable chemicals and bioenergy.

Two methodologies are distinguished for providing kinetic outcomes: single-step and multistep kinetic analysis (DA SILVA et al., 2020; LOPES; TANNOUS, 2020; VYAZOVKIN et al., 2020). The pyrolysis of lignocellulosic biomass involves multiple partial overlapping reactions, leading to a complex scheme with an overall kinetic expression that may not be represented entirely by a single-step kinetic analysis (DA SILVA et al., 2020). Under a multicomponent kinetic perspective, pyrolysis is typically interpreted based on hypothetical reactional kinetic schemes, where the overall behavior is considered a combination of multiple independent parallel reactions (CHEN et al., 2022b; DA SILVA et al., 2020). Recent studies

highlight the importance of comprehending the kinetics and characterization of volatile products of lignocellulosic residues to achieve a thorough understanding of the pyrolysis process (NISAR et al., 2022; REHMAN et al., 2023). These studies also showcase how this research aligns with contemporary efforts to enhance the value of lignocellulosic residues through pyrolysis, which can be applied as a circular economy solution for cashew nutshell residues.

The current state of knowledge regarding the valorization of cashew nutshell residues through the pyrolysis process is summarized below. Previous research by Ahmadou et al. (AHMADOU et al., 2019) explored the influence of pyrolysis temperature on biochar production and adsorption capacity. Another study aimed to investigate the pyrolysis of cashew nutshells using a muffle furnace under several distinct operating conditions to understand and control the resulting product characteristics (NAM et al., 2020). Additional research has examined microwave-assisted pyrolysis and the characteristics of the resulting products (AMALIYAH; EKA PUTRA, 2021). Kinetic and thermodynamic properties were analyzed in a study on the copyrolysis of low ash content biomass (coconut shell and cashew nutshell) with high ash content biomass (rice husk) (KAZAWADI; NTALIKWA; KOMBE, 2022). Finally, the products resulting from the slow pyrolysis of three different cashew waste samples in a lab-scale tubular reactor were thoroughly characterized, encompassing the analysis of bio-oil and biochar properties (KAUR et al., 2023). However, to the authors' knowledge, no studies have been reported regarding the valorization of cashew nutshell residues through pyrolysis, focusing on the kinetic triplet, thermodynamic parameters under a multicomponent approach, and the characterization of volatile products.

The relevance of this literature gap is underscored by the potential of cashew nutshell residues as abundant and readily available feedstock to produce bioenergy and renewable chemicals within the framework of the circular economy. This study aids in addressing this gap in the literature by offering new insights into the valorization of cashew nutshell residues through pyrolysis. In this context, this study’s contribution to the current state of knowledge is its investigation of the pyrolysis characteristics of cashew nutshell residues, with a focus on analyzing the kinetic triplet, thermodynamic parameters, and characterization of volatile products using TGA and Py–GC/MS techniques. Another contribution of this study to the current state of knowledge lies in the assessment of kinetic triplet and thermodynamic parameters for cashew nutshell residue pyrolysis, employing a multicomponent methodology. This involved determining the devolatilization rates of individual biomass pseudocomponents by deconvolution with the

Asym2Sig fitting function. The activation energy was determined from the classical isoconversional methods of Friedman, Flynn−Wall−Ozawa, Kissinger−Akahira−Sunose, and Starink; the frequency factor was calculated from the compensation effect method; and the proper form of the reaction model was identified by integral master plots. A complementary step of this study was to obtain the physicochemical characteristics of raw (RCNS) and pressed (PCNS) cashew nutshell residues. Analytical Py–GC/MS analysis was employed to investigate the effect of pyrolysis temperature on the distribution of volatile products under fast pyrolysis conditions. This analysis is crucial for adjusting operational parameters and devising more efficient strategies to valorize cashew nutshell residues. Additionally, the thermodynamic parameters, namely, variation in enthalpy (ΔH), variation in Gibb free energy (ΔG), and variation in entropy (ΔS), were determined based on the kinetic results.

3.3 Materials and methods

Figure 3.1 depicts an integrated flowsheet illustrating the methodology employed to investigate the valorization of cashew nutshell residues into bioenergy and biobased chemicals through pyrolysis.

Figure 3.1 − Integrated flowsheet for the methodology employed for investigating the valorization of cashew nutshell residues to bioenergy and bio-based chemicals through pyrolysis.

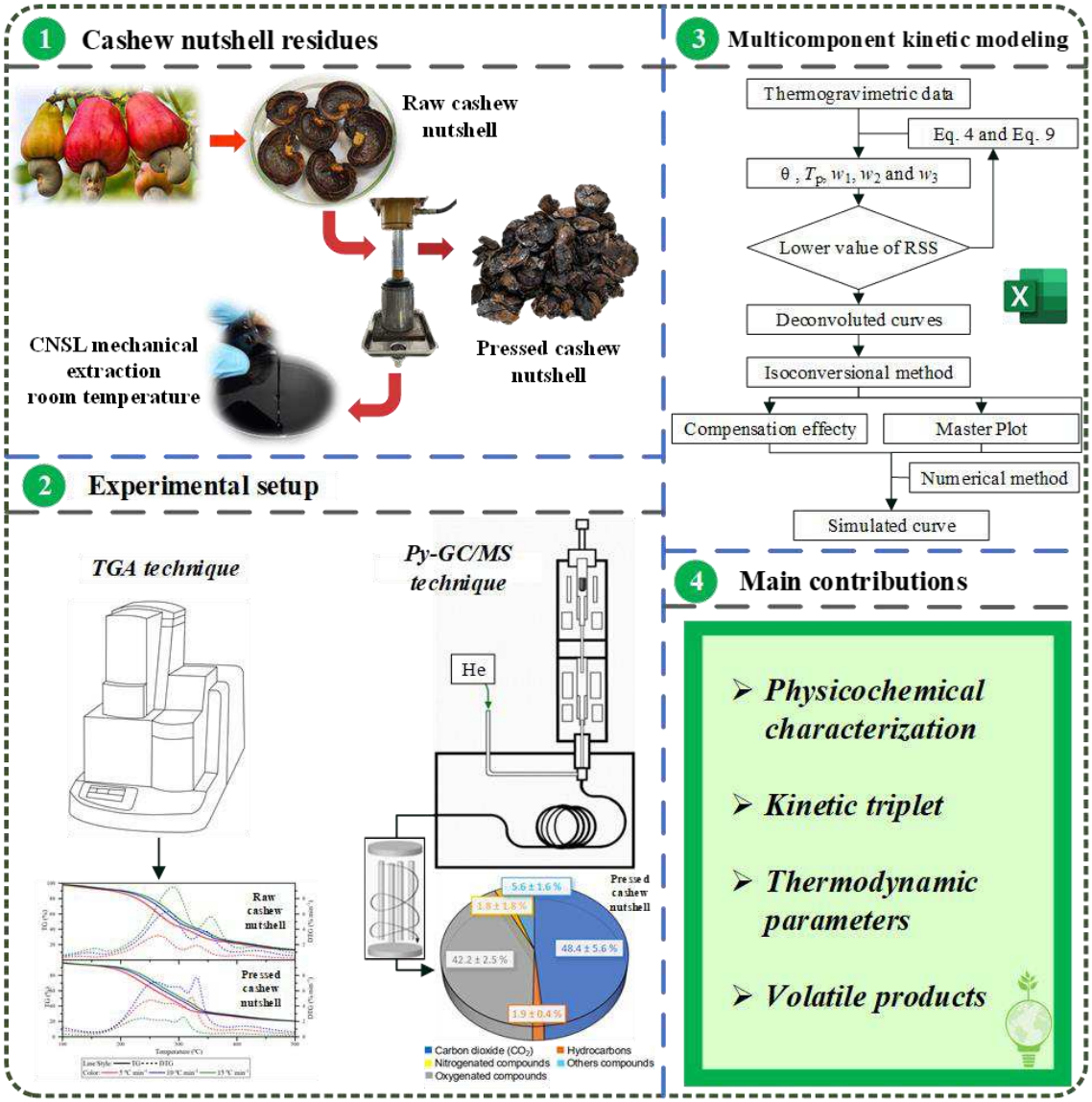

Source: Elaborated by the author

3.3.1 Preparation of raw materials

The cashew nutshells were supplied by a small factory in the city of Pacajus (state of Ceará, Brazil) and were initially obtained from manual (longitudinal) cutting with a blade. Then, the raw shells were pressed in a hydraulic press model MA/098/50A/I (Marconi, Piracicaba, Brazil) under the following conditions: 15 MPa for 3 min at 40 °C (OIRAM FILHO et al., 2019). Approximately 70% of the cashew nutshell liquid (CNSL) was extracted. The raw (RCNS) and pressed (PCNS) cashew nutshells were dried in an oven at 105 °C for 24 h (resulting in moisture contents of 28 wt.% and 13 wt.%, respectively) and mechanically ground using a cutting mill model 55743 (Fritsch, EUA) to achieve powdered samples. Then, each residue was screened through a standard 50-mesh sieve to provide a homogenized material with reduced particle size (< 300 μm). The resulting materials were sealed in plastic airtight zip bags until further characterization and experiments.

3.3.2 Characterization procedures

An adaptation from the ASTM E−1131 standard method was followed to obtain the mass percentages of inherent moisture (IM), volatile matter (VM), fixed carbon (FC), and inorganic matter (ASH), and the procedure was conducted in a thermogravimetric analyzer model TGA-Q50 (TA Instruments, New Castle, United States) (PACIONI et al., 2016). The mass percentage of fixed carbon was indirectly obtained by subtraction based on the known mass percentages of the other three components, as given in Eq. (3.1) (GUPTA; GUPTA; MONDAL, 2020).

$$FC\left(wt.\%\right) = 100\ wt.\% - IM\left(wt.\%\right) - VM\left(wt.\%\right) - ASH\left(wt.\%\right) \tag{3.1}$$

An elemental analyzer model CE 1108 (Carlo Erba Instruments, Wigan, England) was employed to determine carbon (C), hydrogen (H), nitrogen (N) and sulfur (S) mass percentages, following the standard protocol ASTM D3176−15 (ASTM, 2015). The oxygen (O) content was determined from a mass balance, *i.e.*, by subtracting the sum of the mass percentages of C, H, N, S, and ash from the total mass (100 wt.%), on a dry basis (WU et al., 2022).

The well-established correlation stipulated by Channiwala and Parikh (CHANNIWALA; PARIKH, 2002) was employed to calculate the higher heating value (HHV), as shown below:

$$HHV\left(\text{MJ kg}^{-1}\right) = 0.3491 \cdot C\left(wt.\%\right) + 1.1783 \cdot H\left(wt.\%\right) + 0.1005 \cdot S\left(wt.\%\right) - 0.1034 \cdot O\left(wt.\%\right) - 0.0151 \cdot N\left(wt.\%\right) - 0.0211 \cdot ASH\left(wt.\%\right) \quad (3.2)$$

Leveraging the results of HHV and ultimate analysis on a dry basis, Eq. (3.2) (KAN; STREZOV; EVANS, 2016) was used to calculate the lower heating value (LHV) of each cashew nutshell residue.

$$LHV\left(MJ \cdot kg^{-1}\right) = HHV\left(MJ \cdot kg^{-1}\right) - 0.2183 \cdot H\left(\%\right) \quad (3.3)$$

The bulk density was determined as the ratio of the sample mass introduced into a known volume of a closely packed sample, based on the standard protocol ASTM E873-82 (ASTM, 2019).

Each physicochemical characterization analysis was conducted in triplicate, so this study displays the average results.

3.3.3 Thermogravimetric analysis

The pyrolysis behavior of each sample under nonisothermal conditions (5, 10, 15, and 20 °C min^{-1}) was acquired using a thermogravimetric analyzer model STA 6000 (PerkinElmer, Waltham, United States). Only high-purity nitrogen under a constant flow rate of 50 mL min^{-1} was applied during the tests. Approximately 10 mg of each prepared solid sample was placed inside an open platinum crucible and pyrolyzed from room temperature up to 900 °C. Given the reduced size (< 350 μm) and small mass (10 mg) of solid particles, it was assumed that the thermogravimetric study was conducted with negligible heat and mass transfer restrictions (DAMARTZIS et al., 2011). Two replicates of the thermogravimetric experiments were also performed to guarantee repeatability estimates. The average TGA results were applied to calculate the pyrolysis kinetic triplet, *i.e.*, the activation energy, the pre-exponential factor, and the reaction model.

3.3.4 Pyrolysis kinetic modeling

Previous kinetic studies on biomass pyrolysis have shown multicomponent kinetic modeling to be more suitable and consistent in providing kinetic triplets with the ability to reconstruct and predict experimental curves (MUMBACH et al., 2022b; ROMERO MILLÁN; SIERRA VARGAS; NZIHOU, 2017). Nevertheless, this approach is aligned with recent guidelines for analyzing multistep kinetics published by the ICTAC Kinetics Committee (VYAZOVKIN et al., 2020).

The kinetic reaction scheme chosen for the modeling of raw cashew nutshell pyrolysis was a simplified one (given by Eq. (R-1)) contemplating a summative reaction of five independent devolatilization reactions attributed to the extractives, hemicellulose, cellulose, primary lignin, and secondary lignin (DA SILVA et al., 2020; MUMBACH et al., 2022c).

$$\text{Raw cashew nutshell} \begin{cases} \text{Extractives} \xrightarrow{k_e} \text{Volatiles} + \text{Char} \\ \text{Hemicellulose} \xrightarrow{k_h} \text{Volatiles} + \text{Char} \\ \text{Cellulose} \xrightarrow{k_c} \text{Volatiles} + \text{Char} \\ \text{Primary lignin} \xrightarrow{k_{pl}} \text{Volatiles} + \text{Char} \\ \text{Secondary lignin} \xrightarrow{k_{sp}} \text{Volatiles} + \text{Char} \end{cases} \quad \text{(R-1)}$$

Regarding the pyrolysis of the pressed cashew nutshell, the kinetic reaction scheme (given by Eq. (R-2)) is a summative reaction of four independent devolatilization reactions attributed to primary hemicellulose, secondary hemicellulose, cellulose, and lignin.

$$\text{Pressed cashew nutshell} \begin{cases} \text{Primary hemicellulose} \xrightarrow{k_{ph}} \text{Volatiles} + \text{Char} \\ \text{Secondary hemicellulose} \xrightarrow{k_{sh}} \text{Volatiles} + \text{Char} \\ \text{Cellulose} \xrightarrow{k_c} \text{Volatiles} + \text{Char} \\ \text{Lignin} \xrightarrow{k_l} \text{Volatiles} + \text{Char} \end{cases} \quad \text{(R-2)}$$

3.3.5 Pyrolysis deconvolution

After adopting the kinetic reaction scheme, the pyrolysis profiles of each sample were deconvoluted into several independent parallel reactions, which were further assessed for their kinetic triplet and thermodynamic parameters. A similar approach has been successfully followed in preceding research with analogous objectives (LI et al., 2022; MUMBACH et al., 2022a; PINZI et al., 2020).

Most noticeable is the ability of the asymmetric double sigmoidal (Asym2Sig) fitting function to address the asymmetric nature of the pyrolysis behavior of lignocellulosic biomass by deconvoluting three (or more) independent parallel reactions (DA SILVA et al., 2020; MUMBACH et al., 2022c). In this sense, the Asym2Sig function with the mathematical expression presented by Eq. (3.4) was chosen to fit the current data (DA SILVA et al., 2020).

$$\frac{d\alpha}{dT} = \frac{\theta}{1+\exp\left(\dfrac{-\left(T-T_p+w_1/2\right)}{w_2}\right)}\left[1-\frac{1}{1+\exp\left(\dfrac{-\left(T-T_p+w_1/2\right)}{w_3}\right)}\right] \tag{3.4}$$

Each pseudo-component was characterized by four adjustable parameters: the maximum amplitude of the curve (θ), the curve width (w_1), and two shape parameters (w_2 and w_3) (MUMBACH et al., 2022a). The following restrictions were assumed: $w_1 > 0$; $w_2 > 0$; and $w_3 > 0$. The four adjustable parameters were determined so that the objective function, defined as the residual sum of squares (*RSS*), converged to a minimum value. In Eq. (3.5), M refers to the total points of experimental data used to fit the Asym2Sig function, $(d\alpha/dT)_{exp}$ refers to the experimental conversion rates, and $(d\alpha/dT)_{dec}$ refers to the conversion rates deconvoluted by the Asym2Sig function.

$$RSS = \sum^{M}\left[\left(\frac{d\alpha}{dT}\right)_{exp} - \left(\frac{d\alpha}{dT}\right)_{dec}\right]^2 \tag{3.5}$$

3.3.6 Methods for extracting the kinetic triplet from the TGA data

The fundamentals of kinetic analysis of biomass pyrolysis presume a heterogeneous reaction in which the solid particle is thermally converted into volatiles and biochar under a deficient atmosphere of oxygen. A temperature-dependent reaction constant [*k(T)*] and a conversion-dependent reaction model [*f(α)*] specify the expression of the conversion rate as given by Eq. (3.6). Here, α refers to the conversion extent, t refers to the reaction time, *k(T)* refers to the reaction constant, and *f(α)* represents the conversion-dependent reaction model.

$$\frac{d\alpha}{dt} = k(T) f(\alpha) \tag{3.6}$$

Assuming the temperature-dependent reaction constant (*k(T)*) based on the Arrhenius law, Eq. (6) becomes Eq. (3.7), where T refers to the reaction temperature (K), R refers to the gas constant (8.3145×10^{-3} kJ mol^{-1} K^{-1}) and the kinetic parameters A and E_a refer to the pre-exponential factor (min^{-1}) and the activation energy (kJ mol^{-1}), respectively.

$$\frac{d\alpha}{dt} = Ae^{-E_a/RT} f(\alpha) \tag{3.7}$$

Considering a nonisothermal condition with a constant heating rate ($\beta = dT/dt$), Eq. (4.7) is rearranged as Eq. (3.8) (YAO et al., 2020c).

$$\frac{d\alpha}{dT} = \beta\frac{d\alpha}{dT} = \frac{A}{\beta}e^{-E_a/RT} f(\alpha) \tag{3.8}$$

Assuming that the pyrolysis of raw and pressed cashew nutshell residue is a process with five and four independent devolatilization reactions, respectively, its overall conversion rate is the combination of the five and four partial conversion rates, considering the mass fraction of each pseudo-component, i, as presented in Eq. (3.9) (where "*c*" refers to the mass fraction of each pseudo-component i).

$$\left(\frac{d\alpha}{dt}\right)_{\text{Cashew nutshell residues}} \equiv \sum_{i=1}^{N} c_i \left(\frac{d\alpha}{dt}\right)_i = \sum_{i=1}^{N} c_i A_i e^{Ea_i/RT} f(\alpha)_i \tag{3.9}$$

Additionally, Eq. (3.10) represents the integral form of Eq. (3.8). Although there is no analytical solution for the temperature integral [*p(x)*], this term can be solved using mathematical approximations.

$$g(\alpha)_i = \int_0^1 \frac{d\alpha}{f(\alpha)_i} = \frac{A_i}{\beta}\int_{T_0}^{T} e^{-E_{ai}/RT}dT \equiv \frac{A_i}{\beta} I(E_{ai},T) = \frac{A_i E_{ai}}{R\beta} p(x) \tag{3.10}$$

The dependence of activation energy on the degree of conversion from the DTG data can be determined by several available isoconversional (model-free) methods (VYAZOVKIN et al., 2011; YAO et al., 2020a). These methods are based on different mathematical approximations or direct differentiation made to simplify the complexity of the resolution of Eq. (3.10).

3.3.6.1 Activation energy from model-free methods

In the scope of this study, four isoconversional methods, namely, Friedman (FR), Flynn-Wall-Ozawa (FWO), Kissinger-Akahira-Sunose (KAS), and Starink (STK), were employed to calculate the activation energy as a function of the extent of conversion. The literature extensively documents the derivation of these isoconversional methods (CHEN et al., 2023; STARINK, 2003; VYAZOVKIN et al., 2011), utilized in their linearized forms (Eqs. (3.11) to (3.14)) to obtain activation energy values. Additionally, two different calculation algorithms (integral and differential) were employed to assess the consistency of activation energy values, applying various methods (AHMAD et al., 2021; MUMBACH et al., 2022a).

FR: $$\ln\left(\frac{d\alpha}{dt}\right) = \ln\left[\beta\left(\frac{d\alpha}{dT}\right)\right] = \ln\left[Af(\alpha)\right] - \frac{E_a}{RT} \tag{3.11}$$

FWO: $$\log\beta = \log\left(\frac{AE_a}{Rg(\alpha)}\right) - 2.315 - 0.4567\frac{E_a}{RT} \tag{3.12}$$

KAS: $$\ln\left(\frac{\beta}{T^2}\right) = \ln\left(\frac{AR}{E_a}\right) + 0.6075 - \frac{E_a}{RT} \tag{3.13}$$

$$\text{STK: } \ln\left(\frac{\beta}{T^{1.92}}\right) = \text{Constant} - 1.0008\frac{E_a}{RT} \tag{3.14}$$

The left-hand side of Eqs. (3.11) to Eq. (3.14) is plotted against *1/T* for each extent of conversion, providing a slope that involves the apparent activation energy (ALVES et al., 2023; WU et al., 2022). In this work, experimental conversions of $0.05 < \alpha < 0.95$ were chosen to derive the E_a values for the four isoconversional methods.

As described, assuming a reaction model for isoconversional methods is unnecessary, so these modes are not used to determine the reaction model and the frequency factor (LÓPEZ-FONSECA et al., 2005). Accordingly, sets of reaction models, both in the differential form ($f(\alpha)$) and integral form ($g(\alpha)$), are conventionally derived from different reaction mechanisms, such as power-law (P-type), Avrami-Erofeev (A-type), reaction order (F-type), geometrical contraction (R-type), and diffusion (D-type) (DA SILVA et al., 2020; MUMBACH et al., 2022a). **Table A1** of the Appendix A contains the seventeen reaction models used to determine the pre-exponential factor and the reaction model (KHAWAM; FLANAGAN, 2006).

3.3.6.2 Reaction model from master plots

The methodology applied for elucidating the most likely reaction model was integral master plots, which use the graphical comparison between experimental and theoretical master plot curves (this latter considers seventeen classical reaction models, presented in **Table A1** of Appendix A). First, the experimental master plot curves represent the normalized form of the experimental kinetic curves at the reference extent of conversion $\alpha = 0.5$. According to Eq. (3.15), if the experimental master plot curve [*p(x)/p(x0.5) versus* α] coincides with one of the seventeen theoretical master plot curves [*g(α)/g(0.5) versus* α], the most plausible reaction model is defined.

$$\frac{g(\alpha)}{g(0.5)} = \frac{p(x)}{p(x_{0.5})} \tag{3.15}$$

Here, $g(0.5)$ refers to the integral form of the reaction model at $\alpha = 0.5$, and $p(x_{0.5})$ refers to the approximate function (with $x=E_a/RT_{0.5}$).

3.3.6.3 Pre-exponential factor from kinetic compensation effect

The kinetic compensation effect (KCE) states a characteristic pattern – a linear relationship among Arrhenius parameters (activation energy and pre-exponential factor) – in thermally induced solid-state reactions, such as the pyrolysis of lignocellulosic biomass. The KCE method, as given by Eq. (3.16) (GOGOI et al., 2018; YAO et al., 2020b), was applied by plotting the values of E_a against $\ln A$ concerning the distinct reaction models, thus obtaining the coefficients a and b (from the slope and y-intercept of the plot, respectively).

$$\ln(A)_i = a_i.E_{ai} + b \tag{3.16}$$

Here, a and b refer to the compensation parameters, and the subscript i refers to the assumed and tested reaction model $g(\alpha)$, which is able to characterize the pyrolysis process (listed in **Table A1** of Appendix A).

3.3.6.4 Statistics-based verification criteria

Statistical-based verification criteria are necessary to accept the acquired multiple kinetic triplets. To validate the summative kinetic expressions and assess the applicability of the estimated kinetic triplets for predicting pyrolysis behavior, an additional heating rate of 20 °C min^{-1} was selected, supplementing the heating rates employed in the kinetic computations. This validation approach aligns with the guidelines published by the Kinetics Committee of the International Confederation for Thermal Analysis and Calorimetry (ICTAC) regarding the conduction of kinetic calculations using thermal analysis data (VYAZOVKIN et al., 2011). Three statistical test correlations were used in this work to confirm the agreement between the simulated and experimental pyrolysis progress profiles, namely, the coefficient of determination (R^2), the quality of agreement (*Fit*), and the residual sum of squares (*RSS*) (MUMBACH et al., 2022a). These three statistical test correlations are given by Eq. (3.17), Eq. (3.18), and Eq. (3.19), where N refers to the total number of experimental determinations used during simulations, and $(d\alpha/dt)_{exp}$, $[(d\alpha/dt)_{exp}]_{max}$, $(d\alpha/dt)_{average}$, and $(d\alpha/dt)_{sim}$ are, sequentially: the conversion rates (measured experimentally), the maximum value of the conversion rates (measured experimentally), the average value of

the conversion rates (measured experimentally), and the conversion rates (calculated numerically from the Runge–Kutta 4th-order method).

$$R^2 = 1 - \frac{\sum\left[\left(\frac{d\alpha}{dt}\right)_{\exp} - \left(\frac{d\alpha}{dt}\right)_{\mathrm{sim}}\right]^2}{\sum\left[\left(\frac{d\alpha}{dt}\right)_{\exp} - \left(\frac{d\alpha}{dt}\right)_{average}\right]^2} \tag{3.17}$$

$$Fit(\%) = \left(1 - \frac{\sqrt{\sum\left[\left(\frac{d\alpha}{dt}\right)_{\exp} - \left(\frac{d\alpha}{dt}\right)_{\mathrm{sim}}\right]^2 \Big/ N}}{\left[\left(\frac{d\alpha}{dt}\right)_{\exp}\right]_{\max}}\right) \cdot 100 \tag{3.18}$$

$$RSS = \sum\left[\left(\frac{d\alpha}{dt}\right)_{\exp} - \left(\frac{d\alpha}{dt}\right)_{\mathrm{sim}}\right]^2 \tag{3.19}$$

3.3.7 Pyrolysis−gas chromatography/mass spectrometry (Py−GC/MS) procedure

Analytical fast pyrolysis tests were performed on each sample using a microfurnace pyrolyzer model Rx-3050TR (Frontier Laboratories Ltd., Fukushima, Japan) coupled to gas chromatography/mass spectrometry analysis equipment model QP2020 (Shimadzu, Tokyo, Japan). The CG/MS system was connected to the microfurnace pyrolyzer by a transfer line, heated and maintained at 300 °C to reduce the possibility of premature condensation of the light volatile species. Approximately 150 μg of the sample was placed in an inert stainless-steel cup and then analytically pyrolyzed at the setpoint temperatures of 450, 550, and 650 °C at a ramp rate of 1000 °C min^{-1} with a final dwell time of 18 s in the heated zone. The separation of volatile products occurred on a fused-silica capillary column SH-Rtx-5 (Shimadzu, Tokyo, Japan) of 60 m in length and 0.25 mm in inner diameter with a film thickness of 0.25 μm. The column contained 5% diphenyl dimethylpolysiloxane as the stationary phase. The process started with the gas chromatograph oven at 45 °C (maintained for 5 min), followed by continuous heating up to 280 °C at 5 °C min^{-1}, and remaining unchanged for 10 min. The operating parameters for GC/MS analysis were as follows: carrier gas of high-purity helium (at 1 mL min^{-1}); injector temperature of 250 °C; ionization energy

of 70 eV; ion source temperature of 250 °C; and interface temperature of 290 °C. The GC injector was operated in split mode at a split ratio of 1:50, and the mass spectrometer was operated in full-scan acquisition mode with mass-to-charge (m z^{-1}) ratios from 40 to 400. The experimental conditions and operating parameters used for the Py−GC/MS analysis were chosen based on previous studies by our research group (MUMBACH et al., 2022a). Volatile species were semi-quantitatively quantified using chromatographic peak areas, focusing on organic compounds with spectral similarity of 90% or higher. Volatile species were prospectively identified through mass spectral detection and compared with the NIST08 Mass Spectral Library. Analytical pyrolysis tests were repeated at least two times to ensure repeatability, and average values with corresponding standard deviations were calculated.

3.3.8 Equations for determining the thermodynamic parameters

The thermodynamic parameters contribute to establishing the feasibility and energy requirements of the pyrolysis process (GUPTA; GUPTA; MONDAL, 2020; MUMBACH et al., 2022a), providing important information for the design and optimization of equipment for this purpose. In this work, the TGA data, along with the kinetic outcomes, were applied to calculate the thermodynamic parameters, *i.e.*, change in enthalpy (ΔH), change in Gibb's free energy (ΔG), and change in entropy (ΔS). The related equations for estimating the thermodynamic parameters are shown in Eqs. (3.20) to (3.22) (CHEN et al., 2023; GUPTA; GUPTA; MONDAL, 2020).

$$\Delta H = E_a - RT \tag{3.20}$$

$$\Delta G = E_a + RT_m \ln\left(\frac{k_B T_m}{hA}\right) \tag{3.21}$$

$$\Delta S = \frac{\Delta H - \Delta G}{T_m} \tag{3.22}$$

In the above equations, T_m is the maximum temperature peak obtained through the differential thermogravimetric curve (DTG), k_B is the Boltzmann constant (1.381×10^{-23} J K^{-1}), and h is the Plank constant (6.626×10^{-34} J s^{-1}).

3.4 Results and discussion

3.4.1 Physicochemical characterization of cashew nutshell residues

The results of the physicochemical characterization of RCNS and PCNS are reported in **Table 3.1**.

Table 3.1 − Physicochemical characterization of the raw and pressed cashew nutshell, including proximate analysis, ultimate analysis, heating values and chemical composition.

	Raw cashew nutshells	Pressed cashew nutshells	Cashew nutshells (MYTHILI et al., 2013)
Proximate analysis (wt.%)			
Moisture	6.78 ± 0.19 [a]	6.34 ± 0.51 [a]	6.93
Volatile matter	86.23 ± 0.80 [b]	84.28 ± 0.84 [b]	70.44
Fixed carbon	11.98 ± 0.79 [b, c]	14.85 ± 0.82 [b, c]	14.73
Ash	1.79 ± 0.01 [b]	0.87 ± 0.02 [b]	7.90
Ultimate analysis (wt.%)			
Carbon	54.65 ± 0.18 [b]	47.26 ± 0.20 [b]	46.02
Hydrogen	7.68 ± 0.06 [b]	5.81 ± 0.05 [b]	5.83
Nitrogen	0.65 ± 0.01 [b]	0.85 ± 0.02 [b]	5.44
Sulfur	0 [b]	0 [b]	-
Oxygen	35.23 ± 0.12 [b, c]	45.21 ± 0.13 [b, c]	34.22
Heating values (MJ kg^{-1})			
HHV	23.72 ± 0.15 [b]	17.01 ± 0.17 [b]	
LHV	22.04 ± 0.14 [b]	15.75 ± 0.16 [b]	
Bulk density (kg m^{-3})	220.50 ± 1.47 [b]	180.20 ± 0.87 [b]	231.60
Chemical composition (wt.%)			
Hemicellulose	58.34 ± 0.25 [d]	70.42 ± 0.45 [d]	
Cellulose	12.78 ± 0.07 [d]	11.78 ± 0.10 [d]	
Lignin	24.30 ± 0.12 [d]	17.80 ± 0.15 [d]	
Extractives	4.58 ± 0.04 [d]	-	

[a] Air dried basis.
[b] Dry basis.
[c] Calculated by difference.
[d] Dry ash-free basis.

Source: Elaborated by the author

Based on the proximate analysis, it is verified that the RCNS has a higher content of volatile matter (86.23 wt.%) and ash (1.79 wt.%) compared to the PCNS, with 84.28 wt.% and 0.87 wt.%, respectively. The low ash content present in both residues is interesting for thermochemical processes, since ash contents above 10% suggest the formation of slag, which can lead to fouling problems inside the equipment, as well as a decrease in the efficiency of the conversion process (SINGH et al., 2021; CHEN et al., 2023). PCNS contains a considerable amount of fixed carbon, comparable to the results found in the literature (MYTHILI et al., 2013). García et al. (GARCÍA et al., 2014a) performed the proximate analysis of several commercially applied lignocellulosic materials and found the following results: volatile matter ranging from 66.0 to 85.0 wt.%; fixed carbon ranging from 11.2 to 30.5 wt.%; and ash content ranging from 0.8 to 17.0 wt.%. Thus, the proximate analysis of both residues is in accordance with that obtained in lignocellulosic materials exploited as solid fuels, suggesting the feasibility of these lignocellulosic residues as bioenergy feedstocks.

From the ultimate analysis results, it is observed that the percentages of carbon, hydrogen, nitrogen, and oxygen for RCNS and PCNS were 54.65 wt.% and 47.26 wt.%, 7.68 wt.% and 5.81 wt.%, 0.65 wt.% and 0.85 wt.%, and 35.23 wt.% and 45.21 wt.%, respectively. The values for PCNS are close to the range reported in the literature for cashew nutshell waste (carbon content of 46.02 wt.%, hydrogen content of 5.44 wt.%, and oxygen content of 34.22 wt.%) (MYTHILI et al., 2013). The ultimate analysis of both residues was consistent with that obtained in lignocellulosic materials commercially employed as solid fuels (38.9−48.2 wt% for carbon, 45.2−54.1 wt% for oxygen, 4.8−6.4 wt% for hydrogen, 0.1−1.8 wt% for nitrogen, and 0.1−2.0 wt% for sulfur) (GARCÍA et al., 2014b), indicating once again their suitability as bioenergy feedstocks. Nevertheless, low contents of nitrogen and negligible contents of sulfur suggest that both residues have the potential to produce clean bioenergy, resulting in low levels of sulfur and nitrogen oxides present in gaseous emissions (from their thermochemical conversion), without contributing to acid rain formation and the destruction of the ozone layer.

According to the calculated values of HHV and LHV for RCNS (23.72 MJ kg^{-1} and 22.04 MJ kg^{-1}, respectively) and PCNS (17.01 MJ $kg^{-1}$and 15.75 MJ kg^{-1}, respectively), it

is inferred that both residues have potential as a source of bioenergy: the heating values are close to those from the literature for biomasses such as corn brakes (16.72 MJ kg^{-1} and 15.10 MJ kg^{-1}) (JANKOVI; STOJILJKOVI; JOVANOVI, 2018), hazelnut shells (18.20 MJ kg^{-1} and 16.21 MJ kg^{-1}) (JANKOVI; STOJILJKOVI; JOVANOVI, 2018), and apricot kernel shells (20.26 MJ kg^{-1} and 18.72 MJ kg^{-1}) (MANIĆ et al., 2020).

The raw and pressed cashew nutshell residues presented bulk densities of 220.5 kg m^{-3} and 180.2 kg m^{-3}, respectively. The bulk density of RCNS is close to the values found for lignocellulosic materials suggested as bioenergy feedstocks, such as sugarcane bagasse (119.1 kg m^{-3}) (KUMAR; UPADHYAY; MISHRA, 2019), wheat straw (200.0 kg m^{-3}) (KUMAR; UPADHYAY; MISHRA, 2019), and rice straw (208.3 kg m^{-3}) (KUMAR; UPADHYAY; MISHRA, 2019). Additionally, the apparent density of the PCNS is close to the density of the banana tree trunk (161.29 kg m^{-3}) (KUMAR; UPADHYAY; MISHRA, 2019) and *Pinus* wood (186.04 kg m^{-3}) (LENIS; OSORIO; PÉREZ, 2013).

The chemical composition of biomass is an important factor in its yield and characteristics (COLLARD; BLIN, 2014). As displayed in **Table 3.1**, the lignocellulosic composition analysis revealed that RCNS comprises 4.58 wt.% extractives, 58.34 wt.% hemicellulose, 12.78 wt.% cellulose, and 24.30 wt.% lignin on a dry and ash-free basis. Regarding PCNS, the results reported were 70.42 wt.% for hemicellulose, 11.78 wt.% for cellulose, and 17.80 wt.% for lignin on a dry and ash-free basis.

Finally, the percentages of extractives, hemicellulose, cellulose, and lignin align with literature values for lignocellulosic biomass. For example, the extractive content obtained for the RCNS matches that of coconut shells, Brazil nutshells, and almond shells (4.00 wt.%, 3.60 wt.%, and 3.50 wt.%, respectively) (BLASI; GALGANO; BRANCA, 2019). The hemicellulose contents (58.34 wt.% and 70.42 wt.%) observed for RCNS and PCNS exceed those reported for lignocellulosic biomass such as rice straw (19.0 wt.%–27.0 wt.%) (BISWAS et al., 2018), plum pits (21.34 wt.%) (FERNANDEZ et al., 2020) and olive pits (18.41 wt.%) (FERNANDEZ et al., 2020). Regarding the cellulose content, the values found in cashew nutshells were lower than those found in rice straw (32.00 wt.%–47.00 wt.%) (BISWAS et al., 2018), hazelnut shells (29.50 wt.%) (TYAGI; ANAND, 2023) and plum pits

(24.46 wt.%) (MANIĆ et al., 2020). Finally, the lignin content is consistent with other shells, such as pistachio shells, almond shells, and peanut shells (19.0 wt.%, 28.0 wt.%, and 28.2 wt.%) (BLASI; GALGANO; BRANCA, 2019). The physicochemical characteristics of cashew nutshell residues make them promise for bioenergy production.

3.4.2 Mass loss characteristics of cashew nutshell residues

Figure 3.2 shows the pyrolysis behavior of raw and pressed cashew nutshells at different heating rates (5, 10, and 15 °C min^{-1}) by presenting the thermogravimetric curves (TG) and the differential thermogravimetric curves (DTG) with varying temperatures.

Figure 3.2 − Results from thermogravimetric analysis (TG/DTG) for raw **(a)** and pressed **(b)** cashew nutshells using heating rates of 5, 10, and 15 °C min^{-1} in the temperature range from 100 to 500 °C.

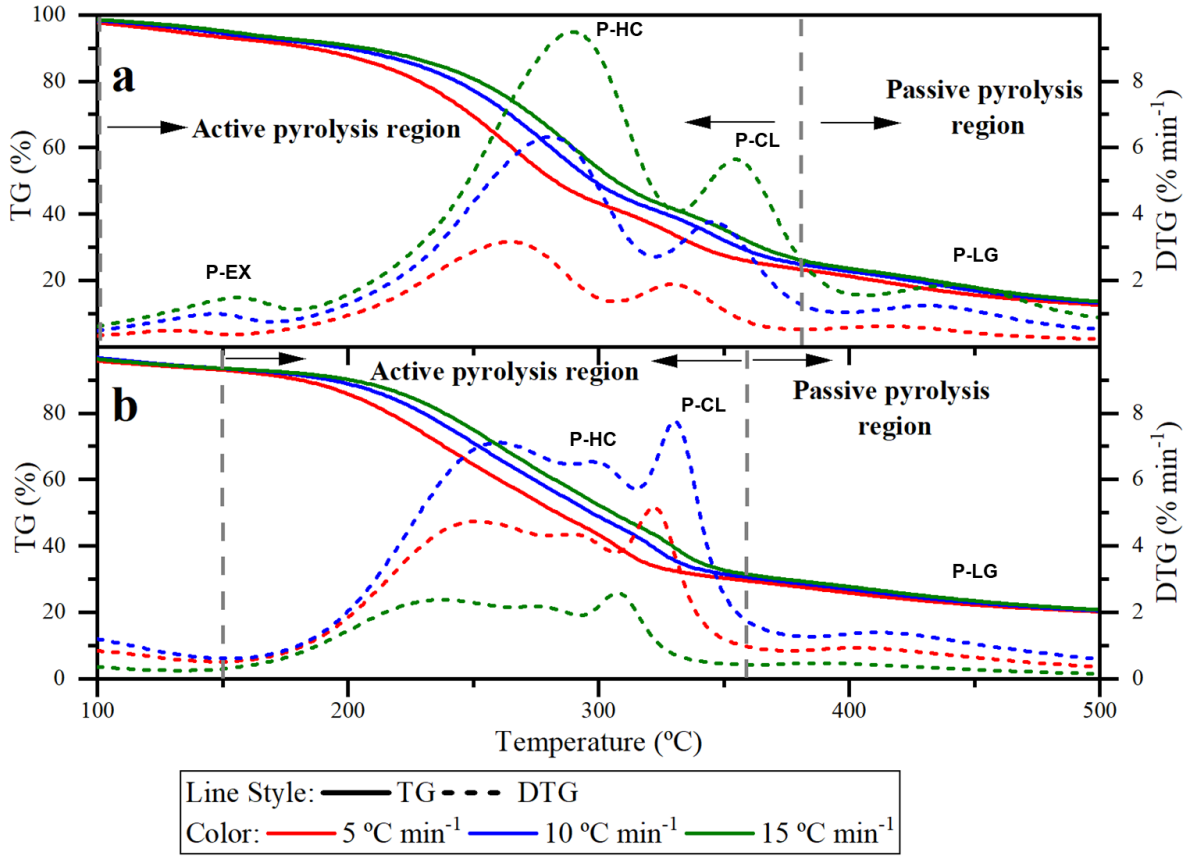

Source: Elaborated by the author

Based on the TG/DTG curves in **Figure 3.2a**, the zone of mass loss below 170 °C is due to the removal of moisture and low-temperature light volatile compounds present in the RCNS, with an average mass loss of 8.25 ± 2.77 wt.%. The temperature interval in which the RCNS experienced the more significant mass loss was 170–380 °C, classified as the active pyrolysis region. In this region, the mass loss of approximately 65.53 wt% corresponds to the concomitant devolatilization of hemicellulose and cellulose, with a minor amount of lignin, all present in RCNS. Examining the DTG curves in the active pyrolysis region highlights the prevalent mass loss peak at a lower temperature range (maximum between 265.0−290.0 °C), which is credited to the devolatilization of hemicellulose. However, the well-defined mass loss peak (330.0–355.0 °C) indicates the thermal decomposition of cellulose. As verified in the literature, the devolatilization of hemicellulose and cellulose usually occurs in the temperature ranges of 200–320 °C and 320–400 °C, respectively (GUPTA; GUPTA; MONDAL, 2022; MUMBACH et al., 2022b). These findings support the observed pyrolysis behavior of RCNS. The passive pyrolysis region, which immediately follows the active region, occurred in the 380–500 °C temperature range. The passive pyrolysis of RCNS was slower and presented a larger mass loss of approximately 9.75 ± 3.39 wt.%, related to lignin decomposition (and finally, biochar formation).

In **Figure 3.2b**, below 150 °C, the mass loss zone is due to moisture evaporation from PCNS, with an average mass loss of 7.50 ± 2.63 wt.%. The second mass loss zone, spanning from 150 °C to 360 °C, accounts for 57.97 wt.% of the mass loss. This zone, known as active pyrolysis, was prevalent for converting volatile matter into condensable vapors and noncondensable gases through overlapping devolatilization of hemicellulose, cellulose, and part of the lignin (primary pyrolysis components). The third mass loss zone, occurring from 360 to 500 °C, leads to a mass loss of 10.99 wt.%. This region, known as passive pyrolysis, was prevalent for losing mass through the slow decomposition of lignin and subsequent biochar formation. The first two peaks appearing in the DTG profiles designate the devolatilization of hemicellulose, *i.e.*, the decomposition of many polysaccharides that occur at lower temperatures (glucose, xylose, galactose, and mannose) than that of the devolatilization of cellulose (KIRTI et al., 2022). Thus, the following projecting peak is related to the devolatilization of cellulose that typically occurs from 315 to 400 °C and presents greater thermal stability than hemicellulose (GUPTA; GUPTA; MONDAL, 2022).

Finally, the following long tail appearing in the DTG profiles designates the devolatilization of lignin at higher temperatures.

It is important to note that lignin usually decomposes in both active and passive pyrolysis regions, which is also observed in the pyrolysis of raw and pressed cashew nutshells: lignin decomposes continuously and slowly over a wide temperature range, from approximately 180-800 °C (GUPTA; GUPTA; MONDAL, 2022; PINZI et al., 2020). The structural differences between the three major biomass components can explain this decomposition order: hemicellulose has an amorphous and random molecular structure, thus presenting lower strength, while cellulose has a crystalline structure (formed by linear and repetitive units of glucose monomers) (YANG et al., 2007), and lignin is a highly complex three-dimensional polymer with multiple chemical functions that present significant differences in thermal stability (COLLARD; BLIN, 2014).

As shown in **Figure 3.2**, the increase in heating rates promoted a shift in the TG/DTG curves to higher temperatures; for example, the most expressive mass loss peak moved from 265 °C (at 5 °C min^{-1}) to 290 °C (at 15 °C min^{-1}) for the RCNS and from 320 °C (at 5 °C min^{-1}) to 330 °C (at 15 °C min^{-1}) for the PCNS. This phenomenon aligns with literature reports (GUPTA; GUPTA; MONDAL, 2022; MÜSELLIM et al., 2018), where a higher heating rate slows down the pyrolysis reaction, delaying its progression toward higher temperature regions. In contrast, a lower heating rate enhances heat transfer to the biomass particles, leading to increased pyrolysis devolatilization time.

3.4.3 Results from deconvolution analysis using Asym2Sig fitting function

Figure 3.3 shows the simultaneous fit of the deconvoluted DTG curves (solid lines) to the experimental DTG curves (open circles), assuming five and four independent devolatilization reactions concerning the DTG curves related to the pyrolysis behavior of the **(a)** raw and **(b)** pressed cashew nutshells, respectively. It was demonstrated that modeling the pyrolysis behavior of raw and pressed cashew nutshells using five and four independent devolatilization reactions, respectively, adequately described the process. This result was evidenced by the coefficients of determination (R^2) estimated at 0.99 or higher. Adjustable parameters of the Asym2Sig function (θ, w_1, w_2, and w_3) for each pseudo-component

deconvoluted from the pyrolysis behavior of raw and pressed cashew nutshells are shown in Appendix A (**Table A2** and **Table A3**).

The pyrolysis of raw cashew nutshells (**Figure 3.3a**) was modeled by deconvolution of five independent parallel reactions. The first deconvoluted reaction occurred over a temperature range of 100 to 190 °C and comprised extractive devolatilization. The second deconvoluted reaction involved pseudo-hemicellulose devolatilization within the temperature range of 100 to 380 °C. The third deconvoluted reaction, attributed to pseudo-cellulose devolatilization, took place from 220 to 470 °C. The fourth and fifth reactions, observed in **Figure 3.3a,** involve the devolatilization of pseudo-lignin and occur over a wide temperature range of 150 to 600 °C. The premise of two pseudo-components related to lignin (P-LG1 and P-LG2) is seen as well-plausive since lignin is a highly complex three-dimensional biopolymer with multiple chemical functions that present significant differences in thermal stability (COLLARD; BLIN, 2014), justifying its complex devolatilization behavior (MUMBACH et al., 2022b). This singular behavior concurs with the findings observed for the pyrolysis of coffee silver skin, with a two-step reaction process involving the devolatilization of pseudo-lignin (PINZI et al., 2020) and the pyrolysis of apricot kernel shell, resulting in the thermal conversion of primary and secondary lignin fragments (MANIĆ et al., 2020).

Figure 3.3 − Plots of the deconvoluted DTG curves (solid lines), using the Asym2Sig fitting function, against the experimental DTG curves (open circles), presuming multiple independent devolatilization reactions, related to the pyrolysis behavior of the **(a)** raw and **(b)** pressed cashew nutshells at a heating rate of 5 °C min^{-1}.

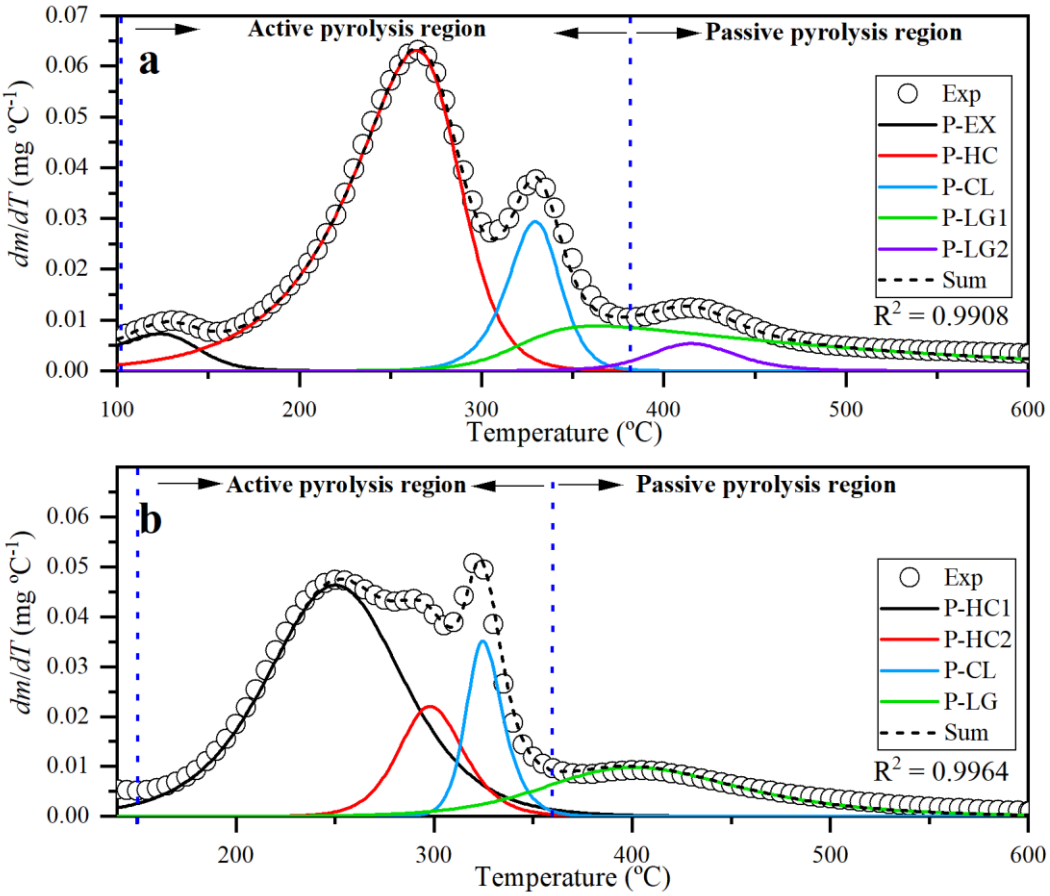

Source: Elaborated by the author

The deconvolution analysis of PCNS pyrolysis (**Figure 3.3b**) revealed four well-defined peaks, referring to four independent devolatilization reactions. The first and second peaks refer to the devolatilization of primary and secondary pseudo-hemicellulose (P-HC1 and P-HC2, respectively) within the temperature range of 140-430 °C. The assumption of two pseudo-components associated with hemicellulose (P-HC1 and P-HC2) is plausible since hemicellulose is a mixture of several polysaccharides (such as glucose, xylose, galactose, and mannose), resulting in a complex devolatilization behavior (MUMBACH et al., 2022b). This characteristic is similar to that observed in the literature for wood pyrolysis, where two well-defined peaks represent hemicellulose devolatilization (VÁRHEGYI, 2007). The third peak

corresponds to the devolatilization of pseudo-cellulose (P-CL) in the range of 250 to 470 °C. The last deconvoluted reaction (fourth peak), referred to as pseudo-lignin (P-LG), occurred over a wide temperature range of 140 to 600 °C. These results are consistent with the deconvoluted mass loss peaks linked to devolatilization reactions of hemicellulose, cellulose, and lignin, as previously published for cocoa shell biomass and coffee silver husk (MUMBACH et al., 2022b; PINZI et al., 2020).

3.4.4 Results for kinetic triplet under a multicomponent approach

3.4.4.1 Estimates of activation energy from isoconversional methods

When the isoconversional methods of FR, FWO, KAS, and STK were applied to the mass loss profiles of raw and pressed cashew nutshells under an atmosphere of nitrogen, they provided the average values of activation energy and coefficient of determination listed in **Table 3.2** and **Table 3.3,** respectively. The four isoconversional methods equally gave high values of R^2 (higher than 0.998), confirming their accuracy in fitting the experimental kinetic data for the pyrolysis of both residues. The resulting activation energy values from the FWO, KAS, and STK integral methods are relatively similar and lower than those found from the differential method of FR, except for the devolatilization of P-EX involved in the pyrolysis of RCNS. One major drawback of the FR differential method is related to the experimental noise found in the numerical differentiation of nonisothermal thermogravimetry data (MA et al., 2015; YAO et al., 2022), thus affecting the activation energy calculation. This aligns with literature findings, where the FR method typically provides a higher E_a than classical integral methods (MISHRA; KUMAR; BHASKAR, 2015; MOINE et al., 2016).

Table 3.2− Mean activation energy (E_a) and coefficient of determination (R^2) for pyrolysis of RCNS applying FR, FWO, KAS, and STK isoconversional methods, assuming five independent parallel reactions.

Isoconversional method	**P-EX**			**P−HC**			**P−CL**			**P−LG1**			**P-LG2**		
	E_a (kJ mol^{-1})	R^2	ε (%)	E_a (kJ mol^{-1})	R^2	ε (%)	E_a (kJ mol^{-1})	R^2	ε (%)	E_a (kJ mol^{-1})	R^2	ε (%)	E_a (kJ mol^{-1})	R^2	ε (%)
FR	63.81	0.9989	21.88	102.32	0.9991	5.05	133.88	0.9991	5.20	249.28	0.9991	7.32	202.20	0.9993	15.78
FWO	88.98	0.9993	8.93	98.13	0.9991	0.75	127.27	0.9991	0.00	226.57	0.9991	2.46	167.25	0.9992	4.24
KAS	86.80	0.9993	6.26	94.36	0.9990	3.12	123.70	0.9990	2.80	226.32	0.9990	2.57	164.27	0.9991	5.94
STK	87.15	0.9993	6.69	94.79	0.9990	2.68	124.21	0.9990	2.40	226.98	0.9990	2.28	164.87	0.9991	5.60

Abbreviations: P−EX: pseudo-extractives; P−HC: pseudo-hemicellulose; P−CL: pseudo-cellulose; P−LG1: primary pseudo-lignin; and P−LG2: secondary pseudo-lignin.

Table 3.3− Mean activation energy (E_a) and coefficient of determination (R^2) for pyrolysis of PSNC applying FR, FWO, KAS, and STK isoconversional methods, assuming four independent parallel reactions.

Isoconversional method	**P−HC1**			**P−HC2**			**−CL**			**P-LG**		
	E_a (kJ mol^{-1})	R^2	ε (%)	E_a (kJ mol^{-1})	R^2	ε (%)	E_a (kJ mol^{-1})	R^2	%)	E_a (kJ mol^{-1})	R^2	
FR	97.48	0.9991	3.99	115.01	0.9991	5.53	126.43	0.9991	5.32	167.42	0.9992	7
FWO	94.82	0.9993	1.15	109.32	0.9991	0.31	120.18	0.9991	0.12	158.92	0.9992	6
KAS	91.12	0.9992	2.79	105.57	0.9990	3.13	116.53	0.9990	2.92	155.84	0.9991	9
STK	91.54	0.9992	2.35	106.03	0.9990	2.71	117.02	0.9990	2.52	156.42	0.9991	2

Abbreviations: P−HC1: primary pseudo-hemicellulose; P−HC2: secondary pseudo-hemicellulose; P−CL: pseudo-cellulose; and P−LG: pseudo-lignin. (Source: Elaborated by the author)

The minimum amount of energy required by the pyrolysis reaction to produce bioenergy products, otherwise known as the activation energy, was determined, with average values ranging from 63.8 to 249.3 kJ mol^{-1} and 91.1 to 167.4 kJ mol^{-1} for the pyrolysis of raw and pressed cashew nutshells, respectively. Within the above, both residues can be considered as feedstocks with significant potential for use in bioenergy/biofuel production, with average E_a values that are smaller or similar to those found for other lignocellulosic biomass suggested as bioenergy feedstocks, such as grapefruit residue (160.7 to 293.8 kJ mol^{-1}) (NISAR et al., 2022), bamboo guadua (163.2 to 221.2 kJ mol^{-1}) (ROMERO MILLÁN; SIERRA VARGAS; NZIHOU, 2017), oil palm shells (194.6 to 249.5 kJ mol^{-1}) (ROMERO MILLÁN; SIERRA VARGAS; NZIHOU, 2017), coconut shells (175.9 to 235.8 kJ mol^{-1}) (ROMERO MILLÁN; SIERRA VARGAS; NZIHOU, 2017), and soybean stalk (124.1 to 136.3 kJ mol^{-1}) (AGNIHOTRI; MONDAL, 2023).

Figure 3.4 illustrates the dependence of activation energy on the extent of conversion for each pseudo-component provided by the FR, FWO, KAS, and STK isoconversional methods related to the pyrolysis of raw **(a)** and pressed **(b)** cashew nutshells. In the pyrolysis of RCNS, the dependence of E_a on the conversion extent is similar for the FWO, KAS, and STK integral methods. Nevertheless, it presents an evident discrepancy for the FR method, particularly for the devolatilization of P-EX and P-LG2. Focusing on the pyrolysis of the PCSN, the dependence of E_a on the conversion extent for the three integral methods almost overlaps with a similar trend. On the other hand, for the FR method, the E_a values similarly vary with the conversion degree compared to integral isoconversional methods, with slightly larger values.

Figure 3.4 − Dependency of the activation energy on the degree of conversion for each pseudo-component according to four isoconversional methods related to the pyrolysis of raw (a) and pressed (b) cashew nutshells.

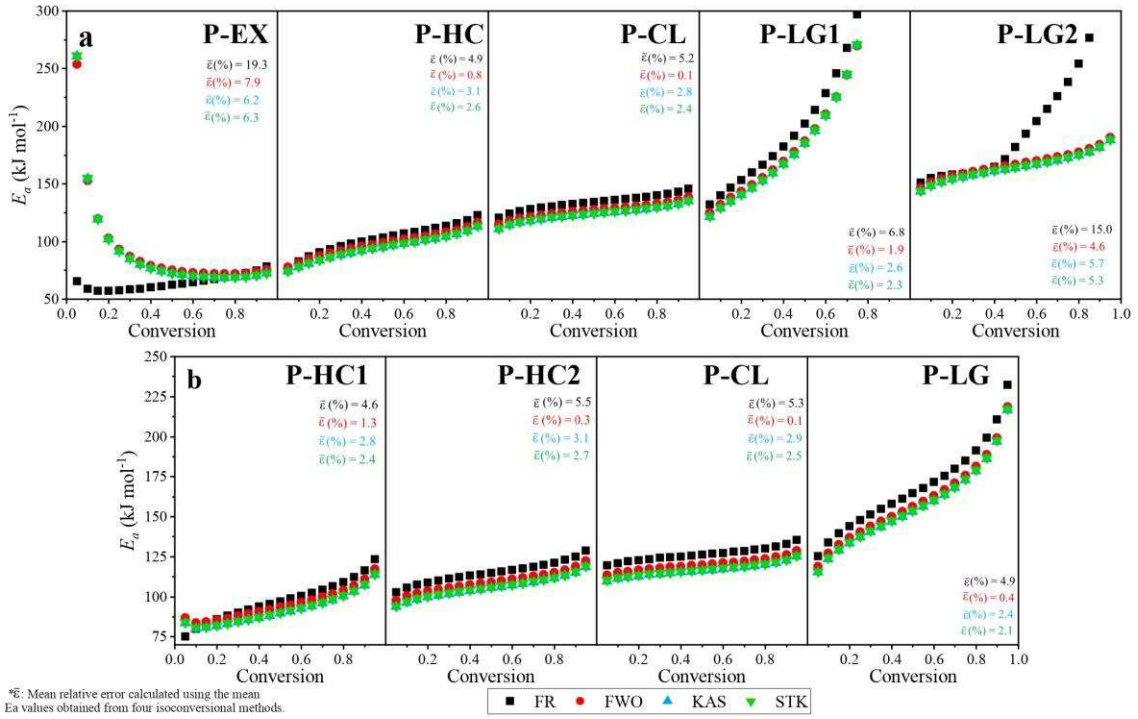

Source: Elaborated by the author

From the four isoconversional methods and considering the pyrolysis of both cashew nutshell residues, the maximum and minimum average E_a values obtained for the devolatilization of pseudo−extractives, pseudo−hemicellulose, pseudo−cellulose, and pseudo−lignin were 63.8 and 89.0 kJ mol^{-1}, 91.1 and 115.0 kJ mol^{-1}, 116.5 and 133.9 kJ mol^{-1}, and 155.8 and 249.3 kJ mol^{-1}, respectively. As previously mentioned, pseudo-lignin has a complex three-dimensional aromatic structure, thus requiring higher amounts of energy to break its long chains. This explanation is why pseudo-lignin presents a higher E_a than the other two lignocellulosic pseudo-components (MUMBACH et al., 2022a; PINZI et al., 2020). Formerly published works (on biomass pyrolysis) showed E_a values ranging from 77.2 to 89.2 kJ mol^{-1} for pseudo−extractives (DA SILVA et al., 2020), from 74.39 to 108.99 kJ mol^{-1} for pseudo−hemicellulose (JANKOVI; STOJILJKOVI; JOVANOVI, 2018; MUMBACH et al., 2022a), from 124.3 to 135.2 kJ mol^{-1} for pseudo−cellulose (JANKOVI; STOJILJKOVI; JOVANOVI, 2018), and from 140.4 to 249.5 kJ mol^{-1} for pseudo−lignin (DA SILVA et al., 2020; ROMERO MILLÁN; SIERRA VARGAS; NZIHOU, 2017). Thus, the average E_a values for each independent

parallel reaction acquired in this study are close to the literature reports. Also, the average activation energy values for the pyrolysis of sugarcane bagasse, a well-known bioenergy feedstock, ranged from 71.1 to 127.4 kJ mol^{-1} for hemicellulose, 121.2 to 166.3 kJ mol^{-1} for cellulose, and 126.5 to 232.8 kJ mol^{-1} for lignin (NISAR et al., 2021). These average activation energy values are close to those obtained in this study for the pseudo-components involved in the pyrolysis of cashew nutshell residues.

According to several studies, the STK method is recognized for its accuracy and efficiency in estimating the activation energy of pyrolysis. Therefore, the average E_a values calculated from this method were used to estimate the pre-exponential factors and thermodynamic parameters and applied to the summative kinetic expression (DA SILVA et al., 2020; STARINK, 2003).

3.4.4.2 Results from the compensation effect method for the pre-exponential factor

Figure 3.5 illustrates the linear correlation between the pre-exponential factor in its logarithmic form (ln A) and the activation energy (E_a) for raw **(a)** and pressed **(b)** cashew nutshell. It is important to highlight those high values of R^2 (above 0.9492) attest to the validity of estimates of pre-exponential factors from the kinetic compensation effect method for both cashew nutshell residues. Regarding the pyrolysis of RCNS, the estimates of pre-exponential factors of the pseudo-components were 2.78×10^{10} min^{-1} for P-EX, 4.25×10^{8} min^{-1} for P-HC, 8.33×10^{9} min^{-1} for P-CL, 6.89×10^{16} min^{-1} for P-LG1, and 3.89×10^{11} min^{-1} for P-LG2, which are comparable to values found in previous works. The value of A for the devolatilization of pseudo-extractives is between 10^{8} and 10^{11} min^{-1}, as reported for lignocellulosic biomass pyrolysis (examples include cashew nutshell (DA SILVA et al., 2020) and butia seed (MUMBACH et al., 2022c) residues). The pre-exponential factor for the devolatilization of pseudo-hemicellulose and pseudo-cellulose in biomass agrees with the values previously reported (DA SILVA et al., 2020). Regarding the devolatilization of pseudo-lignin, kinetic studies on the pyrolysis of another cashew nutshell (DA SILVA et al., 2020) and pecan nutshell (MUMBACH et al., 2022a)) indicated A values between 10^{10} and 10^{19} min^{-1}, agreeing with the estimates acquired in this study.

Figure 3.5 – Linear correlation between the pre-exponential factor in its logarithmic form and the activation energy (ln *A versus* E_a) for raw (**a**) and pressed (**b**) cashew nutshells.

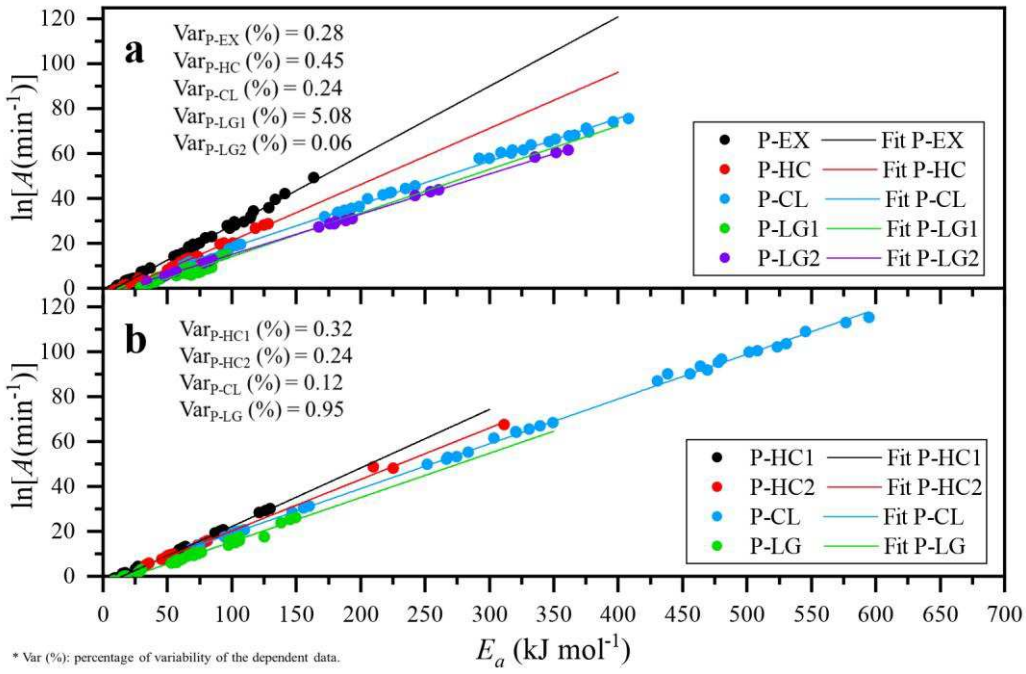

Source: Elaborated by the author

The pre-exponential factors of the individual devolatilization events derived from the pyrolysis of PCNS were calculated to be equal to 4.80×10^{8} min^{-1} for P-HC1, 2.32×10^{9} min^{-1} for P-HC2, 5.80×10^{9} min^{-1} for P-CL, and 3.24×10^{11} min^{-1} for LG. The value of *A* for the devolatilization of pseudo-hemicellulose aligns with those reported in kinetic studies involving the pyrolysis of hazelnut and cashew nutshells, with *A* values between 10^{6} and 10^{9} min^{-1} (DA SILVA et al., 2020; JANKOVIĆ et al., 2018). Regarding the devolatilization reactions of pseudo-cellulose and pseudo-lignin, the values of *A* are in accordance with those commonly reported in the literature for lignocellulosic biomass pyrolysis, which range from 10^{9} to 10^{10} min^{-1} (DA SILVA et al., 2020) and from 10^{10} to 10^{14} min^{-1} (DA SILVA et al., 2020; MA et al., 2022), respectively.

The order of the pre-exponential factor value can indicate the kind and nature of the chemical reaction that occurs during pyrolysis. For an order of magnitude lower than or equal to 10^{9} min^{-1}, the occurrence of a surface chemical reaction is presumed. In contrast, a simpler reaction chemistry path is presumed for an order of the pre-exponential factor higher than 10^{9} min^{-1} (AHMAD et al., 2017, 2021). Thus, for both cashew nutshell samples, the devolatilizations of pseudo-hemicellulose and pseudo-cellulose is typified

as surface chemical reaction, while the devolatilization of pseudo-lignin is typified as a chemical reaction with a simpler nature. Regarding the devolatilization of pseudo-extractives for the RCSN, a chemical reaction with a simpler nature is also presumed.

Knowledge about the type and nature of chemical reactions during pyrolysis is crucial for selecting the most suitable pyrolysis processes and conditions. The devolatilization of pseudo-hemicellulose and pseudo-cellulose are slower and more complex processes, requiring higher temperatures and longer residence times for complete conversion, thereby increasing the potential for coke formation. In contrast, the devolatilization of pseudo-lignin and pseudo-extractives is a faster and simpler process, with lower coke and byproduct formation, thus offering greater potential for the production of biofuels and other high-value products (YEO et al., 2019). Kinetic characterization of pyrolysis can therefore assist in selecting more efficient conversion processes.

3.4.4.3 Evaluating the most probable reaction model

Table 3.4 and **Table 3.5** present the comparison between the experimental master curves and theory adopting seventeen candidate reaction models for raw and pressed cashew nutshells, respectively. The reaction model that describes the most likely process for devolatilization of pseudo-extractives and pseudo-hemicellulose involved in the pyrolysis of cashew nutshell residues was represented by the second-order reaction model $F2 = (1- \alpha)^2$, which is in agreement with the literature (DA SILVA et al., 2020). Regarding the devolatilization of pseudo-cellulose, for both residues, it was well described by an Avrami-Erofeev nucleation reaction model, type A2 and A3, respectively (characterized by reactions in which the growth of nuclei is observed). Published data on pseudo-cellulose devolatilization also tend toward nucleation reaction models (MAMLEEV; BOURBIGOT; YVON, 2007; ZHANG et al., 2019).

Table 3.4 shows that the devolatilization reactions of P−LG1 and P−LG2 in the pyrolysis of RCSN align with order-based reaction models. In particular, the high reaction order for the devolatilization of P−LG1 (n = 9) agrees with the findings of Chen et al. (CHEN et al., 2017) for bamboo waste pyrolysis. These authors verified that the devolatilization of pseudo-lignin follows a n^{th}-order-based reaction model, with n between 6 and 8.

Table 3.4− Relative errors resulting from comparing experimental master plot curves and theoretical curves for pyrolysis of the raw cashew nutshell, assuming seventeen candidate reaction models.

Model	$f(\alpha)$	Relative error (%)				
		P−EX	**P−HC**	**P−CL**	**P−LG1**	**P−LG2**
P2	$2\alpha^{1/2}$	0.9497	0.7493	0.1922	168.6907	0.5608
P3	$3\alpha^{2/3}$	1.0655	0.8395	0.2836	186.2553	0.6640
P4	$4\alpha^{3/4}$	1.1253	0.8862	0.3274	195.7238	0.7157
P2/3	$2/3\,\alpha^{-1/2}$	0.3585	0.2392	0.6669	93.2343	0.4249
A2	$2(1-\alpha)\left[-\ln(1-\alpha)\right]^{1/2}$	0.7103	0.5657	**0.0589**	121.4450	0.3744
A3	$3(1-\alpha)\left[-\ln(1-\alpha)\right]^{2/3}$	0.8867	0.7029	0.1905	149.4799	0.5280
A4	$4(1-\alpha)\left[-\ln(1-\alpha)\right]^{3/4}$	0.9830	0.7777	0.2554	165.9022	0.6085
F1	$1-\alpha$	0.2579	0.2172	0.4121	65.5584	**0.1504**
F2	$(1-\alpha)^2$	**0.0869**	**0.1649**	0.7338	23.5734	0.4103
F3	$(1-\alpha)^3$	0.3515	0.3134	1.1191	7.3285	0.7369
F9	$(1-\alpha)^9$	5.0967	3.4605	13.3929	**0.3754**	9.0870
R2	$2(1-\alpha)^{1/2}$	0.4426	0.2528	0.5591	95.3722	0.2013
R3	$3(1-\alpha)^{2/3}$	0.3811	0.2767	0.6131	85.1603	0.1804
D1	$1/2\,\alpha^{-1}$	0.4961	0.6313	2.7604	69.3919	0.9877
D2	$\left[-\ln(1-\alpha)\right]^{-1}$	0.5355	2.0062	3.3170	51.0735	1.2132
D3	$3/2(1-\alpha)^{2/3}\left[1-(1-\alpha)^{1/3}\right]^{-1}$	0.6809	2.4815	4.0342	32.5283	1.5604
D4	$3\left[2\left((1-\alpha)^{-1/3}-1\right)\right]^{-1}$	0.5562	2.1578	3.5434	44.0878	1.3211

Abbreviations: P-EX: pseudo-extractives; P−HC: pseudo-hemicellulose; P−CL: pseudo-cellulose; P−LG1: primary pseudo-lignin; and P−LG2: secondary pseudo-lignin.

Source: Elaborated by the author

Table 3.5− Relative errors resulting from comparing experimental master plot curves and theoretical curves for pyrolysis of the pressed cashew nutshell, assuming seventeen candidate reaction models.

Model	$f(\alpha)$	Relative error (%)			
		P−HC1	**P−HC2**	**P−CL**	**P−LG**
P2	$2\alpha^{1/2}$	1.0921	0.2651	0.1319	3.4622
P3	$3\alpha^{2/3}$	1.2198	0.3619	0.1234	3.8111
P4	$4\alpha^{3/4}$	1.2863	0.4086	0.1676	3.9971
P2/3	$2/3\alpha^{-1/2}$	0.4022	0.6421	1.1700	1.8534
A2	$2(1-\alpha)\left[-\ln(1-\alpha)\right]^{1/2}$	0.8189	**0.1176**	0.1287	2.6021
A3	$3(1-\alpha)\left[-\ln(1-\alpha)\right]^{2/3}$	1.0146	0.2578	**0.0665**	3.1503
A4	$4(1-\alpha)\left[-\ln(1-\alpha)\right]^{3/4}$	1.1226	0.3277	0.0989	3.4646
F1	$1-\alpha$	0.3356	0.3696	0.7279	1.4279
F2	$(1-\alpha)^2$	**0.0707**	0.7041	0.1285	0.5371
F3	$(1-\alpha)^3$	0.3026	1.0937	1.6502	**0.1362**
F5	$(1-\alpha)^5$	0.8722	2.3713	5.5232	0.4657
R2	$2(1-\alpha)^{1/2}$	0.5400	0.2528	0.5591	2.0031
R3	$3(1-\alpha)^{2/3}$	0.4717	0.2767	0.6131	1.8081
D1	$1/2\alpha^{-1}$	0.4608	0.6313	2.7604	1.2690
D2	$\left[-\ln(1-\alpha)\right]^{-1}$	0.4514	2.0062	3.3170	0.9183
D3	$3/2(1-\alpha)^{2/3}\left[1-(1-\alpha)^{1/3}\right]^{-1}$	0.5308	2.4815	4.0342	0.5912
D4	$3\left[2\left((1-\alpha)^{-1/3}-1\right)\right]^{-1}$	0.4607	2.1578	3.5434	0.7912

Abbreviations: P−HC1: primary pseudo-hemicellulose; P−HC2: secondary pseudo-hemicellulose; P−CL: pseudo-cellulose; and P−LG: pseudo-lignin.

Source: Elaborated by the author

Literature evidence suggests that lignin pyrolysis is governed by the combined effect of different mechanisms, such as nucleation, diffusion, geometrical contraction, and power law (ZHANG et al., 2019;MAMLEEV; BOURBIGOT; YVON, 2007), which justifies the higher-order reaction model observed in the devolatilization of pseudo-lignin. For the PCNS, the third-order reaction model is plausible for the devolatilization of pseudo-lignin, consistent with literature reports (HIDAYAT et al., 2021). The complex phenolic structure and rigidity of cross-linked lignin can explain the difference observed in reaction orders found for pseudo-lignin devolatilization (YEO et al., 2019). In summary, the reaction models for lignocellulosic pseudo-components in both cashew nutshell residues align with the literature.

3.4.4.4 Application of the summative kinetic expression for reproducing the experimental pyrolysis behavior

Two summative kinetic expressions, Eq. (R-3) and Eq. (R-4), were proposed by combining calculated kinetic triplets to represent the pyrolysis behavior of raw and pressed cashew nutshells, respectively. The five and four kinetic triplets describing the pyrolysis behavior are summarized in the Appendix A (**Table A4** and **Table A5**, respectively).

$$\left(\frac{d\alpha}{dt}\right)_{raw} = \sum_{i=1}^{5} c_i \left(\frac{d\alpha}{dt}\right)_i = \left\{ \begin{array}{l} C_{P-EX}\left(2.78\times10^{10}\right)e^{-87150/RT}(1-\alpha)^2 \\ C_{P-HC}\left(4.25\times10^{8}\right)e^{-94790/RT}(1-\alpha)^2 \\ C_{P-CL}\left(8.33\times10^{9}\right)e^{-124210/RT}2(1-\alpha)\left[-\ln(1-\alpha)^{1/2}\right] \\ C_{P-LG1}\left(6.89\times10^{16}\right)e^{-226980/RT}(1-\alpha)^9 \\ C_{P-LG2}\left(3.89\times10^{11}\right)e^{-164870/RT}(1-\alpha) \end{array} \right\} \quad \text{(R-3)}$$

$$\left(\frac{d\alpha}{dt}\right)_{pressed} = \sum_{i=1}^{4} c_i \left(\frac{d\alpha}{dt}\right)_i = \left\{ \begin{array}{l} C_{P-HC1}\left(4.80\times10^{8}\right)e^{-91540/RT}(1-\alpha)^2 \\ C_{P-HC2}\left(2.32\times10^{9}\right)e^{-106030/RT}2(1-\alpha)\left[-\ln(1-\alpha)^{1/2}\right] \\ C_{P-CL}\left(5.80\times10^{9}\right)e^{-117020/RT}3(1-\alpha)\left[-\ln(1-\alpha)^{2/3}\right] \\ C_{P-LG}\left(3.24\times10^{11}\right)e^{-156420/RT}(1-\alpha)^3 \end{array} \right\} \quad \text{(R-4)}$$

Figure 3.6 represents the conversion and conversion rate plots concerning pyrolysis temperature for the raw (**Figure 3.6a** and **Figure 3.6b**) and pressed (**Figure 3.6c** and **Figure 3.6d**) cashew nutshells at heating rates of 5, 10, and 15 °C min^{-1}.

Figure 3.6 − Comparison of reconstructed pyrolysis behaviors with experimental data at 5, 10, and 15 °C min^{-1} for raw (**a** and **b**) and pressed (**c** and **d**) cashew nutshells.

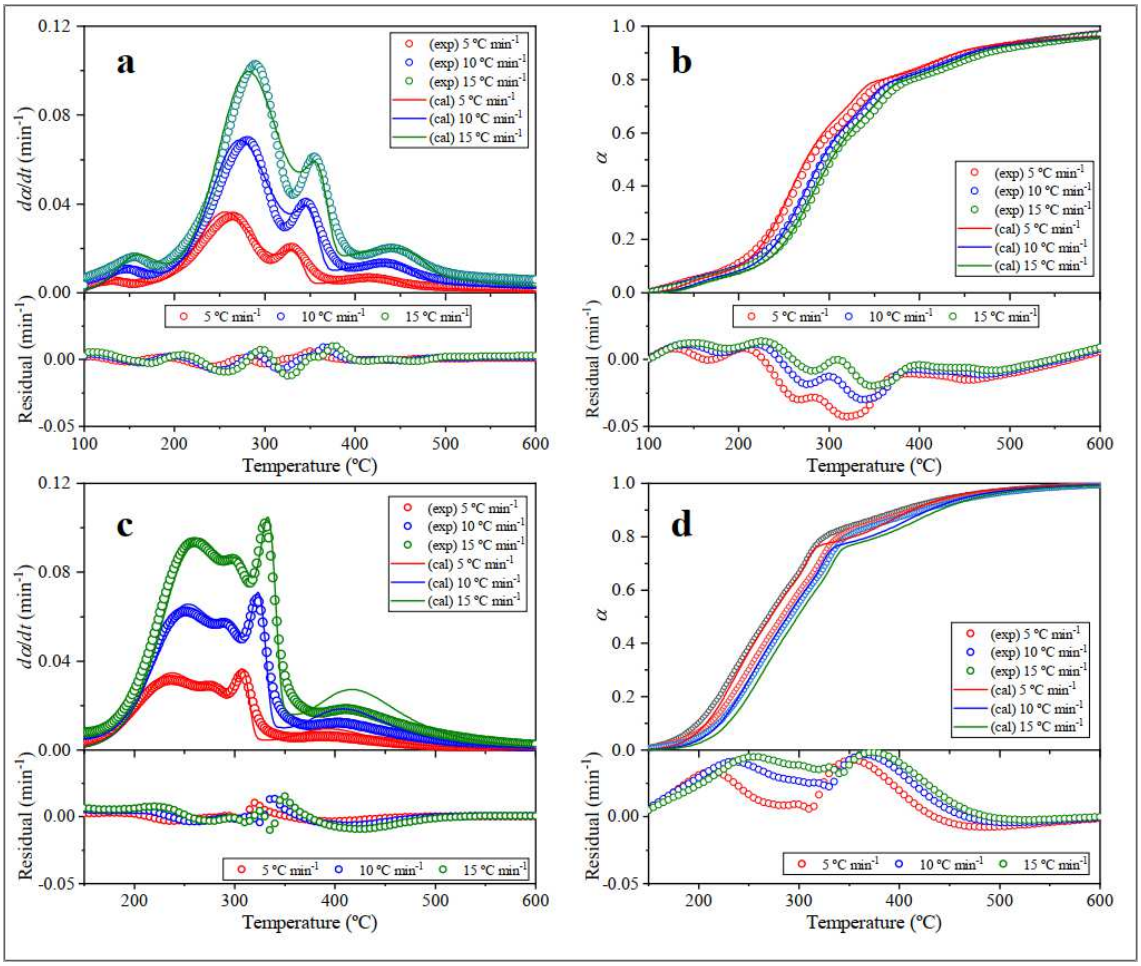

Source: Elaborated by the author

Both summative kinetic expressions were resolved with the spreadsheet software Microsoft Excel version Office 365 (Microsoft Corporation, United States) to compare the reconstructed curves (continuous lines) with experimental data (open circles). The proposed summative kinetic expressions Eq. (R-3) and Eq. (R-4) can describe with excellent agreement the experimental pyrolysis behavior of RCNS and PCNS, respectively, over the entire temperature range, as shown in **Figure 3.6** and confirmed by statistical correlations with $R^2 > 0.958$, $QOF > 93.1\%$ and $RSS < 0.443$.

In addition, as shown in **Figure 3.7,** the nonisothermal pyrolysis of raw (**Figure 3.7a** and **Figure 3.7b**) and pressed (**Figure 3.7c** and **Figure 3.7d**) cashew nutshells

collected at a heating rate of 20 °C min^{-1} was used to validate the summative kinetic expressions.

Figure 3.7− Graph of the pyrolysis behavior reconstructed with experimental data at 20 °C min^{-1} for raw (**a** and **b**) and pressed (**c** and **d**) cashew nutshells. Open circles and solid continuous lines represent the experimental and predicted curves, respectively (latter defined by summative kinetics expressions).

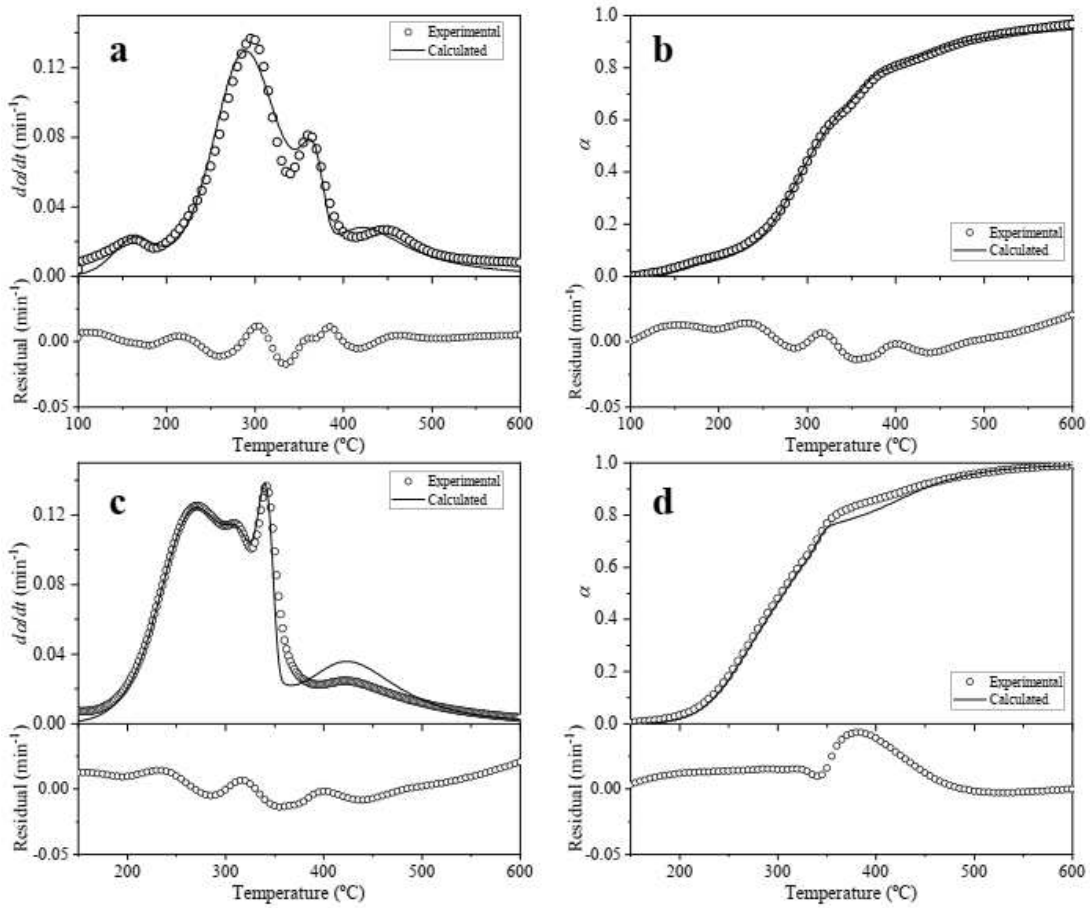

Source: Elaborated by the author

As displayed in **Figure 3.7**, by comparing the predicted curves (solid lines) with experimental data (open circles), it is confirmed that the summative expressions also correctly predict the additional nonisothermal pyrolysis behavior, giving excellent consistency ($R^2 > 0.972$, $Fit > 94.51\%$ and $RSS < 0.144$). These findings suggest that both proposed expressions (Eq. (R-3) and Eq. (R-4)) can be employed for simulation studies, process optimization, and equipment design involving the conversion of raw and pressed cashew nutshell residues into bioenergy and renewable chemicals.

3.4.5 Results for thermodynamic parameters

Table 3.6 and **Table 3.7** show the estimated thermodynamic parameters (ΔH, ΔG, and ΔS) as a function of the degree of conversion for pyrolysis of RCNS and PCNS, respectively. The conversion process for both residues is endothermic, as evident from the positive values of ΔH. Positive ΔH values were also found in the literature for pyrolysis of corn cob residue biomass, ranging from 174.2 to 180.2 kJ mol^{-1} (GUPTA; MONDAL, 2019), canola residue, ranging from 135.8 to 385.3 kJ mol^{-1} (TAHIR et al., 2019), and pistachio shell, ranging from 106.6 to 272.0 kJ mol^{-1} (GUPTA; GUPTA; MONDAL, 2022). Compared with the abovementioned bioenergy feedstocks, the low values of ΔH for raw and pressed cashew nutshells indicate their viability as raw materials for bioenergy production. Furthermore, the difference between the average values determined for E_a and ΔH, known as the potential energy barrier, directly expresses the difficulty a reagent molecule faces in overcoming the barrier for activated complex formation. The calculated values of $E_a - \Delta H$, which are less than 6.8 kJ mol^{-1}, indicate that the pyrolysis of both residues tends to be energetically viable due to the small amount of energy required to convert these lignocellulosic feedstocks into bioenergy (KUMAR MISHRA, 2022).

Table 3.6− Thermodynamic parameters (ΔH, ΔG, and ΔS) as a function of the extent of conversion for pyrolysis of the raw cashew nutshell, assuming five independent parallel reactions.

α	P−EX			P−HC			P−CL			P-LG1			P-LG2		
	ΔH (kJ mol^{-1})	ΔG (kJ mol^{-1})	ΔS (J mol^{-1} K^{-1})	ΔH (kJ mol^{-1})	ΔG (kJ mol^{-1})	ΔS (J mol^{-1} K^{-1})	ΔH (kJ mol^{-1})	ΔG (kJ mol^{-1})	ΔS (J mol^{-1} K^{-1})	ΔH (kJ mol^{-1})	ΔG (kJ mol^{-1})	ΔS (J mol^{-1} K^{-1})	ΔH (kJ mol^{-1})	ΔG (kJ mol^{-1})	ΔS (J mol^{-1} K^{-1})
0.05	84.00	117.85	-89.32	90.99	148.35	-125.64	117.75	177.78	-102.93	221.95	204.29	29.20	159.39	206.86	-72.00
0.10	83.95	118.28	-89.42	90.80	151.24	-126.05	117.68	178.66	-103.05	221.82	203.83	28.99	159.30	207.65	-72.14
0.15	83.92	118.66	-89.51	90.69	153.00	-126.29	117.64	179.18	-103.12	221.72	203.49	28.83	159.24	208.13	-72.22
0.20	83.89	119.00	-89.59	90.60	154.34	-126.46	117.61	179.59	-103.18	221.63	203.18	28.69	159.20	208.52	-72.29
0.25	83.86	119.31	-89.67	90.53	155.38	-126.60	117.58	179.91	-103.22	221.54	202.88	28.56	159.16	208.83	-72.34
0.30	83.83	119.60	-89.73	90.47	156.26	-126.71	117.56	180.18	-103.26	221.46	202.58	28.42	159.13	209.11	-72.38
0.35	83.81	119.87	-89.80	90.42	157.02	-126.81	117.54	180.42	-103.29	221.37	202.27	28.29	159.10	209.36	-72.43
0.40	83.78	120.13	-89.86	90.38	157.71	-126.89	117.52	180.65	-103.32	221.27	201.96	28.15	159.07	209.59	-72.47
0.45	83.76	120.38	-89.91	90.34	158.33	-126.97	117.50	180.86	-103.35	221.17	201.62	28.01	159.05	209.82	-72.50
0.50	83.74	120.63	-89.97	90.30	158.91	-127.04	117.49	181.06	-103.37	221.07	201.27	27.86	159.02	210.05	-72.54
0.55	83.71	120.88	-90.02	90.26	159.46	-127.11	117.47	181.27	-103.40	220.96	200.89	27.70	159.00	210.28	-72.58
0.60	83.69	121.12	-90.08	90.23	159.98	-127.17	117.45	181.46	-103.42	220.84	200.50	27.54	158.97	210.50	-72.61
0.65	83.67	121.38	-90.14	90.19	160.51	-127.23	117.44	181.67	-103.45	220.70	200.05	27.36	158.94	210.75	-72.65
0.70	83.64	121.65	-90.19	90.16	161.03	-127.29	117.42	181.89	-103.48	220.56	199.58	27.17	158.91	211.01	-72.70
0.75	83.62	121.94	-90.26	90.12	161.57	-127.36	117.40	182.12	-103.51	220.40	199.05	26.96	158.88	211.31	-72.74
0.80	83.59	122.27	-90.33	90.08	162.18	-127.43	117.38	182.39	-103.54	220.20	198.43	26.72	158.84	211.65	-72.80
0.85	83.55	122.65	-90.41	90.04	162.84	-127.50	117.36	182.70	-103.58	219.99	197.75	26.46	158.79	212.05	-72.86
0.90	83.50	123.16	-90.52	89.98	163.70	-127.60	117.32	183.12	-103.64	219.72	196.89	26.15	158.73	212.62	-72.95
0.95	83.43	123.93	-90.68	89.90	164.95	-127.74	117.27	183.75	-103.72	219.38	195.84	25.77	158.63	213.50	-73.08
Average	**83.73**	**120.67**	**-89.97**	**90.34**	**158.25**	**-126.94**	**117.49**	**180.98**	**-103.36**	**220.93**	**200.86**	**27.73**	**159.02**	**210.08**	**-72.54**
± SD	**0.13**	**1.36**	**0.31**	**0.23**	**3.44**	**0.43**	**0.10**	**1.22**	**0.16**	**0.60**	**1.98**	**0.81**	**0.16**	**1.36**	**0.22**

Abbreviations: P−EX: pseudo-extractives; P−HC: pseudo-hemicellulose; P−CL: pseudo-cellulose; P−LG1: primary pseudo-lignin; and P−LG2: secondary pseudo-lignin. (Source: Elaborated by the author)

Table 3.7− Thermodynamic parameters (Δ*H*, Δ*G*, and Δ*S*) as a function of the extent of conversion for pyrolysis of the pressed cashew nutshell, assuming four independent parallel reactions.

	P−HC1			**P−HC2**			**P−CL**			**P-LG**		
α	**Δ*H***	**Δ*G***	**Δ*S***	**Δ*H***	**Δ*G***	**Δ*S***	**Δ*H***	**Δ*G***	**Δ*S***	**Δ*H***	**Δ*G***	**Δ*S***
	(kJ mol^{-1})	**(kJ mol^{-1})**	**(J mol^{-1} K^{-1})**	**(kJ mol^{-1})**	**(kJ mol^{-1})**	**J mol^{-1} K^{-1})**	**kJ mol^{-1})**	**(kJ mol^{-1})**	**(J mol^{-1} K^{-1})**	**(kJ mol^{-1})**	**(kJ mol^{-1})**	**(J mol^{-1} K^{-1})**
0.05	87.75	144.57	-124.62	101.56	163.77	-115.62	111.09	173.70	-107.89	151.48	194.62	-72.63
0.10	87.62	146.49	-124.89	101.49	164.67	-115.74	111.06	174.11	-107.94	151.32	196.09	-72.91
0.15	87.54	147.73	-125.07	101.45	165.23	-115.81	111.04	174.37	-107.98	151.21	197.01	-73.08
0.20	87.47	148.72	-125.20	101.42	165.66	-115.87	111.02	174.58	-108.00	151.13	197.76	-73.22
0.25	87.42	149.53	-125.31	101.40	166.01	-115.92	111.01	174.76	-108.03	151.06	198.38	-73.33
0.30	87.37	150.24	-125.41	101.37	166.32	-115.96	110.99	174.91	-108.05	150.99	198.93	-73.42
0.35	87.33	150.89	-125.49	101.35	166.61	-115.99	110.98	175.05	-108.07	150.93	199.45	-73.51
0.40	87.29	151.50	-125.57	101.34	166.88	-116.03	110.97	175.19	-108.08	150.88	199.95	-73.60
0.45	87.25	152.09	-125.65	101.32	167.13	-116.06	110.96	175.32	-108.10	150.82	200.44	-73.68
0.50	87.21	152.66	-125.72	101.30	167.39	-116.09	110.95	175.46	-108.12	150.77	200.94	-73.76
0.55	87.17	153.24	-125.79	101.28	167.64	-116.12	110.94	175.59	-108.14	150.71	201.45	-73.85
0.60	87.13	153.81	-125.86	101.26	167.90	-116.15	110.93	175.73	-108.15	150.65	201.97	-73.93
0.65	87.09	154.43	-125.94	101.24	168.18	-116.19	110.92	175.89	-108.17	150.58	202.56	-74.03
0.70	87.05	155.06	-126.02	101.22	168.47	-116.22	110.91	176.05	-108.19	150.52	203.17	-74.12
0.75	87.00	155.78	-126.11	101.20	168.79	-116.27	110.89	176.24	-108.22	150.44	203.89	-74.24
0.80	86.95	156.61	-126.21	101.17	169.18	-116.31	110.88	176.47	-108.25	150.34	204.74	-74.37
0.85	86.89	157.57	-126.32	101.14	169.63	-116.37	110.85	176.73	-108.28	150.22	205.77	-74.52
0.90	86.80	158.90	-126.48	101.09	170.25	-116.44	110.83	177.11	-108.33	150.06	207.23	-74.74
0.95	86.66	160.95	-126.71	101.02	171.22	-116.56	110.78	177.72	-108.40	149.81	209.54	-75.07
Average	**87.21**	**152.67**	**-125.70**	**101.30**	**167.42**	**-116.09**	**110.95**	**175.53**	**-108.13**	**150.73**	**201.26**	**-73.79**
± SD	**0.22**	**3.40**	**0.43**	**0.11**	**1.53**	**0.19**	**0.06**	**0.82**	**0.11**	**0.34**	**3.05**	**0.50**

Abbreviations: P−HC1: primary pseudo-hemicellulose; P−HC2: secondary pseudo-hemicellulose; P−CL: pseudo-cellulose; and P−LG: pseudo-lignin. (Source: Elaborated by the author)

The thermodynamic parameter change in Gibbs free energy (ΔG) of the pyrolysis process depicts the available bioenergy that can potentially be recovered from biomass (GUPTA; MONDAL, 2019; GUPTA; GUPTA; MONDAL, 2022). The results found for both cashew nutshell residues are comparable with those obtained for corn cob (ranging from 174.20 to 180.20 kJ mol^{-1}) (GUPTA; MONDAL, 2019), canola residue (ranging from 158.30 to 212.10 kJ mol^{-1}) (TAHIR et al., 2019), and pistachio shell (ranging from 179.34 to 184.11 kJ mol^{-1}) (GUPTA; GUPTA; MONDAL, 2022), being favorable for pyrolytic conversion and reflecting their potential for transformation into bioenergy and renewable chemicals. ΔH and ΔG showed positive values during the pyrolysis process of both cashew nutshell residues across all conversion degrees, indicating a nonspontaneous reaction. The increase in conversion had a minimal effect on ΔH and ΔG values, suggesting a relatively constant energy requirement within the entire conversion range.

The degree of disorder in a pyrolysis reaction can be measured by the state function named the change in entropy (ΔS). A "slow" or a "fast" reaction can be identified according to the sign of ΔS (BOONCHOM, 2008). Negative values for ΔS indicate that the products formed by volatile release and molecular rearrangement are more ordered (XU et al., 2020). Since the products' disorder degree is inferior to the reactants' disorder degree, a lower reactivity characteristic occurs, and the conversion process is governed mainly through "slow" reactions. Thus, the negative values of ΔS for the pyrolysis of PCNS suggest a low reactivity characteristic. According to the literature (KIRTI et al., 2022; MAIA; DE MORAIS, 2016), uniquely negative ΔS values are associated with biomass pyrolysis, corroborating the thermodynamic findings achieved for the pyrolysis of PCNS. On the other hand, as the ΔS value was positive for the devolatilization of P-LG1 involved in the pyrolysis of RCNS, the degree of disorder of the products was higher than that of the initial reactants. This statement directs the rapid formation of the activated complex as a result of volatile release and molecular rearrangement (MAIA; DE MORAIS, 2016). The negative and positive ΔS values indicate the complexity of the pyrolysis process RCNS. This behavior is also commensurate with reports from the literature (GUPTA; GUPTA; MONDAL, 2022; TAHIR et al., 2019). From the analysis of the thermodynamic parameters, both cashew nutshell residues have the potential for use in producing bioenergy and renewable chemicals.

3.4.6 Composition of volatile products (Py-GC/MS analysis)

Figure 3.8 illustrates the impact of pyrolysis temperature on the distribution of the volatile products arising from the fast pyrolysis of raw (**a**) and pressed (**b**) cashew nutshells. For this illustration, the oxygenated compound group includes alcohols, aldehydes, carboxylic acids, esters, ethers, ketones, phenols, and furans. Additionally, the hydrocarbon group is listed in **Table A6, Table A7**, and **Table A8** in the Appendix A. As shown in **Figure 3.8**, increasing the temperature (from 450 °C to 650 °C) caused a decrease in the CO_2 concentration. For the raw cashew nutshell, the concentration of CO_2 decreased from 43.5% at 450 °C to 30.5% at 650 °C. Likewise, for the pressed cashew nutshell, the relative CO_2 concentration decreased from 48.8% at 450 °C to 28.5% at 650 °C. At a temperature of 550 °C, the raw cashew nutshell showed a lower concentration of CO_2 (27.4%) compared to the other concentrations of the same component and an increase in the concentration of oxygenated compounds, nitrogenous compounds, and hydrocarbons. According to reports in the literature, the decomposition of cellulose and hemicellulose directly influences the high concentration of CO_2 at temperatures of 450 °C. Furthermore, the production of CO_2 from the decomposition of lignin showed the same trend reported in this study: a decrease in CO_2 concentration with increasing temperature (CHEN et al., 2022a). Regarding the nitrogenous compounds in the volatile products, the concentration of nitrogen-containing compounds decreased from 4.0% to 1.1% for the raw cashew nutshell and from 1.8% to 1.2% for the pressed cashew nutshell with increasing temperature from 450 °C to 650 °C. Mumbach et al. (MUMBACH et al., 2022a) found that the relative concentration of nitrogen compounds in the volatile fraction of the fast pyrolysis of royal palm tree agroindustrial waste is above 8.0% at 450 °C.

Figure 3.8 − Distribution of volatile products arising from fast analytical pyrolysis of raw **(a)** and pressed **(b)** cashew nutshells, based on the relative concentration, in relation to reaction temperature.

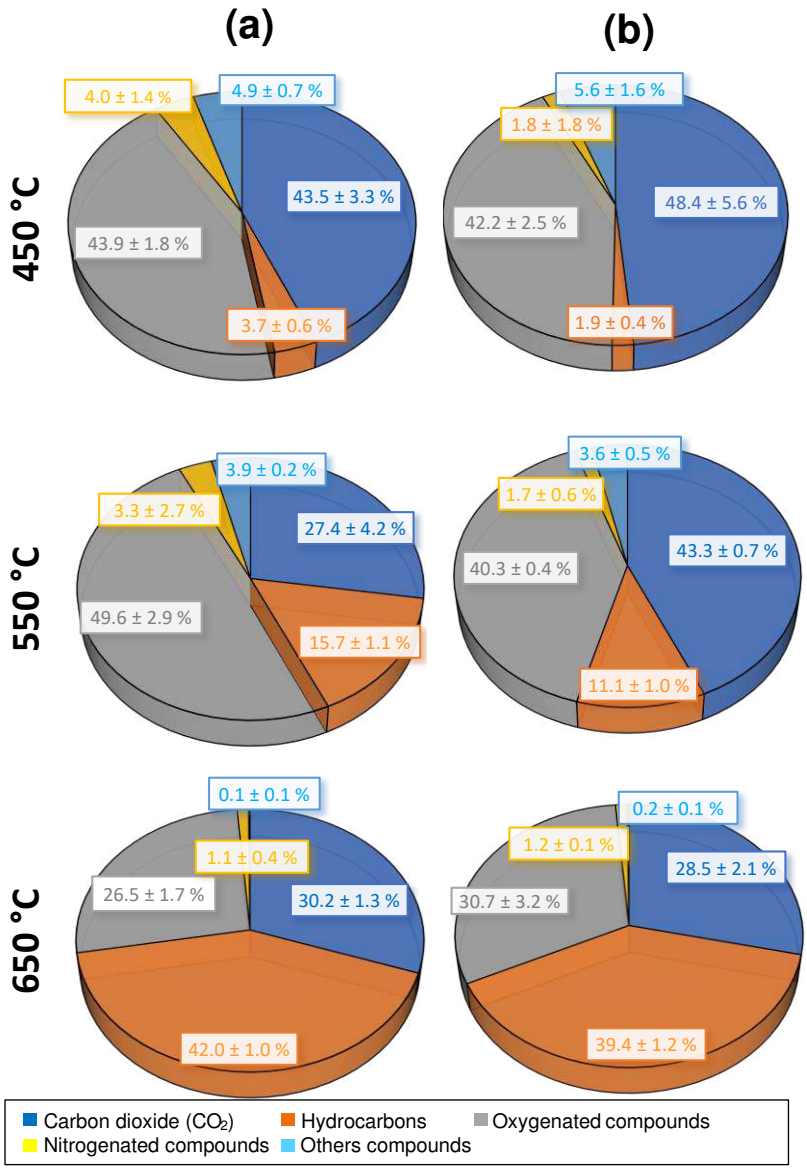

Source: Elaborated by the author

Figure 3.9 shows the effect of reaction temperature on the distribution of the main organic compounds in the condensable fraction of the volatile products arising from the fast pyrolysis of raw and pressed cashew nutshell residues. An increase in pyrolysis temperature is associated with an observed increase in the relative concentration of hydrocarbons. For PCNS, the hydrocarbon concentration is lower than that of RCNS in the studied temperature

range. In addition, a reduction in the relative concentration of oxygenated compounds from 4.0% to 1.1% for RCNS and from 1.8% to 1.2% for PCNS was found with increasing pyrolysis temperature from 450 °C to 650 °C. This trend aligns with a previous report (MUMBACH et al., 2022a) that indicates a decline in the concentration of oxygenated compounds in volatile pyrolysis products as the reaction temperature increases.

Figure 3.9 − Distribution of the condensable fraction of the volatile products arising from fast analytical pyrolysis of raw **(a)** and pressed **(b)** cashew nutshells, based on the relative concentration excluding the noncondensable fraction, in relation to reaction temperature.

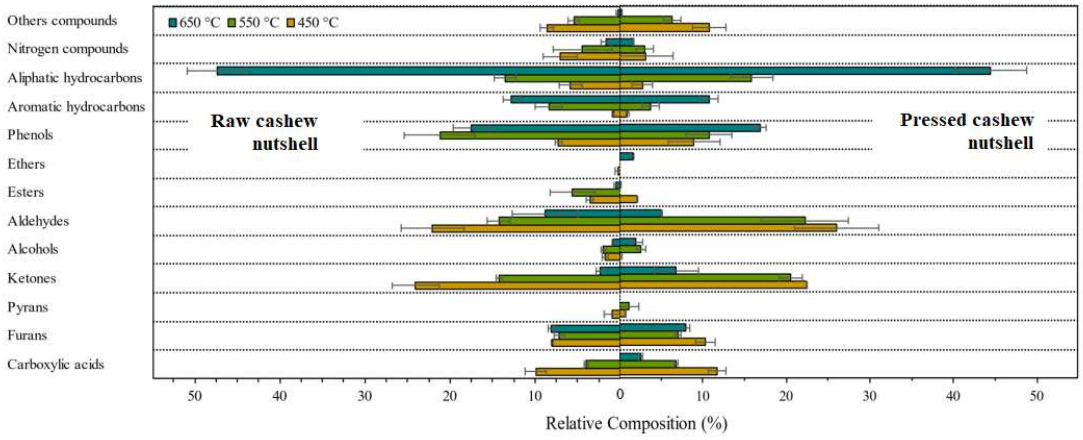

Source: Elaborated by the author

As shown in **Figure 3.9**, the relative concentration of aliphatic hydrocarbons presents in the condensable fraction of volatile products increased for both residues when the final pyrolysis temperature increased from 450 °C to 650 °C. The relative concentrations of aliphatic hydrocarbons in RCNS and PCNS of 5.83 ± 1.33% and 2.75 ± 1.24% at 450 °C increased to maximum relative concentrations of 47.42 ± 3.47% and 44.46 ± 4.29% at 650 °C, respectively. This increase in the fraction of aliphatic hydrocarbons is favorable and may be an alternative for the use of the condensable fraction of organic volatiles in the production of biofuels (ASHOKKUMAR et al., 2022).

Increasing the pyrolysis temperature also caused an increase in the concentration of aromatic hydrocarbons, as shown in **Figure 3.9**. The relative concentrations of 0.84 ± 0.12% and 0.98 ± 0.16% at 450 °C increased to approximately 12.83 ± 0.92% and 10.73 ± 1.09% at 650 °C in the volatile products of the pyrolysis of RCNS and PCNS, respectively. At a

temperature of 550 °C, raw cashew nutshell had a relative concentration of 8.37 ± 1.59%, and pressed cashew nutshell had a relative concentration of 3.75 ± 1.01%. The increase in temperature leads to a higher concentration of aromatic hydrocarbons due to secondary reactions that cause aromatization, polymerization, condensation, and cracking (UZUN; PÜTÜN; PÜTÜN, 2007). The chemical composition of the cashew nutshell liquid can contribute to polymerization reactions at 550 °C, leading to an increase in the concentration of aromatic hydrocarbons (UZUN; PÜTÜN; PÜTÜN, 2007). This finding is interesting since aromatic hydrocarbons are commonly used as industrial raw materials, solvents, and components of numerous commercial and consumer products (Ã; BINGHAM; PH, 2012).

As shown in **Figure 3.9**, at a pyrolysis temperature of 450 °C, aldehydes and ketones are the oxygenated groups with the highest concentration in both cashew nutshell residues. Regarding phenolic compounds, the relative concentrations significantly increased from 7.20 ± 0.40% and 8.9 ± 3.10% at 450 °C to maximum concentrations of 17.48 ± 2.14% and 16.90 ± 0.68% at 650 °C for the pyrolysis of RCNS and PCNS, respectively. The concentration of alcohols in the pyrolysis of PCNS slightly increased from 0.15 ± 0.15% at 450 °C to 2.00 ± 0.75% at 650 °C. Devolatilization reactions associated with the oxygenated compounds present in hemicellulose and cellulose are related to this increase. The furan contents in volatile gases were also detected, and their relative concentrations increased slightly from 7.12 ± 0.58% and 6.99% ± 0.38% at 450 °C to 8.11 ± 0.34% and 7.97 ± 0.45% at 650 °C for RNCS and PCNS, respectively. Furans originate from the primary decomposition of hemicellulose at lower temperatures (BRANCA; GIUDICIANNI; BLASI, 2003). Finally, in **Figure 3.9**, the relative concentrations of the "other" compounds were 8.59 ± 0.78% and 10.73 ± 2.01% at 450 °C, decreasing by 0.20 ± 0.20% and 0.26 ± 0.10% at 650 °C.

The current results add to previous literature data that the volatile products derived from fast pyrolysis of cashew nutshell residues have potential sustainable and renewable sources of valuable chemicals. Py–GC/MS analysis revealed that aliphatic hydrocarbons were the dominant components in the condensable volatile products at a pyrolysis temperature of 650 °C, indicating the production of liquid fuel with high calorific value and low viscosity. In summary, the fast pyrolysis process offers an alternative approach to enhance the value of cashew nutshell residues and mitigate environmental impacts related to

their improper disposal.

3.5 Conclusions

The present study investigated four facets of valorizing raw and pressed cashew nutshells as new feedstocks for producing bioenergy and renewable chemicals using pyrolysis through (1) physicochemical characterization of these agro-industrial residues, (2) knowing the reaction by determining the kinetic triplets under a multicomponent perspective, (3) estimation of thermodynamic parameters, and (4) characterization of volatile products. First, both residues have promising properties for bioenergy exploitation, such as considerable HHV (17.0–22.1 MJ kg^{-1}), satisfactory bulk density (180.2–220.5 kg m^{-3}), ash content below 1.8 wt.%, nitrogen content below 0.9 wt.%, and negligible sulfur content.

The following conclusions have been drawn as a result of TGA and Py-GC/MS experiments:

1. The determination coefficients (R^2) above 0.99 from the deconvoluted curves confirmed that the pyrolytic behavior of raw and pressed cashew nutshells occurred satisfactorily in the form of five and four parallel devolatilization events, respectively.
2. Regard to the pyrolysis of the raw cashew nutshell, the isoconversional methods indicated average activation energies in the range of 63.81–88.98 kJ mol^{-1} for P-EX, 94.36–102.32 kJ mol^{-1} for P-HC, 123.70–133.88 kJ mol^{-1} for P-CL, and 164.27–249.28 kJ mol^{-1} for P-LG. For the pyrolysis of the pressed cashew nutshell, the average activation energies were between 91.12–115.01 kJ mol^{-1} for P-HC, 116.53–126.43 kJ mol^{-1} for P-CL, and 155.84–167.42 kJ mol^{-1} for P-LG. The average activation energies for both residues are lower than those reported in the literature for well-established bioenergy feedstocks.
3. The estimated pre-exponential factors for the pyrolysis of raw cashew nutshell were 2.78×10^{10} min^{-1} for P-EX, 4.25×10^{8} min^{-1} for P-HC, 8.33×10^{9} min^{-1} for P-CL, 6.89×10^{16} min^{-1} for P-LG1, and 3.89×10^{11} min^{-1} for P-LG2. For the pyrolysis of the pressed cashew nutshell, the pre-exponential factors were estimated as 4.80×10^{8} min^{-1} for P-HC1, 2.32×10^{9} min^{-1} for P-HC2, 5.80×10^{9} min^{-1} for P-CL, and 3.24×10^{11} min^{-1} for P-LG. These values are comparable to those found in previous works.

4. From the integral master plot method, for both cashew nutshell residues, the devolatilization of P-CL adhered to nucleation-growth mechanisms, while the devolatilization of P-LG was within the nth-order-based reaction mechanisms. Depending on the cashew nutshell residue, the devolatilization of P-HC follows nucleation-growth or nth-order-based reaction mechanisms. The most suitable reaction model for the devolatilization of P-EX involved in the pyrolysis of the raw cashew nutshell belongs to the n-order reaction mechanism.
5. The proposed summative kinetic expressions can describe with excellent agreement the experimental pyrolysis behavior of raw and pressed cashew nutshells over the entire temperature range, as confirmed by statistical correlations with $R^2 > 0.958$, $QOF > 93.1\%$, and $RSS < 0.443$.
6. The thermodynamic parameters for the raw cashew nutshell ranged from 83.73 to 220.93 kJ mol^{-1} for ΔH, from 120.67 to 210.08 kJ mol^{-1} for ΔG, and from − 126.94 to 27.23 J mol^{-1} K^{-1} for ΔS. Concerning the pressed cashew nutshell, the thermodynamic parameters ranged from 87.21 to 175.53 kJ mol^{-1} for ΔH, from 152.67 to 201.26 kJ mol^{-1} for ΔG, and from − 125.70 to -73.79 J mol^{-1} K^{-1} for ΔS. These values suggest the suitability of both residues as promising raw materials for producing bioenergy and renewable chemicals.
7. As verified by Py-GC/MS analysis, aliphatic hydrocarbons were the dominant components of the condensable volatile products at 650 °C, while reaction temperatures of 450 and 550 °C favored the production of oxygenated compounds.

For future investigations, the following recommendations are suggested: (a) optimize operational parameters for the thermochemical conversion of cashew nutshell residues into bioenergy and renewable chemicals via pyrolysis; (b) investigate the catalytic pyrolysis of cashew nutshell residues and assess its impact on activation energy and volatile product composition; (c) conduct lab-scale experiments to achieve mass and energy balance for converting cashew nutshell residues into bioenergy and renewable chemicals; and (d) scale up the pyrolysis process and perform techno-economic analyses using Super Pro Design software. In the industrial sector, the outcomes of this comprehensive investigation are anticipated to aid in the formulation and design of large-scale pyrolysis reactors for the

conversion of cashew nutshell residues into bioenergy and renewable chemicals. As a result, the potential energy valorization of these residues through pyrolysis could facilitate energy matrix diversification and advance the circular economy of agro-industrial waste materials.

3.6 References

Ã, P. F. I.; BINGHAM, E.; PH, D. Aromatic Hydrocarbons — Benzene and Other Alkylbenzenes. v. 2, p. 153–220, 2012.

AGENCY, I. E. **World Energy Balances**. Available at: <https://www.iea.org/data-and-statistics/data-product/world-energy-balances>. Accessed on: June 26, 2022.

AGNIHOTRI, N.; MONDAL, M. K. Thermal analysis, kinetic behavior, reaction modeling, and comprehensive pyrolysis index of soybean stalk pyrolysis. **Biomass Conversion and Biorefinery**, n. 0123456789, 2023.

AHMAD, M. S. et al. Kinetic analyses and pyrolytic behavior of Para grass (Urochloa mutica) for its bioenergy potential. **Bioresource Technology**, v. 224, p. 708–713, jan. 2017.

AHMAD, M. S. et al. Elucidating the pyrolysis reaction mechanism of Calotropis procera and analysis of pyrolysis products to evaluate its potential for bioenergy and chemicals. **Bioresource Technology**, v. 322, n. November 2020, p. 124545, fev. 2021.

AHMADOU, A. et al. Effect of pyrolysis temperature on ochratoxin A adsorption mechanisms and kinetics by cashew nut shell biochars. **Journal of Food and Technology**, v. 4, n. 7, p. 877–888, 2019.

ALVES, J. L. F. et al. Physicochemical properties, pyrolysis kinetics, thermodynamic parameters of activation, and evolved volatiles of mango seed waste as a bioenergy feedstock: A potential exploration. **Thermochimica Acta**, v. 725, n. April, p. 179519, jul. 2023.

AMALIYAH, N.; PUTRA, A. E. E. Microwave-Assisted Pyrolysis of Cashew Nut Shell. **International Journal of Design & Nature and Ecodynamics**, v. 16, n. 2, p. 227–232, 30 abr. 2021.

ASHOKKUMAR, V. et al. Recent advances in lignocellulosic biomass for biofuels and value-added bioproducts - A critical review. **Bioresource Technology**, v. 344, n. PB, p. 126195, 2022.

ASTM. D3176-15: Standard Practice for Ultimate Analysis of Coal and Coke. In:

Annual Book of ASTM Standards. West Conshohocken: ASTM International, 2015. p. 1–4.

ASTM. E873-82: Standard Test Method for Bulk Density of Densified Particulate Biomass Fuels. In: **Annual Book of ASTM Standards**. West Conshohocken: [s.n.].

BISWAS, B. et al. Pyrolysis behavior of rice straw under carbon dioxide for production of bio-oil. **Renewable Energy**, v. 129, p. 686–694, 2018.

BLASI, C. DI; GALGANO, A.; BRANCA, C. Exothermic Events of Nut Shell and Fruit Stone Pyrolysis. **ACS Sustainable Chemistry and Engineering**, v. 7, n. 9, p. 9035–9049, 2019.

BOONCHOM, B. Kinetics and Thermodynamic Properties of the Thermal Decomposition of Manganese Dihydrogenphosphate Dihydrate. **Journal of Chemical & Engineering Data**, v. 53, n. 7, p. 1533–1538, jul. 2008.

BRANCA, C.; GIUDICIANNI, P.; BLASI, C. DI. KINETICS , CATALYSIS , AND REACTION ENGINEERING GC / MS Characterization of Liquids Generated from Low-Temperature Pyrolysis of Wood. **Industrial & Engineering Chemistry Research**, p. 3190–3202, 2003.

CHANNIWALA, S. A.; PARIKH, P. P. A unified correlation for estimating HHV of solid, liquid and gaseous fuels. **Fuel**, v. 81, n. 8, p. 1051–1063, maio 2002.

CHEN, C. et al. Bioresource Technology Thermogravimetric pyrolysis kinetics of bamboo waste via Asymmetric Double Sigmoidal (Asym2sig) function deconvolution. **Bioresource Technology**, v. 225, p. 48–57, 2017.

CHEN, D. et al. Insight into biomass pyrolysis mechanism based on cellulose, hemicellulose, and lignin: Evolution of volatiles and kinetics, elucidation of reaction pathways, and characterization of gas, biochar and bio-oil. **Combustion and Flame**, v. 242, 2022a.

CHEN, F. et al. Investigation of non-isothermal pyrolysis kinetics of waste industrial hemp stem by three-parallel-reaction model. **Bioresource Technology**, v. 347, n. November 2021, p. 126402, 2022b.

CHEN, Z. et al. Optimizing co-combustion synergy of soil remediation biomass and pulverized coal toward energetic and gas-to-ash pollution controls. **Science of The Total Environment**, v. 857, n. October 2022, p. 159585, jan. 2023.

COLLARD, F.-X.; BLIN, J. A review on pyrolysis of biomass constituents: Mechanisms and composition of the products obtained from the conversion of cellulose, hemicelluloses and lignin. **Renewable and Sustainable Energy Reviews**, v. 38, p. 594–608, out. 2014.

COSTA, J. E. B. et al. Renewable aromatics through catalytic pyrolysis of coconut fiber (Cocos nucífera Linn.) using low cost HZSM-5. **Renewable Energy**, v. 191, p. 439–446, 2022.

DA SILVA, J. C. G. et al. Single-step and multi-step thermokinetic study – Deconvolution method as a simple pathway for describe properly the biomass pyrolysis for energy conversion. **Energy Conversion and Management**, v. 209, n. March, p. 112653, 2020.

DAMARTZIS, T. et al. Thermal degradation studies and kinetic modeling of cardoon (Cynara cardunculus) pyrolysis using thermogravimetric analysis (TGA). **Bioresource Technology**, v. 102, n. 10, p. 6230–6238, maio 2011.

FERNANDEZ, A. et al. Kinetic analysis and thermodynamics properties of air/steam gasification of agricultural waste. **Journal of Environmental Chemical Engineering**, v. 8, n. 4, p. 103829, 2020.

Food and Agriculture Organization of the United Nations Statistics. Available at: <https://www.fao.org/faostat/en/#data/QCL>. Accessed on: June 26, 2022.

GARCÍA, R. et al. Spanish biofuels heating value estimation. Part II: Proximate analysis data. **Fuel**, v. 117, n. PARTB, p. 1139–1147, jan. 2014a.

GARCÍA, R. et al. Spanish biofuels heating value estimation. Part I: Ultimate analysis data. **Fuel**, v. 117, n. PARTB, p. 1130–1138, jan. 2014b.

GOGOI, M. et al. Assessments of pyrolysis kinetics and mechanisms of biomass residues using thermogravimetry. **Bioresource Technology Reports**, v. 4, n. September, p. 40–49, dez. 2018.

GUPTA, G. K.; MONDAL, M. K. Kinetics and thermodynamic analysis of maize cob pyrolysis for its bioenergy potential using thermogravimetric analyzer. **Journal of Thermal Analysis and Calorimetry**, v. 137, n. 4, p. 1431–1441, ago. 2019.

GUPTA, S.; GUPTA, G. K.; MONDAL, M. K. Thermal degradation characteristics, kinetics, thermodynamic, and reaction mechanism analysis of pistachio shell pyrolysis for its

bioenergy potential. **Biomass Conversion and Biorefinery**, v. 12, n. 11, p. 4847–4861, 2022.

HIDAYAT, S. et al. Comprehensive kinetic study of Imperata Cylindrica pyrolysis via Asym2sig deconvolution and combined kinetics. **Journal of Analytical and Applied Pyrolysis**, v. 156, n. February, p. 105133, 2021.

HU, J. et al. Torrefaction-assisted oxy-fuel co-combustion of textile dyeing sludge and bamboo residues toward enhancing emission-to-ash desulfurization in full waste circularity. **Fuel**, v. 318, n. January, p. 123603, 2022.

HUANG, J. et al. Flue gas-to-ash desulfurization of combustion of textile dyeing sludge: Its dependency on temperature, lignocellulosic residue, and CaO. **Chemical Engineering Journal**, v. 417, n. December 2020, p. 127906, ago. 2021.

JANKOVI, B.; STOJILJKOVI, D.; JOVANOVI, V. TSA-MS characterization and kinetic study of the pyrolysis process of various types of biomass based on the Gaussian multi-peak fi tting and peak- to-peak approaches. v. 234, n. July, p. 447–463, 2018.

JANKOVIĆ, B. et al. TSA-MS characterization and kinetic study of the pyrolysis process of various types of biomass based on the Gaussian multi-peak fitting and peak-to-peak approaches. **Fuel**, v. 234, n. July, p. 447–463, dez. 2018.

KAN, T.; STREZOV, V.; EVANS, T. J. Lignocellulosic biomass pyrolysis: A review of product properties and effects of pyrolysis parameters. **Renewable and Sustainable Energy Reviews**, v. 57, p. 1126–1140, maio 2016.

KAUR, R. et al. Characterization of slow pyrolysis products from three different cashew wastes. **Bioresource Technology**, v. 376, n. March, p. 128859, maio 2023.

KAZAWADI, D.; NTALIKWA, J.; KOMBE, G. Co-pyrolysis of cashew nut, coconut shells, and rice husk waste: kinetic and thermodynamic investigations. **Energy Sources, Part A: Recovery, Utilization, and Environmental Effects**, v. 44, n. 3, p. 5896–5915, 14 set. 2022.

KHAWAM, A.; FLANAGAN, D. R. Solid-State Kinetic Models: Basics and Mathematical Fundamentals. **The Journal of Physical Chemistry B**, v. 110, n. 35, p. 17315–17328, set. 2006.

KIRTI, N. et al. Pyrolysis of pigeon pea (Cajanus cajan) stalk: Kinetics and thermodynamic analysis of degradation stages via isoconversional and master plot methods.

Bioresource Technology, v. 347, n. October 2021, p. 126440, mar. 2022.

KUMAR, M.; UPADHYAY, S. N.; MISHRA, P. K. A comparative study of thermochemical characteristics of lignocellulosic biomasses. **Bioresource Technology Reports**, v. 8, n. April, p. 100186, 2019.

KUMAR MISHRA, R. Pyrolysis of low-value waste switchgrass: Physicochemical characterization, kinetic investigation, and online characterization of hot pyrolysis vapours. **Bioresource Technology**, v. 347, n. January, p. 126720, 2022.

KUMAR, P. P. et al. Process for isolation of cardanol from technical cashew (Anacardium occidentale l.) Nut shell liquid. **Journal of Agricultural and Food Chemistry**, v. 50, n. 16, p. 4705–4708, 2002.

LENIS, Y. A.; OSORIO, L. F.; PÉREZ, J. F. Fixed bed gasification of wood species with potential as energy crops in Colombia: The effect of the physicochemical properties. **Energy Sources, Part A: Recovery, Utilization and Environmental Effects**, v. 35, n. 17, p. 1608–1617, 2013.

LI, W. et al. Kinetic and thermodynamic studies of biomass pseudo-components under thermo-oxidative degradation conditions using asymmetric function of Bi-Gaussian as deconvolution technique. **Renewable Energy**, v. 188, p. 491–503, 2022.

LIBORIO, D. O. et al. Pyrolysis of Energy Cane Bagasse: Investigating Kinetics, Thermodynamics, and Effect of Temperature on Volatile Products. **Energies**, v. 16, n. 15, p. 5669, jul. 2023.

LOPES, F. C. R.; TANNOUS, K. Coconut fiber pyrolysis decomposition kinetics applying single- and multi-step reaction models. **Thermochimica Acta**, v. 691, n. July, p. 178714, set. 2020.

LÓPEZ-FONSECA, R. et al. Non-isothermal analysis of the kinetics of the combustion of carbonaceous materials. **Journal of Thermal Analysis and Calorimetry**, v. 80, n. 1, p. 65–69, mar. 2005.

MA, C. et al. Thermogravimetric pyrolysis kinetics study of tobacco stem via multicomponent kinetic modeling, Asym2sig deconvolution and combined kinetics. **Bioresource Technology**, v. 360, n. June, p. 127539, 2022.

MA, Z. et al. Determination of pyrolysis characteristics and kinetics of palm kernel shell using TGA-FTIR and model-free integral methods. **Energy Conversion and**

Management, v. 89, p. 251–259, 2015.

MA, Z. et al. Pyrolysis behaviors of oilfield sludge based on Py-GC/MS and DAEM kinetics analysis. **Journal of the Energy Institute**, v. 92, n. 4, p. 1053–1063, 2019.

MAIA, A. A. D.; DE MORAIS, L. C. Kinetic parameters of red pepper waste as biomass to solid biofuel. **Bioresource Technology**, v. 204, p. 157–163, mar. 2016.

MAMLEEV, V.; BOURBIGOT, S.; YVON, J. Kinetic analysis of the thermal decomposition of cellulose: The main step of mass loss. **Journal of Analytical and Applied Pyrolysis**, v. 80, n. 1, p. 151–165, 2007.

MANIĆ, N. et al. Apricot kernel shells pyrolysis controlled by non-isothermal simultaneous thermal analysis (STA). **Journal of Thermal Analysis and Calorimetry**, v. 142, n. 2, p. 565–579, jan. 2020.

MARTINS MAYER, F. et al. Characterization of analytical fast pyrolysis vapors of medium-density fiberboard (mdf) using metal-modified HZSM-5. **Journal of Analytical and Applied Pyrolysis**, v. 136, n. October, p. 87–95, nov. 2018.

MISHRA, G.; KUMAR, J.; BHASKAR, T. Kinetic studies on the pyrolysis of pinewood. **Bioresource Technology**, v. 182, p. 282–288, 2015.

MOINE, E. CHEIKH et al. Multistep process kinetics of the non-isothermal pyrolysis of Moroccan Rif oil shale. **Energy**, v. 115, p. 931–941, 2016.

MUMBACH, G. D. et al. Prospecting pecan nutshell pyrolysis as a source of bioenergy and bio-based chemicals using multicomponent kinetic modeling, thermodynamic parameters estimation, and Py-GC/MS analysis. **Renewable and Sustainable Energy Reviews**, v. 153, 2022a.

MUMBACH, G. D. et al. Pyrolysis of cocoa shell and its bioenergy potential: evaluating the kinetic triplet, thermodynamic parameters, and evolved gas analysis using TGA-FTIR. **Biomass Conversion and Biorefinery**, v. 12, n. 3, p. 723–739, 2022b.

MUMBACH, G. D. et al. Investigation on prospective bioenergy from pyrolysis of butia seed waste using TGA-FTIR: Assessment of kinetic triplet, thermodynamic parameters and evolved volatiles. **Renewable Energy**, v. 191, p. 238–250, maio 2022c.

MÜSELLIM, E. et al. Thermokinetic and TG/DSC-FTIR study of pea waste biomass pyrolysis. **Applied Thermal Engineering**, v. 137, p. 54–61, jun. 2018.

MYTHILI, R. et al. Characterization of bioresidues for biooil production through

pyrolysis. **Bioresource Technology**, v. 138, p. 71–78, 2013.

NAM, N. H. et al. Pyrolysis of cashew nut shell: A parametric study. **Vietnam Journal of Chemistry**, v. 58, n. 4, p. 506–511, 2020.

NISAR, J. et al. Kinetics of pyrolysis of sugarcane bagasse: effect of catalyst on activation energy and yield of pyrolysis products. **Cellulose**, v. 28, n. 12, p. 7593–7607, 23 ago. 2021.

NISAR, J. et al. Pyrolysis of juice-squeezed grapefruit waste: effect of nickel oxide on kinetics and bio-oil yield. **International Journal of Environmental Science and Technology**, v. 19, n. 10, p. 10211–10222, 29 out. 2022.

OIRAM FILHO, F. et al. Productivity of a preparative high-performance liquid chromatography isolation of anacardic acids from cashew nut shell liquid. **Separation Science Plus**, v. 2, n. 6, p. 192–199, 2019.

PACIONI, T. R. et al. Bio-syngas production from agro-industrial biomass residues by steam gasification. **Waste Management**, v. 58, p. 221–229, dez. 2016.

PINZI, S. et al. A simplified method for kinetic modeling of coffee silver skin pyrolysis by coupling pseudo-components peaks deconvolution analysis and model free-isoconversional methods. **Fuel**, v. 278, n. February, p. 118260, out. 2020.

QIAO, Y. et al. Thermal behavior, kinetics and fast pyrolysis characteristics of palm oil: Analytical TG-FTIR and Py-GC/MS study. **Energy Conversion and Management**, v. 199, n. August, p. 111964, nov. 2019.

REHMAN, N. U. et al. Production of Bio-Oil from Thermo-Catalytic Decomposition of Pomegranate Peels over a Sulfonated Tea Waste Heterogeneous Catalyst: A Kinetic Investigation. **Energies**, v. 16, n. 4, p. 1908, 15 fev. 2023.

ROMERO MILLÁN, L. M.; SIERRA VARGAS, F. E.; NZIHOU, A. Kinetic Analysis of Tropical Lignocellulosic Agrowaste Pyrolysis. **BioEnergy Research**, v. 10, n. 3, p. 832–845, set. 2017.

SANGARÉ, D. et al. Comparative pyrolysis studies of lignocellulosic biomasses: online gas quantification, kinetics triplets, and thermodynamic parameters of the process. **Bioresource Technology**, v. 346, n. December 2021, p. 126598, 2021.

SANTOS, G. R. et al. Combustion of pellets produced from the powders of coconut and cashew nut shells : Chemical , thermal and emission analyses. 2022.

SINGH, S. et al. Studies on individual pyrolysis and co-pyrolysis of corn cob and polyethylene: Thermal degradation behavior, possible synergism, kinetics, and thermodynamic analysis. **Science of the Total Environment**, v. 783, p. 147004, 2021.

STARINK, M. J. The determination of activation energy from linear heating rate experiments: A comparison of the accuracy of isoconversion methods. **Thermochimica Acta**, v. 404, n. 1–2, p. 163–176, 2003.

TAHIR, M. H. et al. Demonstrating the suitability of canola residue biomass to biofuel conversion via pyrolysis through reaction kinetics, thermodynamics and evolved gas analyses. **Bioresource Technology**, v. 279, n. January, p. 67–73, 2019.

TYAGI, U.; ANAND, N. Prospective of Waste Lignocellulosic Biomass as Precursors for the Production of Biochar: Application, Performance, and Mechanism—A Review. **Bioenergy Research**, n. 0123456789, 2023.

UZUN, B. B.; PÜTÜN, A. E.; PÜTÜN, E. Composition of products obtained via fast pyrolysis of olive-oil residue: Effect of pyrolysis temperature. **Journal of Analytical and Applied Pyrolysis**, v. 79, n. 1–2, p. 147–153, maio 2007.

VÁRHEGYI, G. Aims and methods in non-isothermal reaction kinetics. **Journal of Analytical and Applied Pyrolysis**, v. 79, n. 1–2, p. 278–288, maio 2007.

VYAZOVKIN, S. et al. ICTAC Kinetics Committee recommendations for performing kinetic computations on thermal analysis data. **Thermochimica Acta**, v. 520, n. 1–2, p. 1–19, jun. 2011.

VYAZOVKIN, S. et al. ICTAC Kinetics Committee recommendations for collecting experimental thermal analysis data for kinetic computations. **Thermochimica Acta**, v. 590, p. 1–23, ago. 2014.

VYAZOVKIN, S. et al. Thermochimica Acta ICTAC Kinetics Committee recommendations for analysis of multi-step kinetics. **Thermochimica Acta**, v. 689, n. March, p. 178597, 2020.

WU, X. et al. Oxy-fuel co-combustion dynamics of phytoremediation biomass and textile dyeing sludge: Gas-to-ash pollution abatement. **Science of the Total Environment**, v. 825, p. 153656, 2022.

XU, X. et al. Pyrolysis Kinetics, Thermodynamics, and Volatiles of Representative Pine Wood with Thermogravimetry–Fourier Transform Infrared Analysis. **Energy & Fuels**,

v. 34, n. 2, p. 1859–1869, fev. 2020.

YANG, H. et al. Characteristics of hemicellulose, cellulose and lignin pyrolysis. **Fuel**, v. 86, n. 12–13, p. 1781–1788, ago. 2007.

YAO, Z. et al. Comparative study on the pyrolysis kinetics of polyurethane foam from waste refrigerators. **Waste Management & Research**, v. 38, n. 3, p. 271–278, mar. 2020a.

YAO, Z. et al. Kinetic studies on the pyrolysis of plastic waste using a combination of model-fitting and model-free methods. **Waste Management & Research**, v. 38, n. 1_suppl, p. 77–85, maio 2020b.

YAO, Z. et al. Kinetic study on the slow pyrolysis of nonmetal fraction of waste printed circuit boards (NMF-WPCBs). **Waste Management & Research**, v. 38, n. 8, p. 903–910, ago. 2020c.

YAO, Z. et al. Thermal behavior and kinetic study on the co-pyrolysis of biomass with polymer waste. **Biomass Conversion and Biorefinery**, 2022.

YEO, J. Y. et al. Comparative studies on the pyrolysis of cellulose , hemicellulose , and lignin based on combined kinetics. **Journal of the Energy Institute**, v. 92, n. 1, p. 27–37, 2019.

ZHANG, D. et al. Pyrolysis Characteristics and Reaction Mechanisms of Pine Needles. **Applied Biochemistry and Biotechnology**, v. 189, n. 4, p. 1056–1083, 2019.

Chapter 4

Valorizing cashew nutshell residue for sustainable lignocellulosic panels using a bio-based phenolic resin as a circular economy solution

4 VALORIZING CASHEW NUTSHELL RESIDUE FOR SUSTAINABLE LIGNOCELLULOSIC PANELS USING A BIO-BASED PHENOLIC RESIN AS A CIRCULAR ECONOMY SOLUTION

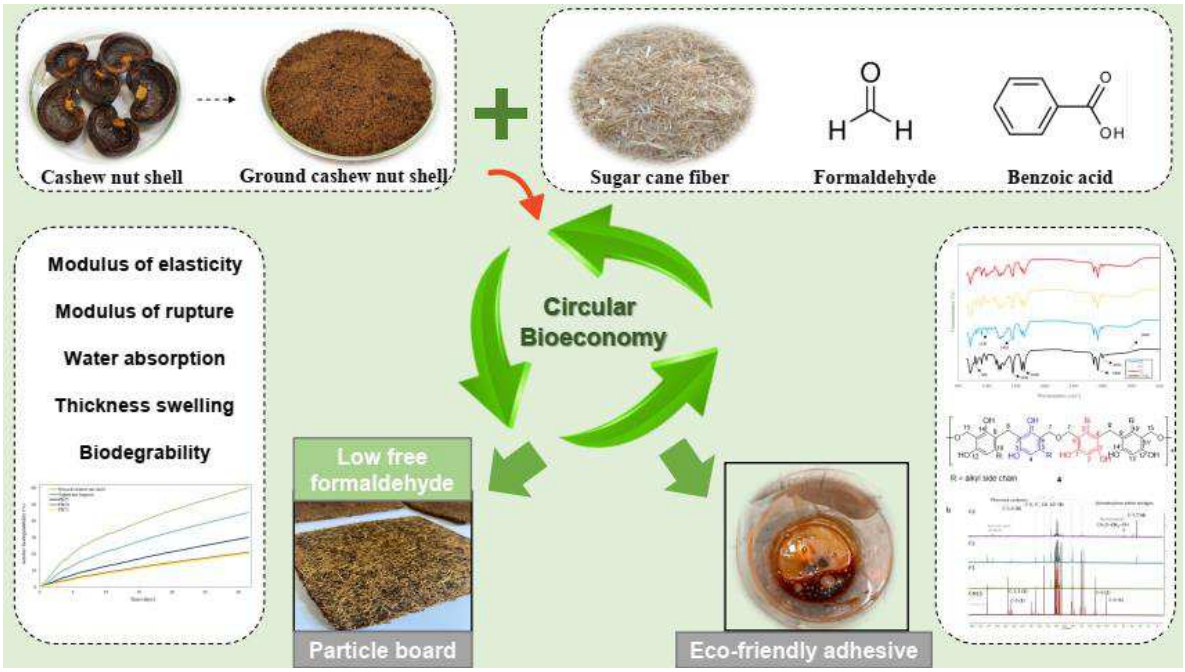

4.1 Abstract

The motivation for this study stems from the significant annual amount of cashew nutshells produced worldwide, which has raised growing concerns about proper environmental disposal. One alternative is to utilize the nutshells to produce particleboards and eco-friendly resin, thereby contributing to the circular economy. The present study proposes an innovation by providing the first insights into particleboard production, utilizing pressed cashew nutshell and a phenolic resin derived from the reaction of cashew nutshell liquid (CNSL) with formaldehyde. The mass proportions of CNSL to formaldehyde were varied at 1:0.25, 1:0.5, and 1:0.75 (w/w) without the necessity for isolating chemical compounds at 105 °C. The resin was characterized using rheology, DSC, FTIR, HPLC, and NMR techniques. The physical and mechanical properties of the particleboard were evaluated through density, tensile, flexural, water absorption, and thickness swelling tests. The formaldehyde emission and biodegradability content of the particleboards were also evaluated. Eco-friendly phenol-formaldehyde resin promoted the modulus of elasticity

(MOE) from 707.06 to 1866.35 MPa and the modulus of rupture (MOR) from 6.38 to 14.25 MPa. In addition, using adhesive with CNSL to formaldehyde mass ratios of 1:0.25 and 1:0.50 resulted in particleboards of class E1 in terms of formaldehyde emissions. The biodegradability of panels PB25, PB50 and PB75 was 30%, 21% and 20%, respectively, in 30 days. These findings demonstrate the potential of cashew nutshell biomass and eco-friendly resin as an adhesive in the particleboard industry.

Keywords: CNSL, eco-friendly adhesive, waste, mechanical properties, free formaldehyde, biodegradability.

4.2 Introduction

The cashew crop is mainly found in tropical and subtropical regions and predominantly in countries such as India, Vietnam, Nigeria, Ivory Coast, and Brazil. According to the Food and Agriculture Organization of the United Nations (FAO), the global production of cashew nuts with shells was approximately 4.0 million tons in 2020 (FAO, 2022). The cashew nut kernel is a nutrient-rich food, and its production is a significant source of income for many countries. However, extracting the kernel generates a considerable volume of cashew nutshells, the improper disposal of which can have serious environmental impacts. The shell accounts for approximately 70% of the weight of processed cashew nuts (FAO, 2022).

In Brazil, cashew nut kernel production is divided between large and small factories. Large factories, with processing capacities of up to 30 thousand tons of cashew nuts per year, produce the largest amount of cashew nutshells, while small factories, with processing capacities of up to 200 tons of cashew nuts per year, contribute a smaller share. Currently, the main destination for the shells is burning in industrial kilns and brickyards.

Improper disposal of this waste can negatively affect both community health and the environment. Burning or landfill disposal of cashew nutshells can release toxic gases and cause environmental problems (SERRA et al., 2021). High concentrations of these pollutants in the atmosphere can lead to lung damage and neurodevelopmental and neurodegenerative diseases (Josino et al., 2017a; Cory-Slechta et al., 2023).

Research studies that have explored the potential for reusing cashew nutshells represent a crucial step towards achieving the United Nations Sustainable Development Goals (SDGs), such as 2 - Zero Hunger and Sustainable Agriculture; 3 - Good Health and Well-being; 9 - Industry, Innovation, and Infrastructure; 11 - Sustainable Cities and Communities; and 12 - Responsible Consumption and Production (UNDP, 2015). In the literature, there is evidence that cashew nutshells can be used as raw material for various products, such as activated carbon (KOUASSI et al., 2020), eco-friendly cement (MANJUNATH et al., 2023), wood waste for the fabrication of particleboards (MARI; VILLENA, 2016), and biochar (TAPAS et al., 2023). However, despite the significant potential, technological routes for reusing cashew nutshells are not yet implemented on a large scale, and studies are conducted only at the laboratory scale.

Currently, there is a significant interest in implementing clean technologies and adopting sustainable waste valorization practices in the industry (Homem et al., 2022). In the Brazilian context, compliance with legislation, specifically Law No. 12.305/2010, which establishes the Política Nacional de Resíduos Sólidos (PNRS), plays a crucial role in promoting the circular economy in the country. Among the initiatives foreseen in this legislation, the implementation of Reverse Logistics and the elaboration of Solid Waste Management Plans stimulate the reuse of waste, contributing to the reduction of the demand for natural resources and the minimization of waste generation.

In this context of searching for more sustainable practices in the industry, particularly in the production of wood derivative, two major challenges are faced: reducing the use of wood and decreasing formaldehyde emissions in the production of particleboards (NGUYEN et al., 2023). A promising alternative to tackle these challenges is to replace commonly used pine and eucalyptus wood with agro-industrial residues, which can add value and reduce the amount of wood used. Recent studies indicate that particleboards derived from various biomass sources, such as rice husk and coconut fiber (CHANDRAN et al., 2022), pine wood, bamboo, yerba (RUSCH et al., 2023), and bean straw (FARIA et al., 2023), have been developed and found to have applications in different sectors, including construction, furniture, and packaging. These options not only help preserve the environment but also bring economic and social advantages, promoting the development of the circular economy.

The utilization of cashew nutshells in particleboard production presents a promising opportunity, thus reducing the amount of waste and contributing to sustainability. Furthermore, the simplified extraction process of cashew nutshell liquid (CNSL) through pressing eliminates the need for high temperatures and solvent usage, making the production process more economical and straightforward. Another advantage is that the residual CNSL present in cashew nutshells can be considered a natural source of phenol, enabling the production of an eco-friendly resin. The cashew nutshell can be processed and combined with other materials, resulting in a sturdy and durable board with a wide range of applications in the furniture and construction industry.

In the manufacture of wood-based particleboards, various resins are used, depending on the type of particleboard and its applications. Adhesives influence all aspects of composites, from their physical-mechanical properties to their performance under wet conditions (DORIEH et al., 2022). The resins commonly used in the composite industry are urea-formaldehyde and melamine-formaldehyde resins (DORIEH et al., 2022). In addition, phenol-formaldehyde resins are also applied as wood adhesives and wood composites. This thermosetting adhesive is produced from the reaction of formaldehyde with phenol (PIZZI; IBEH, 2014), presenting high mechanical strength, high thermal resistance, resistance to various chemicals, low flammability, and good adhesion to wood (PIZZI; IBEH, 2014). It is important to note that the production of particleboards must meet formaldehyde emission restrictions (YADAV, 2021). The European standard EN 13986 establishes limits for the concentration of formaldehyde, categorizing panels into two classes: Class E1 (with less than 8 mg/100 g oven-dry board) and Class E2 (with levels between 8 and 30 mg/100 g oven-dry board) (EN 13986+A1, 2015). In Brazil, regulations require that the emission of formaldehyde in particleboards remains below 8 mg/100 g (ABNT, 2018).

Cashew nutshell liquid (CNSL) is a rich source of phenolic compounds, such as anacardic acid, cardol, and cardanol (SOUZA et al., 2022). The extraction of CNSL can result in two types: natural or technical (SOUZA et al., 2022). When extracted at low temperatures, natural CNSL contains more anacardic acid. Various extraction methods have been used to obtain natural CNSL, including mechanical extraction at low temperatures, which results in a liquid containing approximately 70-80% anacardic acid, 13-20% cardol, and 1-10%

cardanol (SOUZA et al., 2022). Additionally, extraction can be performed using solvents (such as water, hexane, and methanol) or supercritical fluids (such as CO_2) (CRUZ REINA et al., 2023), and it is important to note that the chosen method directly affects the chemical composition of natural CNSL. At high temperatures, decarboxylation of anacardic acid occurs, forming technical CNSL, in which cardanol is the main component (Souza et al., 2022; Mgaya, 2018). Based on available literature evidence (ARAUJO et al., 2021), the high content of anacardic acid in the resin is anticipated to confer an advantage by enhancing the durability of the particleboards, attributed to its antimicrobial property. CNSL has great potential for use in a wide range of industrial applications, such as the production of varnishes (KYEI et al., 2022), adhesives (BRITO et al., 2023) and coatings/resins (RENAN et al., 2020). In the context of particleboard manufacturing, the use of resins of ecological origin is still limited in the scientific literature, making this approach particularly relevant (NARCISO et al., 2021).

Although the literature mentions the utilization of binder/adhesive resins based on CNSL for producing particleboards (AKARANTA, 2000; LUBI; THACHIL, 2007, 2000), the feasibility of experimentally manufacturing particleboards from cashew nutshell residue employing a biobased phenolic resin without the need to isolate chemical compounds has not yet been explored. Therefore, the existence of this knowledge gap has opened a window of opportunity for conducting this study, driven by the considerable quantity of unexploited cashew nutshell residue, which holds potential as a sustainable material for producing particleboards with phenolic resin with low levels of formaldehyde emission.

Therefore, this study represents the first investigation of synthesizing and applying an eco-friendly resin utilizing residual CNSL from cashew nutshell as a natural phenol source, obviating the necessity for employing techniques to isolate chemical compounds within CNSL. Such techniques could result in more intricate processes and increased production costs for particleboards derived from cashew nutshell (NARCISO et al., 2021). In this novel approach, a biobased phenolic resin was synthesized by chemically reacting phenolic compounds present in CNSL with formaldehyde under acidic conditions. The biobased phenolic resin was characterized through rheological studies, as well as FTIR, HPLC, and NMR analyses. In addition, the physical properties (density, water absorption,

and thickness swelling) and mechanical properties (modulus of rupture and modulus of elasticity) of the particleboards were evaluated for various formulations of CNSL and formaldehyde. Biodegradability and free formaldehyde emission tests were also conducted on the particleboards. This study presents an innovative technological pathway for the cashew nut industry to enhance its prospects by effectively utilizing cashew nutshell residue, thereby promoting circularity and sustainability. It offers valuable insights into the valorization of this abundant and underutilized lignocellulosic residue, facilitating the establishment of closed production cycles.

4.3 Materials and methods

4.3.1 Preparation of raw materials and extraction of CNSL

Cashew nutshells used in this project come from Embrapa Tropical Agroindustry in Pacajus – CE, Brazil. The experimental conditions employed were adapted from a previous study of the mechanical extraction of CNSL at 5 MPa (OIRAM FILHO et al., 2019) but carried out at room temperature. The pressing cake, containing approximately 30% by mass of residual CNSL, was ground in a Pulverizette 16 hammer mill (Fritsch, EUA) and passed through a 2.0 mm mesh. The selection of particle sizes was carried out based on preliminary tests to facilitate the chemical polymerization reaction. To quantify the residual CNSL present in the pressed cashew nutshell (PCNS) for particleboard manufacturing, methyl alcohol (Exodo, Sumare, São Paulo, Brazil) was utilized, followed by a vacuum filtration process employing Blue Band Quantitative Filter Paper 70mm for 30 min.

In addition, sugarcane bagasse (SCB) was added to achieve the desired densities and consequently improve the mechanical properties of the particleboards (FARINASSI et al., 2015). The SCB was dried at 105 °C for 12 h. Afterwards, it was processed in a mill (Fritsch, Pulverizette 25) to reduce the particle size to 10 mm before being used in the production of particleboards.

4.3.2 Characterization of the raw material

The pressed cashew nutshell was characterized using proximate analysis, ultimate analysis, and lignocellulosic composition analysis. Procedures for physiochemical characterization analyses were repeated in triplicate. The proximate analysis involved determining the mass percentages of inherent moisture (IM), volatile matter (VM), fixed carbon (FC), and inorganic matter (ASH) using a methodology adapted from ASTM E−1131 (Alves et al., 2023). The mass percentage of fixed carbon was indirectly obtained by subtracting the moisture, volatile matter, and ash, as indicated in Eq. (4.1) (GUPTA; GUPTA; MONDAL, 2022).

$$FC\left(wt.\%\right) = 100\ wt.\% - IM\left(wt.\%\right) - VM\left(wt.\%\right) - ASH\left(wt.\%\right) \qquad (4.1)$$

The elemental composition of the raw material was obtained through ultimate analysis, where the mass percentages of carbon (C), hydrogen (H), nitrogen (N), oxygen (O), and sulfur (S) were obtained. To determine the percentages of C, H, N and S, an elemental analyzer model CE 1108 (Carlo Erba Instruments) was used, following the methodology described in the standard protocol ASTM D3176-15 (ASTM, 2015). To evaluate the mass percentage of oxygen, a mass balance was performed by subtracting the sum of the mass percentages of C, H, N, S, and ash from the total mass (100% by weight) on a dry basis (SANTANA et al., 2021).

The lignocellulosic composition analysis was carried out by means of thermogravimetric analysis (TGA) of the PCSN using the PerkinElmer STA 6000 equipment under a nitrogen atmosphere (50 mL min^{-1}). In this analysis, a 10 mg sample with a particle size of 100 µm was subjected to heating from room temperature to a final temperature of 800 °C at a rate of 10 °C min^{-1}. The lignocellulosic constituents (hemicellulose, cellulose, and lignin) were quantified using the multipeak-fitting deconvolution method. The DTG curve was deconvoluted into the lignocellulosic constituents (hemicellulose, cellulose, and lignin) using the asymmetric double sigmoidal (Asym2Sig) fitting function, implemented in Origin 2018 software. This method has been extensively validated in the literature and has been shown to provide fast and reliable quantification of biomass lignocellulosic composition,

yielding values comparable to those obtained from standard protocols (ALVES et al., 2020; CARRIER et al., 2011).

Using the standard protocol ASTM E873-82 (ASTM, 2019), the bulk density of PCNS residue was calculated by the ratio of the sample mass to the known volume of the compacted sample. For this analysis, a graduated cylindrical container of 5 cm^3 was used.

4.3.3 Synthesis and characterization of phenolic resins

Phenolic resins were synthesized through chemical reaction between phenolic compounds present in CNSL and formaldehyde in an acidic medium. Benzoic acid ($C_7H_6O_2$) (99 wt.% purity, Dinâmica Química, São Paulo, Brazil) was used to make the reaction medium acidic. Three resin formulations were prepared by varying the ratios of CNSL and formaldehyde (37 wt.% purity, Labsynth, São Paulo, Brazil). The ratios were (by mass) 1:0.25 for F1, 1:0.50 for F2, and 1:0.75 for F3. The proportions were selected to achieve the appropriate polymerization reaction for the resin, aiming to use the lowest amount of formaldehyde (PIZZI; IBEH, 2014). Initially, the mass of benzoic acid was weighed (470 mg) and added to formaldehyde (3.58 mL, 7.16 mL, and 10.73 mL for F1, F2, and F3, respectively) under constant stirring at 40 rpm for 10 min. Then, 15.83 mL of CNSL was added to the mixture, and then the solution was heated to 105 °C and stirred for 15 min until complete homogenization. The phenolic resin was slowly cooled to room temperature over an additional 20 min, where the condensation step takes place. The experiment was replicated, revealing that the addition of CNSL favors a reduced reaction time. Such a phenomenon is intrinsically linked to the manufacturing process of this resin.

After phenolic resin formulation, viscosity analysis was performed through rheological tests. The chemical characterization of CNSL and resins was carried out using rheology, differential scanning calorimetry (DSC), Fourier transform infrared spectroscopy (FTIR), high-performance liquid chromatography (HPLC), and nuclear magnetic resonance (NMR) analysis.

4.3.3.1 Rheological analysis

The rheological analysis was performed in a Haake Maars rheometer (Thermo Fisher Scientific, USA) using a concentric cylinder geometry (CC16 Din) designed for measuring the rheological properties of viscous fluids, with a gap of 3.318 mm. The CNSL was evaluated within the linear viscoelastic region: oscillatory time sweep test using 1 Hz, 1.0 Pa, for 15 min (LINCOLN et al., 2023). The flow behavior of CNSL was described in a continuous flow stress sweep test, 0,1 to 100 Pa, 25 °C, 10 min. The Ostwald de Waele model was used, Eq. (4.2):

$$\tau = K \times \bar{y}^{n} \quad (4.2)$$

where τ is the shear stress in Pa, K is the flow consistency index, $\bar{y}$ is the shear rate in s^{-1}, and n is the flow behavior index.

The formulations and CNSL were also evaluated in a continuous flow time sweep test using tension of 5.0 Pa at 105 °C for 5 min.

4.3.3.2 Differential scanning calorimetry (DSC)

Differential scanning calorimetry (DSC) was conducted on phenolic resins using a Q20 instrument (TA Instruments, New Castle, United States) to evaluate their calorimetric behavior in a nitrogen atmosphere (50 mL min^{-1}). Three milligrams of the resin underwent testing at a temperature of 25 °C, employing a heating rate of 10 °C min^{-1}, reaching a maximum temperature of 200 °C. The sample was placed inside an aluminum capsule and hermetically sealed.

4.3.3.3 Infrared spectroscopy with Fourier transformation (FTIR)

The characterization of functional groups in the organic materials of CNLS and different formulations of phenolic resin was performed using a spectrometer (PerkinElmer®, FT-IR/NIR FRONTIER Waltham, MA, U.S.) using an attenuated total reflectance (ATR) accessory with ZnSe crystal surfacewith a resolution of 4 cm^{-1}. The infrared absorption spectrum range was from 400-4000 cm^{-1} with 32 scans.

4.3.3.4 High-performance liquid chromatography (HPLC)

The conditions used in HPLC followed the methodology described in the literature (OIRAM FILHO et al., 2018). HPLC analyses were accomplished on a Shimadzu chromatograph (LC-10AD) equipped with a photodiode array detector (SPD-M10A) at 280 nm. Separation was performed using a C18 column (150 × 4.6 mm × 5 μm, Shimadzu) with a mobile phase composed of 80% acetonitrile or methanol in water in the presence and absence of acetic acid (1% v/v) and with a flow rate of 1.5 mL min^{-1}. CNSL and resin samples were injected in aliquots of 20 μL at a concentration of 1 mg mL^{-1} methanol.

4.3.3.5 NMR analysis

NMR analyses were performed according to methodologies already described in the literature (ALVES FILHO et al., 2022). The NMR analyses were carried out on an Agilent 600 MHz spectrometer (Palo Alto, CA, USA) equipped with a 5 mm One Probe™ inverse detection (HF/^{15}N-^{31}P) probe using the PRESAT pulse sequence to suppress water (δ 4.75) at a temperature of 295 K. CNSL and the phenolic resin samples (10 mg) were solubilized in 600 μL of dimethyl sulfoxide (DMSO) (Cambridge Isotope Lab) and transferred to 5 mm NMR tubes. Component identification was performed through 2D NMR (g-HSQC and g-HMBC).

4.3.4 Production and characterization of particleboard

The fiber fraction of the particleboard consisted of PCNS and SBC (dry basis), with PCNS composed of 70% by mass of residual shell and 30% by mass of residual CNSL. Due to the presence of fibers, the addition of SCB can positively contribute to the mechanical properties of the particleboards. The resin load was prepared with 30% CNSL remaining from dried PCSN, benzoic acid and formaldehyde.

The mass fractions of the particleboards are presented in **Table 4.1**.

Table 4.1 – Mass composition of lignocellulose particleboards.

	PB25 [b]		PB50 [b]		PB75 [b]	
	(g)	(wt. %)	(g)	(wt. %)	(g)	(wt. %)
Residual shell	36.40 [a]	41.57 [a]	36.40 [a]	39.79 [a]	36.40 [a]	38.17 [a]
SCB	31.20 [a]	35.63 [a]	31.20 [a]	34.11 [a]	31.20 [a]	32.71 [a]
Resin Load	19.97	22.80	23.87	26.10	27.77	29.12

[a] Dry basis; [b] PB - Particleboard with a density of 800 kg m^{-3};

Source: Elaborated by the author

The mixtures containing the residual shell, SCB, and resin load were homogenized using an industrial mixer (Skymsen, BPS-05-N, China). After homogenization, the mixtures were molded and pressed in a hydraulic press (Marconi MA/098/50A/I). The polymerization reaction occurs during pressing. Particleboards were manufactured to the dimensions (300 mm x 300 mm x 5 mm) with nominal densities of approximately 800 kg m^{-3} (PB25, PB50 and PB75) and 1000 kg m^{-3} (HD25, HD50 and HD75) (ASTM, 2020).

To produce HD25, HD50 and HD75 particleboard, the mass fraction shown in **Table 4.1** was used. The process of producing particleboards was carried out in seven sequential stages of heating and pressing in a steel mold, as described: (1) Precure: Room temperature, 0.81 MPa, 5 min; (2) curing: 180 °C, 4.05 MPa, 3 min; (3) curing: 180 °C, 3.24 MPa, 2 min; (4) curing: 180 °C, 2.43 MPa, 1 min; (5) curing: 180 °C, 1.62 MPa, 1 min; (6) curing: 180 °C, 0.81 MPa, 1 min; and (7) curing: 180 °C, 0.81 MPa, 1 min. Finally, the particleboards were conditioned in a controlled environment at 25 ± 2 °C and moisture of 50 ± 5% for 24 h to ensure proper resin curing. Subsequently, the particleboards were cut to the needed test size according to standards and subjected to tests to evaluate their physical and mechanical properties (ASTM, 2020; ABNT, 2018). **Figure 4.1** illustrates the proposed production process for producing the particleboards.

Figure 4.1 − Proposed particleboard production process from cashew nutshells.

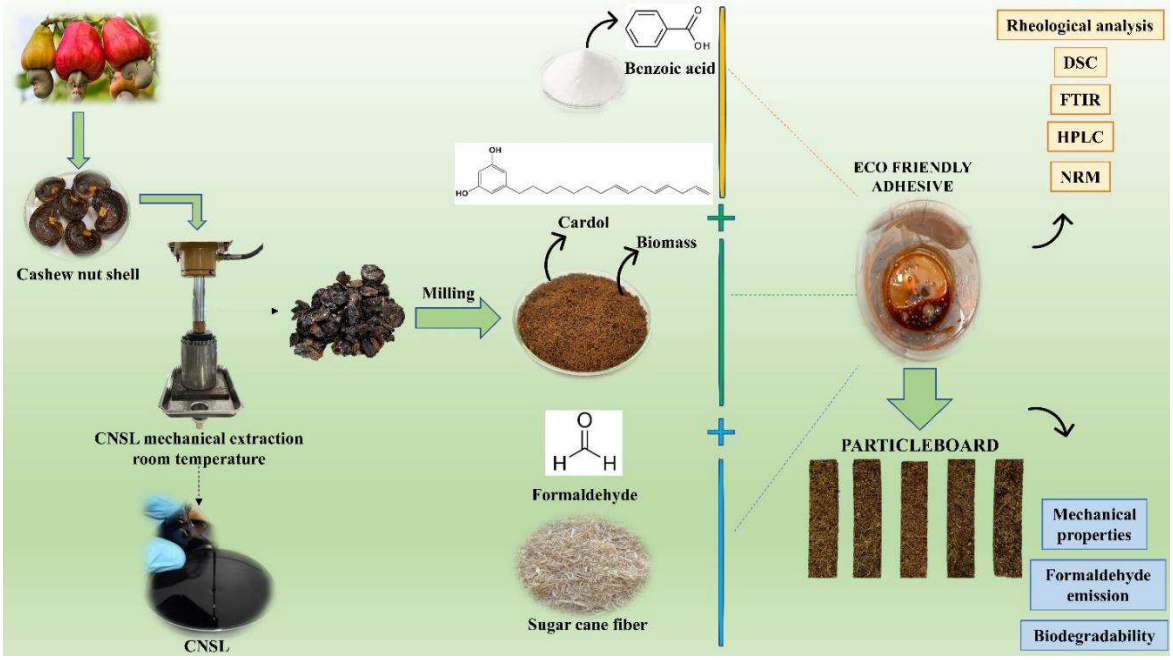

Source: Elaborated by the author

To determine the mechanical behavior, tension and flexural tests (in accordance with the ASTM 1037-12 standard) were conducted on a universal tester machine (DL3000, EMIC, São José dos Pinhais, Brazil) equipped with load cells of 5 kN (for tension) at an assay speed of 1 mm min^{-1} and a distance of 80 mm between the supporters (ASTM, 2020). The test results were expressed as the approximate average of five specimens for each particleboard composition, along with their respective standard deviations.

To evaluate the thickness swelling and water absorption, the particleboards were cut from the original piece, with dimensions of 50 x 50 mm (length x width), according to NBR 14810-2:2018 (ABNT, 2018). Tests were performed according to the D1037-2 standard in five repetitions for each treatment (ASTM, 2020).

Figure 4.2 illustrates the sections of particleboards PB25 (**Figure 4.2a**), PB50 (**Figure 4.2b**), and PB75 (**Figure 4.2c**), produced using different formaldehyde concentrations.

Figure 4.2 − Aspects of the lignocellulosic particleboards produced at 180 °C with different amounts of resin: PB25 (**a**), PB50 (**b**), and PB75 (**c**).

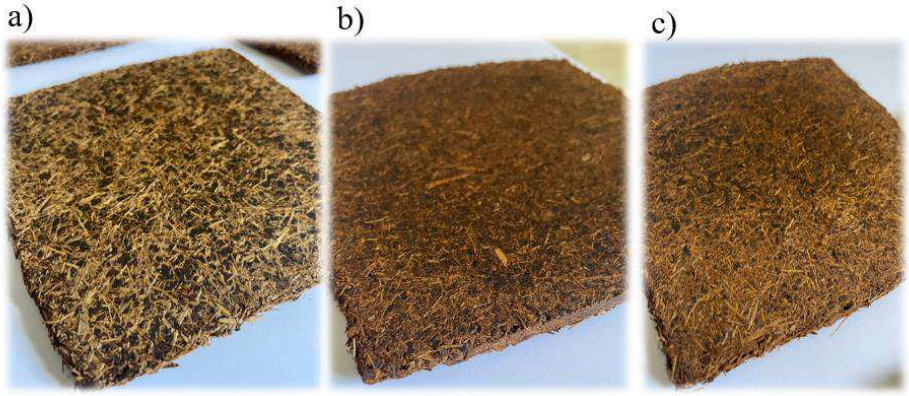

Source: Elaborated by the author

The PB50 and PB75 exhibited a uniform and consistent visual appearance, suggesting a homogeneous distribution of components in the matrix. Additionally, a variation in the color of the particleboards was noted, possibly related to the composition of the resin used. Samples with higher amounts of formaldehyde showed a darker shade, while the PB25 board, with a lower formaldehyde content, exhibited a lighter coloration. Despite the differences in color and resin distribution, all samples presented a smooth surface.

4.3.5 Formaldehyde emission of the particleboard

The determination of free formaldehyde emission from the particleboard was carried out in accordance with standard EN 717-3 (EUROPEAN COMMITTEE FOR STANDARDIZATION, 1996) using the flask method. The flask method is a well-established methodology and adequately meets current requirements for quantitative analysis (FARIA et al., 2023). The particleboards were prepared and placed in 500 mL polyethylene containers containing 50 mL of distilled water. The containers were sealed and maintained at 40 °C for a period of 3 h, followed by cooling to reach room temperature. Formaldehyde was quantified using UV/VIS spectroscopy (DR6000, Hach, Colorado, USA) at 412 nm, employing the acetylacetone method.

4.3.6 Aerobic biodegradability test

The aerobic biodegradability assays were carried out according to the conditions described in the ISO 14851:2019 standard (ISO 14851, 2019) using an automatic Micro-Oxymax respirometer (Columbus Instruments, Ohio, USA). The tests were carried out in 250 mL bottles containing 50 mg of the sample, 5 g of inoculum, and 2 mL of distilled water. Approximately 1.5 mL of distilled water was added to the bottles every 72 h to maintain the ideal moisture in the mixture inoculum with the sample particleboards. The following samples were analyzed: PCSN, SCB, and particleboards (PB25, PB50, and PB75). The samples were subjected to grinding using a Pulverizette 16 hammer mill (Fritsch, USA) with a mesh opening of 2.0 mm. Control tests without substrate (negative control) and with starch (positive control) were conducted to evaluate microbial activity. The inoculum was a mixture of organic compost and worm humus (1:1, w/w), and the test bottles were incubated at 35 °C. The assay was conducted in triplicate.

The biodegradability content was calculated from the ratio between the CO_2 accumulated volume ($V_{CO2\ experimental}$) produced during the test period and the theoretical CO_2 volume ($V_{CO2\ theoretical}$) calculated from the CHNS analysis, as indicated in Eq. (4.3).

$$\%\text{Biodegradability} = \frac{V_{CO_2\ \text{experimental}}}{V_{CO_2\ \text{theoretical}}} x100 \tag{4.3}$$

4.4 Results and discussion

4.4.1 Physicochemical characterization of PCNS residue and SCB

The results of the physicochemical characterization of PCNS and SBC are reported in **Table 4.2**.

Table 4.2 − Physicochemical characterization of the pressed cashew nutshell and sugarcane bagasse, including proximate analysis and chemical composition.

	Pressed cashew nutshells	Sugarcane bagasse (MYTHILI et al., 2013)
Proximate analysis (wt.%)		
Moisture	6.34 ± 0.51 [a]	8.50 ± 1.20 [a]
Volatile matter	84.28 ± 0.84 [b]	70.04 ± 0.03 [b]
Fixed carbon	14.85 ± 0.82 [b, c]	13.44 ± 0.07 [b]
Ash	0.87 ± 0.02 [b]	8.02 ± 0.06 [b]
Bulk density (kg m^{-3})	180.20 ± 0.87 [b]	120.10 ± 5.93 [b]
Chemical composition (wt.%)		
Hemicellulose	70.42 ± 0.45 [d]	22.00 ± 3.60 [d]
Cellulose	11.78 ± 0.10 [d]	29.00 ± 4.80 [d]
Lignin	17.80 ± 0.15 [d]	21.00 ± 3.81 [d]

[a] Air dried basis. [b] Dry basis. [c] Calculated by difference. [d] Dry ash-free basis.
Source: Elaborated by the author

Based on the results obtained, no significant differences were identified in the moisture content, volatile matter, and fixed carbon content between the two biomass sources. It is important to note that, according to EN 312 specifications, the moisture content of particleboards should not exceed 5% to 13% (EUROPEAN COMMITTEE FOR STANDARDIZATION, 2010), emphasizing the need to monitor the moisture content of the raw material used.

Volatile matter consists of compounds that decompose during heating in the production of particleboard, releasing gases and vapors. This component also directly influences the density of the particleboard, as a higher amount of volatile matter results in less dense panels, which can compromise bending and tensile strength (LINCOLN et al., 2023). Therefore, it is preferable for volatile matter content to be low. On the other hand, regarding fixed carbon content, higher levels may be desirable to increase the density and weight of the panel, providing greater strength and durability.

However, a significant difference in ash content was observed between the raw materials. The available literature indicates that utilizing biomass with high ash content in the production of particleboard panels adversely affects their mechanical and physical

properties, leading to a decrease in the overall quality of the final product (MIGNEAULT; KOUBAA; PERRÉ, 2014). Thus, it is expected that the low ash content in PCNS residues positively influences the quality of the particleboard panel produced.

The ash content found in cashew nutshells is in agreement with values reported in the literature for other biomasses, such as coconut shells (0.17 wt.%) (NARCISO et al., 2021) and *Pinus oocarpa* (0.26 wt.%) (NARCISO et al., 2021). Additionally, PCNS and SCB contain 6.34 wt.% and 8.50 wt.% moisture, respectively, which is within the range (5.00 wt.% to 13.00 wt.%) recommended by Brazilian technical standard 14810-2 and European standard EN 312 for particleboard manufacturing (NBR-14810-2, 2018; European Committee for Standardization, 2010). The fixed carbon content in PCNS and SCB (14.85 wt.% and 13.44 wt.%, respectively) is comparable to the result found in the literature for rice husk (14.60 wt.%), which was used in particleboard production in other studies (Wilson et al., 2011; Lee et al., 2022)

The PCNS and SCB presented bulk densities of 180.2 kg m^{-3} and 120.1 kg m^{-3}, respectively. The bulk density of the PCNS is close to the value found in the literature for Pinus wood (186.04 kg m^{-3}) (LENIS; OSORIO; PÉREZ, 2013), which is used as a raw material to manufacture medium density particleboard. It is also noted that the bulk density of the SCB is close to that reported in the literature (119.09 kg m^{-3}) (KUMAR; UPADHYAY; MISHRA, 2019). The bulk density of the particles is a variable that influences the manufacturing costs and quality of particleboards (LEE et al., 2022b).

The analysis of the chemical composition of the biomass (**Table 4.2**) reveals a significant difference between PSCN and SBC. PSCN exhibits a considerably higher hemicellulose content (70.42%) compared to SBC (22.00%). However, the high hemicellulose content in PSCN may negatively affect the mechanical properties and dimensional stability of the particleboard due to its high hydrophilicity, making it susceptible to water absorption and hydrolytic degradation. The water is connected with OH groups on the hemicellulose (BAHAROĞLU et al., 2013). This degradation compromises the integrity of the hemicellulose polymer chains, resulting in a reduction in the flexural, tensile, and compressive strength of the particleboard.

On the other hand, SBC has higher contents of cellulose and lignin compared to PSCN. Cellulose contributes to the strength and stiffness of the panel, while lignin acts as a natural bonding agent, promoting cohesion between the particles (BAHAROĞLU et al., 2013). Due to the favorable chemical composition of SBC, the exclusive production of particleboard with PSCN becomes unfeasible, necessitating the addition of SBC. Preliminary tests confirmed that a proportion of 40% PSCN and 60% SBC in the panel manufacturing provided the best results in terms of mechanical properties.

This trend observed in the composition of SBC is similar to the values found in other biomass sources, such as bamboo biomass (DING et al., 2023), which is composed of hemicellulose (15.00–30.00 wt.%), cellulose (37.00–47.00 wt.%), and lignin (18.00–31.00 wt.%), as well as hardwood (poplar) (CAI et al., 2017) composed of hemicellulose (26.20–28.70 wt.%), cellulose (50.80–53.30 wt.%), and lignin (15.50–16.30 wt.%). The chemical composition of the studied residue aligned with biomass sources previously reported for particleboard production. This observation highlights the promising potential of mixing PCNS and SCB residues in the manufacturing of these boards, with the prospect of achieving improved adhesion and resistance properties.

4.4.2 Characterization of the phenol-formaldehyde adhesive

CNSL at 25 °C is a viscous and dark liquid. The viscosity in the oscillatory test was approximately 700 mPa.s, and the loss modulus (G” ≈ 3.2 Pa) was higher than the storage modulus (G’ ≈ 2.5 Pa); these characteristics are typical of viscous liquids (**Figure 4.3**). This value is close to the data reported in the literature, where the viscosity of CNSL at 25 °C varies between 150 and 600 mPa.s (RODRIGUES et al., 2011). Applying the Ostwald Waele model, the flow consistency index observed was K = 0.01033, and the flow behavior index was n = 1.076. The flow behavior index (n) indicates the deviation from Newtonian behavior. Values of "n" greater than 1 indicate dilatant behavior in non-Newtonian fluids, characterized by a increase in apparent viscosity with an increase in shear rate. However, Cavalcante et al. (2018) found that the flow behavior (n) of CNSL ranges from 0.98 to 1.000 depending on the extraction method. A value of n less than 1 indicates that the fluid is pseudoplastic, while n equal to 1 is characteristic of Newtonian fluid behavior (CAVALCANTE et al., 2018).

Figure 4.3 − Oscillatory time sweep test of Cashew Nutshell Liquid, 1 Hz, 1.0 Pa, 25 °C, 15 min.

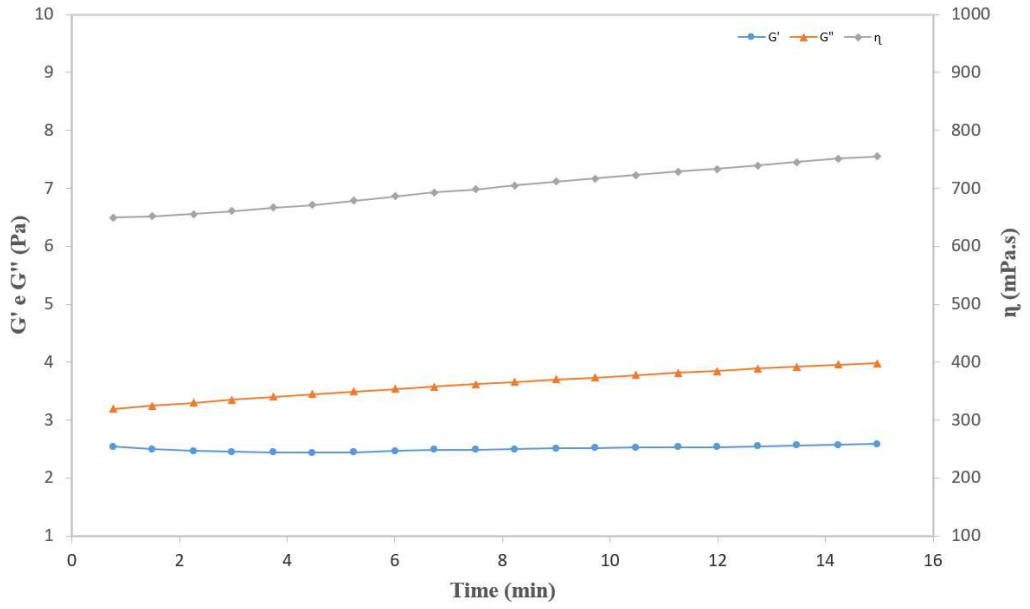

Source: Elaborated by the author

The isothermal rheograms at 105 °C for adhesive formulations F1, F2, F3 and for natural CNSL are shown in **Figure 4.4**, where the viscosity increases in the first 3 min of heating, probably due to the reaction between CNSL phenolic compounds and formaldehyde. In addition, it appears that the CNSL has a viscosity of approximately 7 mPa.s, which proves that the increase in viscosity in adhesive formulations characterizes the occurrence of a chemical reaction of formaldehyde polymerization with the components phenolics present in the CNSL. The increase in temperature to 105 °C resulted in a decrease in the viscosity of CNSL, which aligns with findings from previous studies (PRASANNAKUMAR et al., 2023).

Figure 4.4 − Relationship between viscosity (mPa.s) versus time (min) for adhesive formulations F1, F2, F3; and for the natural CNSL at 105 °C.

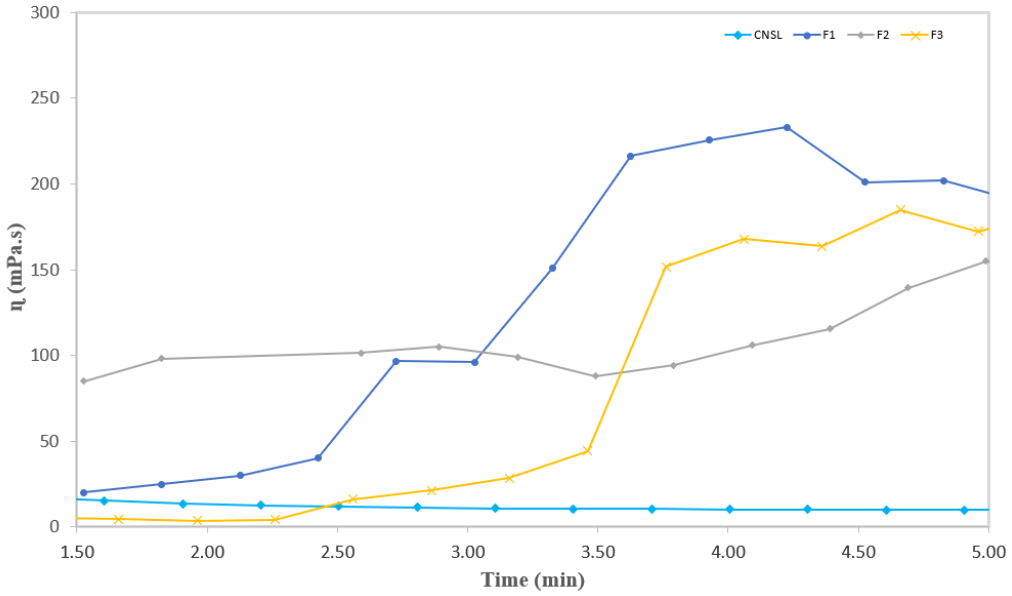

Source: Elaborated by the author

The DSC thermograms of resins F1, F2, and F3 identified a single exothermic peak within 4.5, 5, and 2.4 min, respectively, as shown in **Figure 4.5**. This thermal event is consistent with resin polymerization that occurred at a temperature of up to 120 °C. On the other hand, the absence of an exothermic peak in the CNSL thermogram implies that polymerization reactions do not occur solely through the application of heat to the pure liquid. This result was significant for confirming the adhesive polymerization during pressing (FARIA et al., 2023).

According to reports in the literature, commercial phenolic resins have polymerization reaction conversion temperatures of 128–151 °C (BOTELHO; SCHERBAKOFF; REZENDE, 2000). Thus, it is verified that the phenolic adhesives from CNSL present an advantage because the polymerization conversion temperature is lower than 120 °C (**Figure 4.5**). Ensuring safety and quality in the production of lignocellulosic panels necessitates consideration of polymerization time and temperature, given the thermal constraints of biomass and its degradation. Therefore, the mentioned thermal event was crucial for comprehending adhesive polymerization during biomass pressing.

Figure 4.5 − DSC thermograms of phenolic resins F1 (a), F2 (b), F3 (c) and CNSL (d).

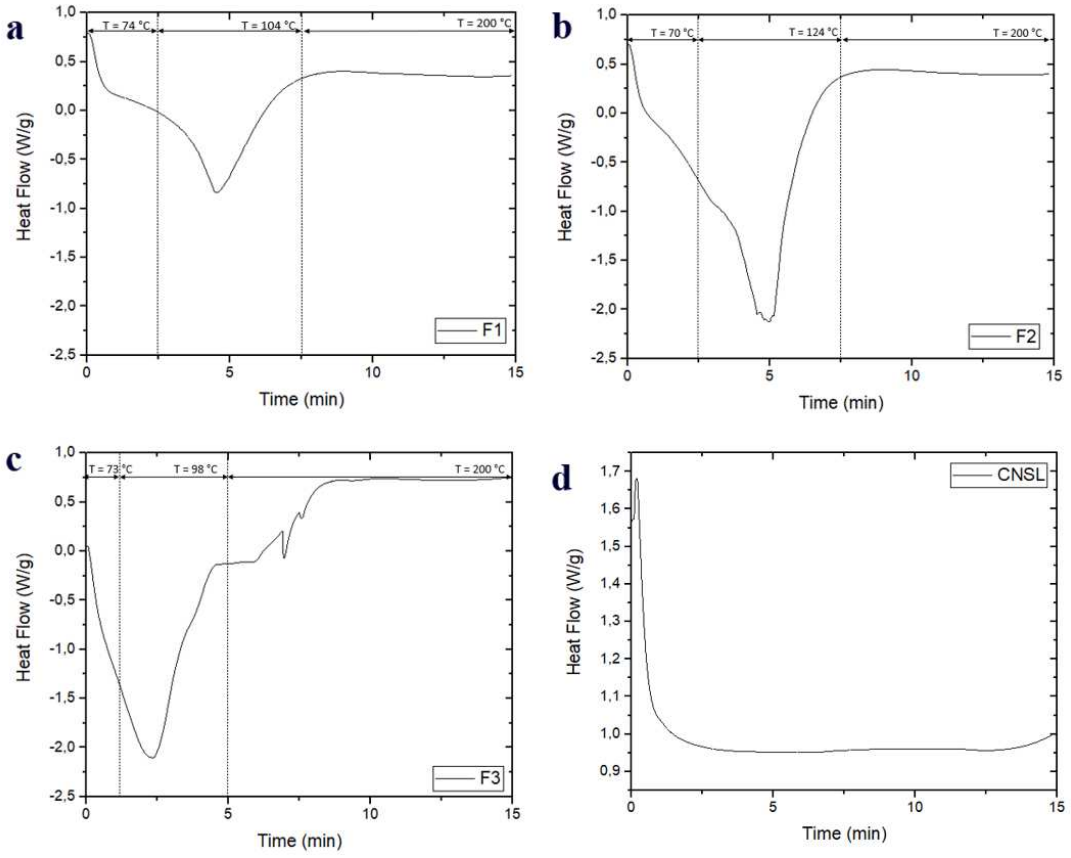

Source: Elaborated by the author

The FTIR spectra of the natural CSNL and adhesives F1, F2 and F3, whose formaldehyde concentrations were varied, are shown in **Figure 4.6**. When comparing the spectrum of natural CNSL with isolated cardol found in the literature, it is possible to observe the presence of similar wavelengths at 3400 cm^{-1} (Phenolic –OH), 3023 cm^{-1} (C=C–H), 2930 cm^{-1} (C–H), and 1609 cm^{-1} (C=C, Aromatic) (MAKWANA et al., 2022).

The spectra of resins F1, F2 and F3 maintain the characteristic broad absorption band between 3700 and 3100 cm^{-1}, which is attributed to the OH stretching of the hydroxyl groups present in the CNSL (SHAHZAIB et al., 2023). Furthermore, at 3023 cm^{-1} the intensity of the aliphatic stretch CH (sp2) was not affected, indicating that the condensation reaction of the CNSL components occurred through a substitution reaction on the hydroxymethyl groups (CH_2OH) and not by double bonds in the side chain.

Figure 4.6 − FTIR spectra of the natural CNSL and of the synthesized adhesives (F1, F2 and F3) from the CNSL varying the concentration of formaldehyde in acidic medium.

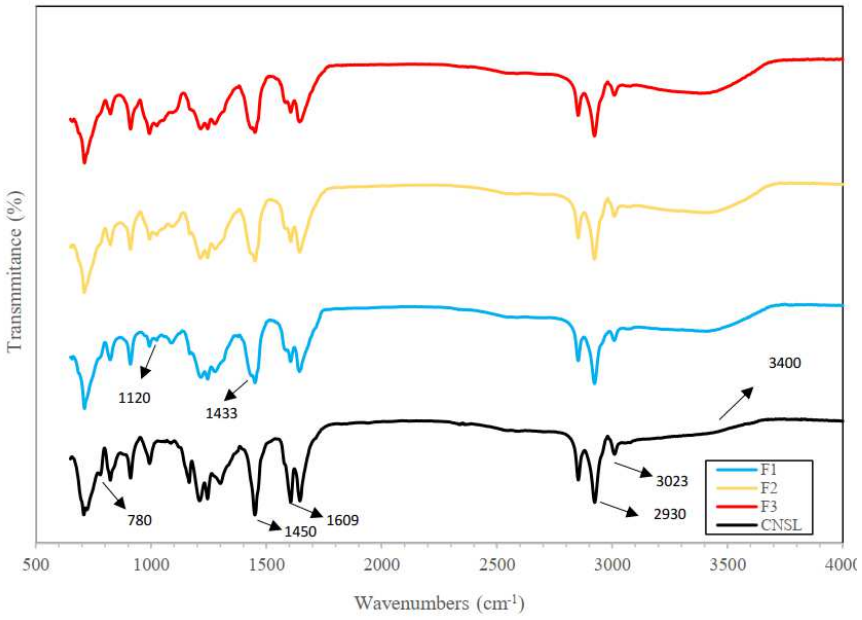

Source: Elaborated by the author

The absorptions observed at 2930 and 2851 cm^{-1} are associated with the CH_2 and CH_3 bonds present in the hydrocarbon chain, respectively (SANTOS et al., 2021). The peaks at 1609 and 1450 cm^{-1} correspond to skeletal vibrations of aromatic bonds (–C=C–), which showed the main changes in the analyzed spectra (MWAIKAMBO; ANSELL, 2001).

In the structure of the resins, the methylene group (CH_2) is considered the most relevant since it interconnects two phenolic units, which is evidenced by the signal observed at 1433 cm^{-1} (ZHANG et al., 2021). At 1120 cm^{-1}, a signal corresponding to aliphatic CO binding appears (SUDPRASERT et al., 2023). Additionally, alterations in the substitution of the aromatic rings can be inferred through the peaks at 780 cm^{-1}, corresponding to the CH deformation of the hydrogen atoms adjacent to an aromatic ring, indicating the substitution of the meta positions in the benzene ring (DA SILVA et al., 2023).

The chromatographic profiles are presented in **Figure B1** of the Appendix B to identify the alkylphenols present in natural CNSL (**Figure B1a**) and in phenolic adhesives

F1 (**Figure B1b**), F2 (**Figure B1c**) and F3 (**Figure B1d**). Peaks were identified based on their retention times, and the chromatographic profile of natural CNSL is shown in **Figure B1a**. Triene cardol (I) was identified at a retention time of 3.47 min, dieno cardol (II) at 4.65 min, and anacardic acids triene (III), diene (IV), and monoene (V) at 6.35, 9.00, and 14.16 min, respectively. The elution order follows the sequence reported in the literature for the components of CNSL (MORAIS et al., 2017; OIRAM FILHO et al., 2019). By comparing the HPLC chromatograms of CNSL with those of adhesives F1 (**Figure B1b**), F2 (**Figure B1c**), and F3 (**Figure B1d**), it can be seen that cardol is only present in the CNSL. This suggests that it participates in the chemical reaction with formaldehyde. **Table B1** of the Appendix B contains information on retention time and area (%) and height (%) for each chromatogram.

As a schematic proposal for the steps of the cardol polymerization reaction in CNLS in the presence of benzoic acid shown in **Figure 4.7**, cardol (**1**) reacts with electrophilic formaldehyde in its protonated form. After that, the electrophile reacts with the nucleophilic phenolic ring, leading to the production of a methyl-ol ketone-type intermediate (**2a** and **2b -** Step I) that gives rise to methylol-phenols (**3a** and **3b**), as commonly reported in novolac-type reactions (Kavita et al., 2016; Nair, 2004; Rego et al., 2004). From that point onwards, successive condensation reactions of the intermediate species and reaction repetitions of steps I - III lead to the formation and growth of the cardol-based resin (**4**).

Figure 4.7 – Schematic polymeric synthesis of phenol-alkyl-formaldehyde (**4**) using CNSL-sourced cardol and benzoic acid at 105 °C.

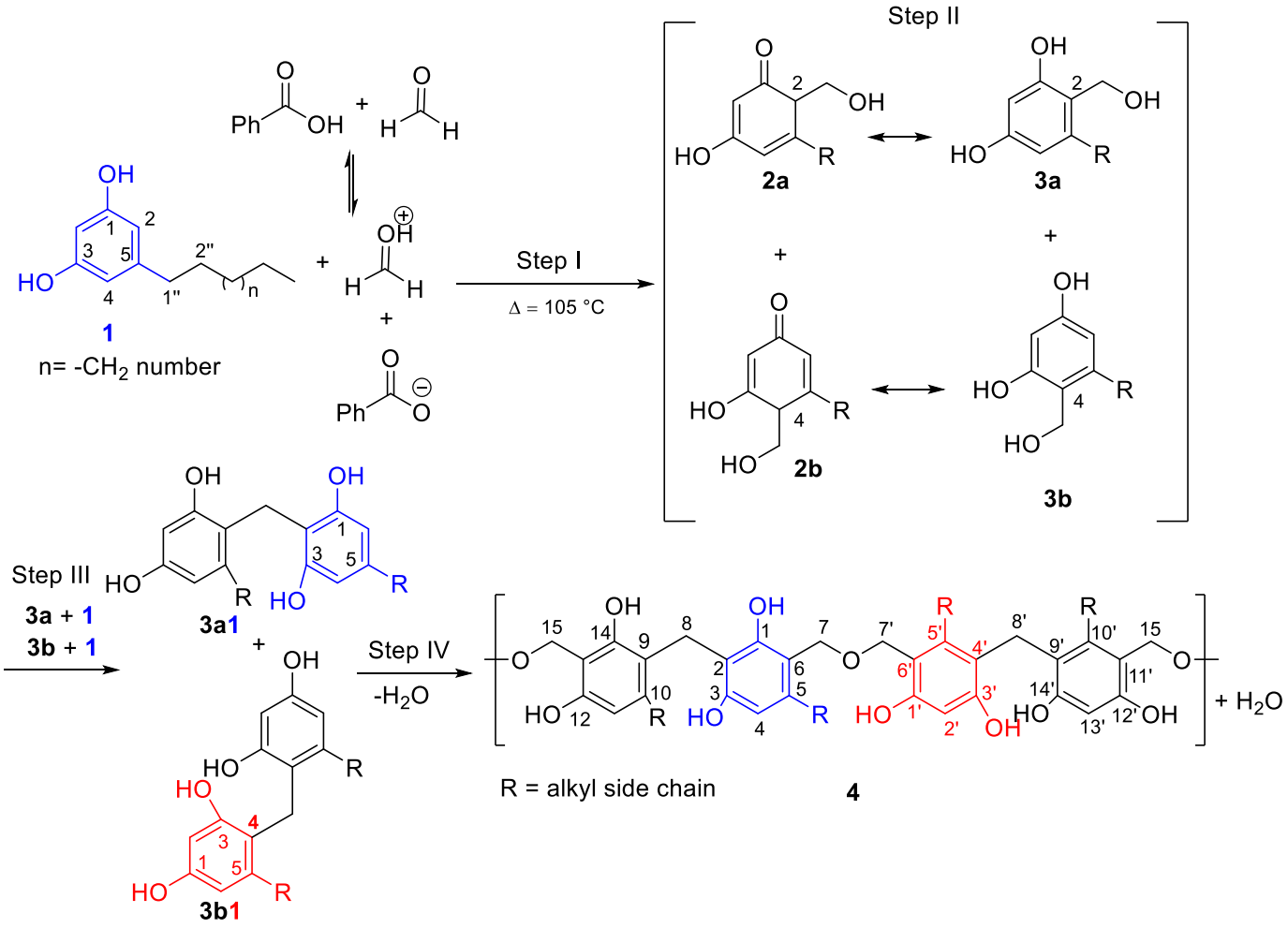

Source: Elaborated by the author

The ^{13}C NMR spectra in **Figure 4.8** highlight the resonance signals belonging to the cardol and the phenol-alkyl-resins in F1, F2 and F3. As we can see in **Figure 4.8a**, the disappearance of the resonance signals related to C-1' and C-2' around δ_C ~ 35.1 ppm from the cardol-alkyl chain present in the starting material indicates the occurrence of the reaction. When comparing the ^{13}C NRM spectra of the F1, F2, and F3 adhesives with the ^{13}C spectrum of cardol (MAKWANA et al., 2022), it is noted that the chemical shift of the alkyl chain in cardol manifests within a wide range of values, ranging from δ 40 to 10 ppm, which suggests a possible relationship with the chemical shift signals at δ_C 35.4 and 33.7 ppm in natural

CNSL. The alteration of the alkyl chain signals in adhesives F1, F2, and F3 occurs as a result of changes in the chemical environment (SILVERSTEIN; BASSLER; MORRILL, 1991).

Figure 4.8 – ^{13}C NMR spectra from CNSL, F1 (1: 0.25, w/w), F2 (1: 0.50, w/w) and F3 (1: 0.75, w/w): before and after the DMSO-*d*6 signal at 39.5 ppm (**a** and **b**), respectively.

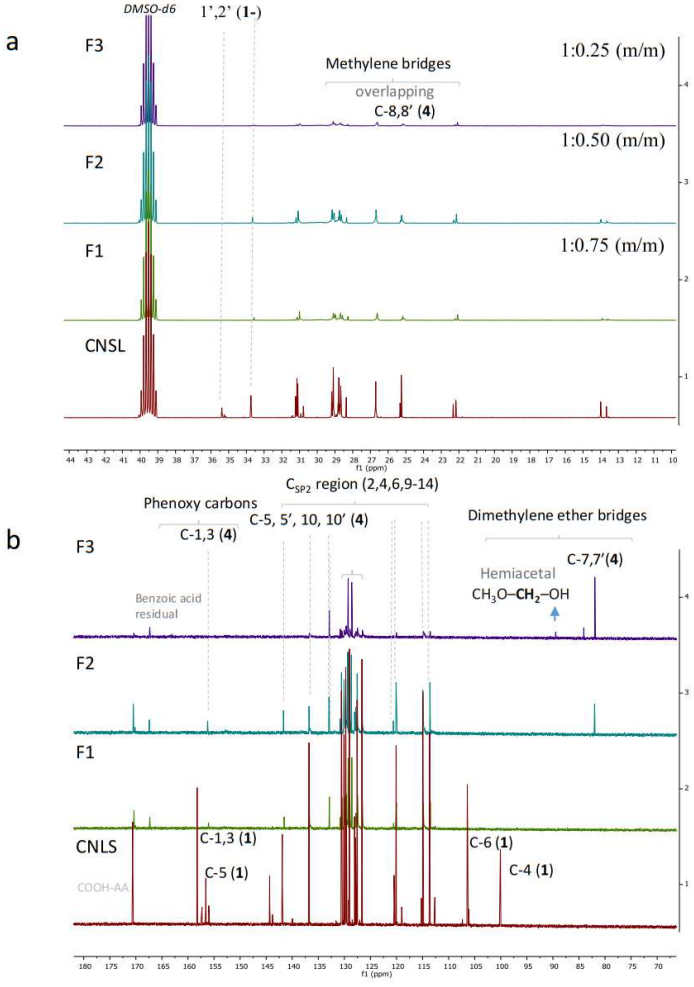

Source: Elaborated by the author

However, new resonance signals are observed due to the formation of a new product. Specifically, the carbon peaks at approximately δ_C 158 and 81.2 ppm were due to the presence of phenoxy carbons (C-1,3, 1',3', 12,14, 12',14') and dimethylene ether bridges (C-7,7'), respectively, as reported in the literature (REGO et al., 2004b). The resin ^{1}H-^{13}C heteronuclear correlation spectrum provides visual evidence of resin structure production and allowed us to assign signals close to the methylene groups formed in the final product.

The expansion of the contour map of gHSQC (**Figure 4.9a**) and gHMBC (**Figure 4.9b**) highlights the resonance signals belonging to the methylene bridges (δ_C ~ 24.9–36.1 ppm) and dimethylene ether bridges (δ_C ~ 80.1 ppm, C-7,7') of phenol-alkyl-resins in F3. As there is a large number of methylene carbons in the resin, a high rate of overlap was observed in the region of the alkyl resonance signals (~ 30–32 ppm) (MAJI; URAKAWA; INOUE, 2014).

The correlations in gHMBC (**Figure 4.9b**) indicate the presence of methylene hydrogens (δ_H 2.75 and 2.98 ppm - C-8 and 8') interacting at long distances with carbons typical of phenoxy-aromatic groups (δ_C 162.3 ppm and 148.7 ppm - C-14 and 3') and Csp2-aromatic rings (δ_C 124.0 ppm and 126 ppm numbered in the structure as C-9 and 10). The protons of the methylene ether moiety (δ_H 3.78 - C-7') couple with aromatic carbons at δ_C 138.1 ppm.

In addition, the appearance of a long-distance correlation in the HMBC contour map (**Figure 4.9b**) in the carbon region between δ_C 89.5–93.7 ppm in F3 corroborates the formation of a hemiacetal adduct from formaldehyde, as reported in the literature (LUBCZAK, 2015).

Figure 4.9 − Selected regions from *g*HSQC (**a**) and *g*HMBC (**b**) contour map (δH 3.5 – 9.5 ppm) showing single bond (HSQC) and multiple bond (HMBC) key correlations of F3-phenol-alkyl-resin highlighting the long-distance linkages of the methylene bridges (*δ*H ~ 2.75–2.98 ppm) and dimethylene ether bridges (*δ*H ~ 3.75–3.79 ppm).

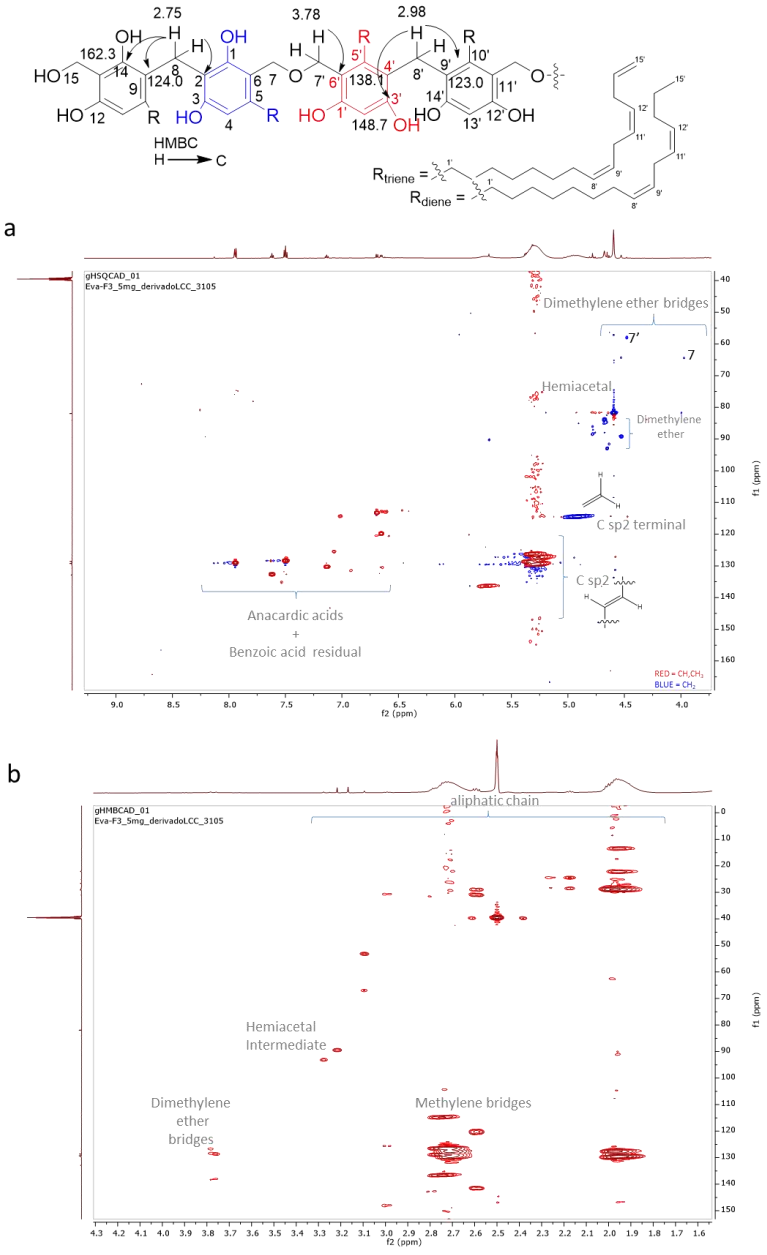

Source: Elaborated by the author

4.4.3 Particleboard from PCNS

Table 4.3 presents the values of the mechanical properties of the particleboard with different concentrations of phenolic resins. The particleboard has a density range of 762 ± 41 to 1076 ± 24 kg m^{-3}. Notably, the particleboard with higher formaldehyde content (PB75 and HD75) has a lower density, which can be attributed to variations in the volatile content of the phenolic resin during the heating stage at 180°C in the manufacture of these panels (JIA et al., 2020).

Table 4.3 – Mechanical properties of particleboards manufactured with PCNS using eco-friendly phenolic resin in different concentrations of formaldehyde.

Sample	Density (kg m^{-3})	Modulus of rupture (MPa)	Modulus of elasticity (MPa)	24 h thickness swelling (%)	24 h water absorption (%)
PB25	799 ± 40	6.4 ± 2.2	769 ± 172	39.5 ± 1.5	60.0 ± 5.5
PB50	796 ± 33	6.6 ± 2.2	707 ± 71	28.1 ± 3.8	40.2 ± 1.2
PB75	762 ± 41	6.5 ± 1.2	855 ± 203	20.8 ± 1.2	42.6 ± 2.3
HD25	1076 ± 24	13.1 ± 2.4	1127 ± 327	16.3 ± 4.4	38.7 ± 6.1
HD50	1063 ± 12	12.9 ± 2.3	1466 ± 100	16.4 ± 0.2	21.1 ± 3.1
HD75	1002 ± 43	14.3 ± 2.2	1866 ± 531	15.0 ± 0.5	29.2 ± 3.2

Source: Elaborated by the author

The effect of increasing density on the mechanical properties of the particleboard panels was investigated, and the results are presented in **Table 4.3**. The average MOR and MOE values varied from 6.4 to 14.3 MPa and from 707 to 1866 MPa, respectively. The increase in particleboard density resulted in an increase in the MOR value, making the HD25, HD50, and HD75 panels compliant with the specifications of EN312 and NBR 14810-2 (12 MPa) (European Committee for Standardization, 2010; ABNT, 2018).

Compared with the literature, particleboards with a density of up to 800 kg m^{-3} exhibit higher MOR values than bean husk particleboards (4.4 MPa) (FARIA et al., 2023) using a cardanol-formaldehyde adhesive. On the other hand, panels with a density of approximately 1000 kg m^{-3} fall within the range of values observed in rice husk panels (9.7 - 16.8 MPa)

using formaldehyde and boric acid-based bio adhesives (BUDDI; VALLI; SAXENA, 2022). A greater amount of compacted material and greater proximity of the particles result in a greater load transfer between them, making the particleboard more resistant to bending efforts.

Regarding the modulus of elasticity (MOE), it is important to note that the HD75 particleboard recorded a higher value, reaching 1866 MPa. However, it is worth mentioning that this value falls below the requirement specified by NBR 14810-2 (ABNT, 2018), which demands an MOE of 1950 MPa. When compared to particleboards made from other agricultural materials, such as a blend of chestnut bark and poplar (75%/25%, w/w), we observed that the MOE of the particleboard was 1850 MPa (LIANG; WU; XU, 2021), a value very close to the MOE of the HD75 particleboard, which was 1866 MPa.

The MOR and MOE of particleboards are inherently linked to the characteristics of the raw materials used in their production, particularly the content of cellulose and hemicellulose (LIANG; WU; XU, 2021). It is worth noting that initial attempts to manufacture particleboard panels using only cashew nutshells and phenolic resin were unsuccessful. This is partly because cashew nutshells have a relatively low cellulose content, approximately 11.78%, while sugarcane bagasse has a significantly higher proportion of this component, approximately 29.00%, which contributes to the increase in MOR and MOE values in particleboard panels.

From the analysis of particleboard water absorption data and swelling, it was verified that the particleboard (HD25, HD50 and HD75) met the thickness absorption/swelling requirement of up to 16% established by European standard EN 312 (EUROPEAN COMMITTEE FOR STANDARDIZATION, 2010). Furthermore, it was observed that particleboards with higher density performed better in terms of water absorption and swelling thickness compared to the lower-density particleboards. This information may be relevant for the selection of suitable materials for certain applications, considering the needed physical properties.

4.4.4 Formaldehyde emission

Table 4.4 outlines the formaldehyde emission outcomes for particleboards PB25, PB50, and PB75, which were fabricated using a biobased phenol-formaldehyde resin. Particleboards PB25, PB50, HD25, and HD50 were categorized as class E1, exhibiting formaldehyde emissions below 8 mg/100 g oven-dry board. In contrast, PB75 and HD75 particleboards were classified as class E2, with formaldehyde emissions ranging between 8 and 30 mg/100 g oven-dry board, as stipulated in EN 13986 (EN 13986+A1, 2015). Also, there was a marginal rise in formaldehyde emissions observed in particleboards with higher density in comparison to those with lower density.

Table 4.4 – Formaldehyde released from particleboards using the flask method, as specified in EN 717-3 (1996).

Sample	Adhesive composition (CNSL : formaldehyde) (w/w)	Formaldehyde release (mg/100 g oven-dry board)
PB25	1 : 0.25	1.97
PB50	1 : 0.50	5.46
PB75	1 : 0.75	9.52
HD25	1 : 0.25	2.15
HD50	1 : 0.50	6.76
HD75	1 : 0.75	12.58

Source: Elaborated by the author

The polyphenols inherent in cashew nutshell (LIANG; WU; XU, 2021) and CNSL undergo a reaction with formaldehyde when phenol-formaldehyde resin is employed as an adhesive in particleboard production. This reaction leads to the formation of stable methylene (CH_2) bridges, thereby reducing formaldehyde emissions from the resulting panels. Formaldehyde emission levels were observed to be lower in particleboard panels manufactured with cardanol-formaldehyde resin compared to those produced with urea-formaldehyde, as reported in literature (FARIA et al., 2023).

Comparing the particleboards in this study with the control particleboard manufactured with urea-formaldehyde (emitting approximately 16 mg/100 g oven-dry board) (FARIA et al., 2023), PB25, PB50, and PB75 particleboards showed reductions of 88%, 66%, and 41%, respectively. Meanwhile, the HD25, HD50, and HD75 particleboards exhibited reductions of 87%, 58%, and 21%, respectively. This highlights the potential of the eco-friendly adhesives in this study, which can be attractive to the wood industry, meeting the requirements for commercialization and use in indoor environments.

4.4.5 Aerobic biodegradability

Figure 4.10 illustrates the variation in biodegradability over time for PCNS, SCB and different particleboards (PB25, PB50 and PB75). A gradual increase in biodegradability content was observed over the degradation period (30 days). The evaluation of particleboards manufactured from eco-friendly resin revealed that the biodegradability content of PB25 (30%) was the highest, followed by PB50 (21%) and PB75 (20%). These results suggest an association between the increased concentration of formaldehyde in the phenolic resin and the decreased biodegradability of the particleboards. This relationship was expected since formaldehyde is toxic to many organisms and can inhibit the activity of microorganisms involved in the biodegradation of other compounds, thus slowing the biodegradation process (ZHANG et al., 2023).

Furthermore, PCNS (60%) exhibited higher biodegradability than SCB (45%). This is because cashew nutshell has a chemical composition that is less recalcitrant to biodegradation, as it contains a lower lignin content (AZMI; OTHMAN, 2023). Specifically, cashew nutshell contains approximately 11.78% cellulose, 70.42% hemicellulose, and 17.80% lignin, while SCB contains approximately 39.00% cellulose, 20.25% hemicellulose, and 23.5% lignin (MAZABA et al., 2022; OTHMAN et al., 2023). This difference in chemical composition explains the greater ease of biodegradation observed in cashew nutshell compared to SCB.

Figure 4.10 − Variation in biodegradability over time for PCNS, SCB and different lignocellulosic particleboards (PB25, PB50 and PB75).

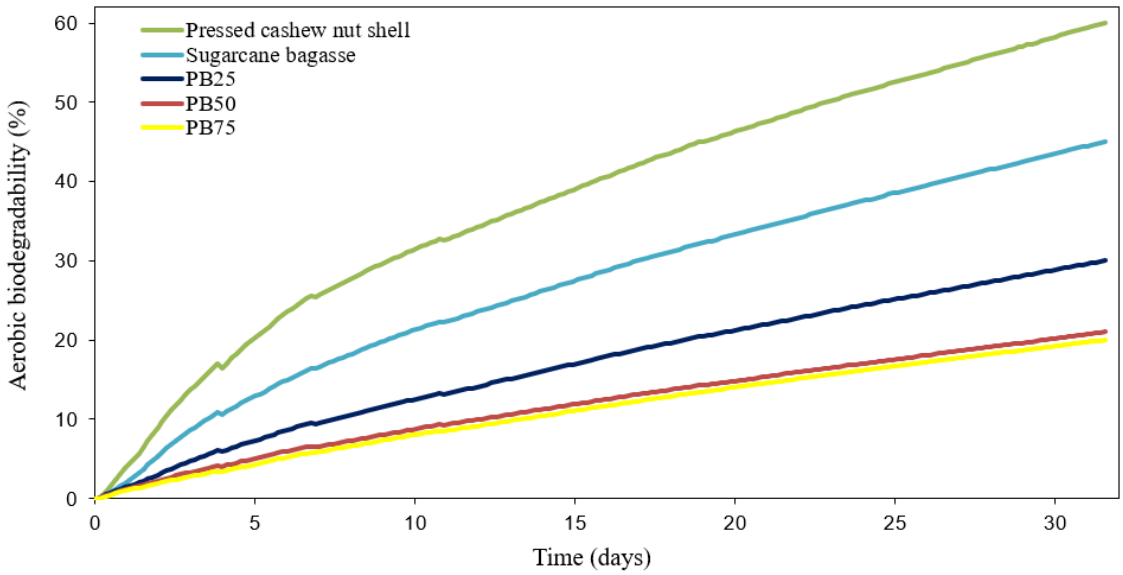

Source: Elaborated by the author

4.5 Conclusion

The study contributed to the existing knowledge on sustainable particleboard production from underutilized and widely available lignocellulosic residues, by presenting a pioneering investigation into the production of particleboards from pressed cashew nutshell and a bio-based resin derived from residual CNSL. Additionally, it paves the way for utilizing this technological route to valorize cashew nutshell residue in the context of the circular economy. The results of the lignocellulosic composition analysis indicated that the mixture of PCNS (high hemicellulose content) and SCB (higher cellulose and lignin contents) shows promising potential to produce particleboards with superior strength properties. The phenolic resin derived from cashew nutshell oil exhibited temperature-dependent crosslinking behavior, with a lower polymerization conversion temperature compared to commercial phenolic resins. The PB25, PB50, HD25, and H50 panels were classified as class E1, with formaldehyde emissions below 8 mg/100 g oven-dry board, while the PB75 and HD75 panels were categorized as class E2. Biodegradability increased gradually during the degradation period, and particleboards produced with higher formaldehyde concentrations showed lower

biodegradability. Based on the evaluated mechanical properties, particleboards with a higher density (HD25, HD50 and HD75) are considered more promising for practical applications. Overall, these results support the potential use of cashew nutshell oil-derived formaldehyde adhesives with PCNS and SCB in particleboard production. Additionally, a techno-economic evaluation using commercial software will be carried out, aiming to scale up the production of these lignocellulosic particleboards.

The pressing time of 14 min for particleboards exceeds the industrially acceptable time, indicating a reduced reactivity of the bio-based resin. Additionally, the particle size of sugarcane bagasse fibers influences resin distribution, which gives way for further research on improving the composite production process.

4.6 References

ABNT. NRB 14810-2 : Painéis de partículas de média densidade Parte 2: Requisitos e métodos de ensaio. In: **Associação Brasileira de Normas Técnicas**. Rio de Janeiro: [s.n.]. p. 71.

AKARANTA, O. Production of particle boards from bioresources. **Bioresource Technology**, v. 75, n. 1, p. 87–89, 2000.

ALVES FILHO, E. G. et al. 1H NMR and UPLC-HRMS-based metabolomic approach for evaluation of the grape maturity and maceration time of Touriga Nacional wines and their correlation with the chemical stability. **Food Chemistry**, v. 382, n. July 2021, p. 132359, jul. 2022.

ALVES, J. L. F. et al. Demonstrating the Suitability of Tamarind Residues to Bioenergy Exploitation Via Combustion Through Physicochemical Properties, Performance Indexes, and Emission Characteristics. **BioEnergy Research**, v. 13, n. 4, p. 1308–1320, dez. 2020.

ALVES, J. L. F. et al. Physicochemical properties, pyrolysis kinetics, thermodynamic parameters of activation, and evolved volatiles of mango seed waste as a bioenergy feedstock: A potential exploration. **Thermochimica Acta**, v. 725, n. April, p. 179519, jul. 2023.

ARAUJO, J. T. C. DE et al. Development of anacardic acid-loaded zein nanoparticles: Physical chemical characterization, stability and antimicrobial improvement. **Journal of Molecular Liquids**, v. 332, p. 115808, jun. 2021.

ASTM. D3176-15: Standard Practice for Ultimate Analysis of Coal and Coke. In: **Annual Book of ASTM Standards**. West Conshohocken: ASTM International, 2015. p. 1–4.

ASTM. E873-82: Standard Test Method for Bulk Density of Densified Particulate Biomass Fuels. In: **Annual Book of ASTM Standards**. West Conshohocken: [s.n.].

ASTM. D1037-12: Standard Test Methods for Evaluating Properties of Wood-Base Fiber and Particle Panel Materials. In: **Annual Book of ASTM Standards**. West Conshohocken: ASTM International, 2020.

AZMI, A. A.; OTHMAN, S. A. **Future of sugarcane bagasse paper: A review**. 2023. Available at: <http://aip.scitation.org/doi/abs/10.1063/5.0117103>

BAHAROĞLU, M. et al. Effects of anatomical and chemical properties of wood on the quality of particleboard. **Composites Part B: Engineering**, v. 52, p. 282–285, set. 2013.

BOTELHO, E. C.; SCHERBAKOFF, N.; REZENDE, M. C. Rheological analysis of the phenolic and furfuryl resins used in the carbon materials processing. **Materials Research**, v. 3, n. 2, p. 19–23, 2000.

BRITO, K. J. S. et al. Sustainable plasticizer from agroindustrial waste for natural rubber compounds: Influence on the curing system and compound properties. **Journal of Elastomers and Plastics**, v. 0, n. 0, p. 1–17, 2023.

BUDDI, T.; VALLI, S.; SAXENA, K. K. Manufacturing and Evaluation of Mechanical Properties for Rice Husk Particle Board Using IoT. **Indian Journal of Engineering & Materials Sciences**, v. 29, n. December, p. 750–754, 2022.

CAI, J. et al. Review of physicochemical properties and analytical characterization of lignocellulosic biomass. **Renewable and Sustainable Energy Reviews**, v. 76, n. March, p. 309–322, set. 2017.

CARRIER, M. et al. Thermogravimetric analysis as a new method to determine the lignocellulosic composition of biomass. **Biomass and Bioenergy**, v. 35, n. 1, p. 298–307, jan. 2011.

CAVALCANTE, J. M. et al. Extração de LCC por Prensagem da Casca da Castanha de Caju Originária de Minifábrica para a Obtenção de Ácidos Anacárdicos. **Embrapa Agroindústria Tropical**, p. 4–12, 2018.

CHANDRAN, A. et al. Particle board using rice husk and coconut fibre . Tablero de partículas con cáscara de arroz y fibra de coco. **Sustainability, Agri, Food and Environmental Research**, v. 11, n. 10, 2022.

CORY-SLECHTA, D. A.; MERRILL, A.; SOBOLEWSKI, M. Air Pollution–Related Neurotoxicity Across the Life Span. **Annual Review of Pharmacology and Toxicology**, v. 63, n. 1, p. 143–163, 2023.

CRUZ REINA, L. J. et al. Compressed fluids and Soxhlet extraction for the valorization of compounds from Colombian cashew (Anacardium occidentale) nut shells aimed at a cosmetic application. **Journal of Supercritical Fluids**, v. 192, n. July 2022, 2023.

DA SILVA, K. T. et al. Bio-based novolac resins from cashew nut processing waste: Alternative resource for the development of high-value sustainable products. **Journal of Applied Polymer Science**, v. 140, n. 13, 5 abr. 2023.

DE MELLO SANTOS, V. H. et al. Towards a green industry through cleaner production development. **Environmental Science and Pollution Research**, v. 29, n. 1, p. 349–370, 21 jan. 2022.

DING, Z. et al. A thermo-chemical and biotechnological approaches for bamboo waste recycling and conversion to value added product : Towards a zero-waste biorefinery and circular bioeconomy. **Fuel**, v. 333, n. P2, p. 126469, 2023.

DORIEH, A. et al. Recent developments in the performance of micro/nanoparticle-modified urea-formaldehyde resins used as wood-based composite binders: A review. **International Journal of Adhesion and Adhesives**, v. 114, n. October 2021, p. 103106, 2022.

EN 13986+A1. EN 13986 + A1 : 2015 : Wood-based panels for use in construction. Characteristics, evaluation of conformity and marking. In: **European Standart**. [s.l: s.n.].

EUROPEAN COMMITTEE FOR STANDARDIZATION. EN 717-3: 1996 : Wood-based panel products - Determination of formaldehyde release by flash method. In: **European Standard**. Brussels: [s.n.].

EUROPEAN COMMITTEE FOR STANDARDIZATION. EN 312:2010 : Particleboards - Specifications. In: **European Standard**. Brussels: [s.n.].

EUROPEAN COMMITTEE FOR STANDARDIZATION. EN ISO14851:2019 : Determination of the ultimate aerobic biodegradability of plastic materials in an aqueous medium - Method by measuring the oxygen demand in a closed respirometer. In: **European Standart**. Brussels: [s.n.]. p. 1–32.

FAO. **FAOSTAT : statistical Cahew nuts (crops production).** Available at: <available: https://www.fao.org/faostat/en/#data/QV>. Accessed on: February 24, 2023.

FARIA, D. L. et al. Cardanol-based adhesive with reduced formaldehyde emission to produce particleboards with waste from bean crops. **Environmental Science and Pollution Research**, v. 30, n. 16, p. 48270–48287, 9 fev. 2023.

FARINASSI, R. et al. Use of sugarcane bagasse for particleboard production. **Key Engineering Materials**, v. 634, p. 163–171, 2015.

GUPTA, S.; GUPTA, G. K.; MONDAL, M. K. Thermal degradation characteristics, kinetics, thermodynamic, and reaction mechanism analysis of pistachio shell pyrolysis for its bioenergy potential. **Biomass Conversion and Biorefinery**, v. 12, n. 11, p. 4847–4861, 25 nov. 2022.

JIA, L. et al. Formaldehyde and VOC emissions from plywood panels bonded with bio-oil phenolic resins. **Environmental Pollution**, v. 264, p. 114819, 2020.

JOSINO, J. B. et al. Changes of respiratory system in mice exposed to PM4.0 or TSP from exhaust gases of combustion of cashew nut shell. **Environmental Toxicology and Pharmacology**, v. 56, p. 1–9, dez. 2017.

KAVITA; MORDINA, B.; TIWARI, R. K. Thermal and mechanical behavior of poly(vinyl butyral)-modified novolac epoxy/multiwalled carbon nanotube nanocomposites. **Journal of Applied Polymer Science**, v. 133, n. 17, p. 1–11, 2016.

KOUASSI, B. G. et al. Preparation of Activated Carbon from Cashew Nut Shells for Water Purification. **Russian Journal of Non-Ferrous Metals**, v. 61, n. 1, p. 112–118, 29 jan. 2020.

KUMAR, M.; UPADHYAY, S. N.; MISHRA, P. K. A comparative study of thermochemical characteristics of lignocellulosic biomasses. **Bioresource Technology Reports**, v. 8, n. April, p. 100186, 2019.

KYEI, S. K. et al. Natural polyhydroxy resins in surface coatings : a review. **Journal of Coatings Technology and Research**, v. 19, n. 3, p. 775–794, 2022.

LEE, S. H. et al. Particleboard from agricultural biomass and recycled wood waste: a review. **Journal of Materials Research and Technology**, v. 20, p. 4630–4658, set. 2022a.

LEE, S. H. et al. Particleboard from agricultural biomass and recycled wood waste: a review. **Journal of Materials Research and Technology**, v. 20, p. 4630–4658, set. 2022b.

LENIS, Y. A.; OSORIO, L. F.; PÉREZ, J. F. Fixed bed gasification of wood species with potential as energy crops in Colombia: The effect of the physicochemical properties. **Energy Sources, Part A: Recovery, Utilization and Environmental Effects**, v. 35, n. 17, p. 1608–1617, 2013.

LIANG, J.; WU, J.; XU, J. Low-formaldehyde emission composite particleboard manufactured from waste chestnut bur. **Journal of Wood Science**, v. 67, n. 1, p. 21, 5 dez. 2021.

LINCOLN, A. et al. Resins and fibers from sugarcane bagasse to produce medium - density fiberboard. **Biomass Conversion and Biorefinery**, n. 0123456789, 2023.

LUBCZAK, R. Thermally resistant carbazole-modified phenol-formaldehyde resins. **Polymer International**, v. 64, n. 9, p. 1163–1171, 2015.

LUBI, C. M.; THACHIL, E. T. Particleboard from cashew nut shell liquid. **Polymer - Plastics Technology and Engineering**, v. 46, n. 4, p. 393–400, 2007.

LUBI, M. C.; THACHIL, E. T. Cashew nut shell liquid (CNSL) - A versatile monomer for polymer synthesis. **Designed Monomers and Polymers**, v. 3, n. 2, p. 123–153, 2000.

MAJI, S.; URAKAWA, O.; INOUE, T. The structure and viscoelasticity of novolac resins. **Polymer Journal**, v. 46, n. 9, p. 584–591, 28 set. 2014.

MAKWANA, K. et al. Cardol: Cashew nut shell liquid (CNSL) - derived starting material for the preparation of partially bio-based epoxy resins. **European Polymer Journal**, v. 166, n. December 2021, p. 111029, mar. 2022.

MANJUNATH, B. et al. Potential utilization of regional cashew nutshell ash wastes as a cementitious replacement on the performance and environmental impact of eco-friendly mortar. **Journal of Building Engineering**, v. 66, n. October 2022, p. 105941, 2023.

MARI, E. L.; VILLENA, E. M. Properties of particleboard from wood wastesand cashew nut shell residue. **Philippine Journal of Science**, v. 145, n. 1, p. 1–8, 2016.

MAZABA, A. V. et al. Multi-response optimization of acid hydrolysis in sugarcane bagasse to obtain high xylose concentration. **Biomass Conversion and Biorefinery**, n. 0123456789, 2022.

MGAYA, E. B. M. J. E. Chemical Valorization of Cashew Nut Shell Waste. **Topics in Current Chemistry**, v. 376, n. 2, p. 1–15, 2018.

MIGNEAULT, S.; KOUBAA, A.; PERRÉ, P. Effect of Fiber Origin, Proportion, and Chemical Composition on the Mechanical and Physical Properties of Wood-Plastic Composites. **Journal of Wood Chemistry and Technology**, v. 34, n. 4, p. 241–261, 2 out. 2014.

MORAIS, S. M. et al. Anacardic acid constituents from cashew nut shell liquid: NMR characterization and the effect of unsaturation on its biological activities. **Pharmaceuticals**, v. 10, n. 1, p. 1–10, 2017.

MWAIKAMBO, L. Y.; ANSELL, M. P. Cure characteristics of alkali catalysed cashew nut shell liquid-formaldehyde resin. **Journal of Materials Science**, v. 36, n. 15, p. 3693–3698, 2001.

MYTHILI, R. et al. Characterization of bioresidues for biooil production through pyrolysis. **Bioresource Technology**, v. 138, p. 71–78, 2013.

NAIR, C. P. R. Advances in addition-cure phenolic resins. **Progress in Polymer Science (Oxford)**, v. 29, n. 5, p. 401–498, 2004.

NARCISO, C. R. P. et al. Potential for the Use of Coconut Husk in the Production of Medium Density Particleboard. **Waste and Biomass Valorization**, v. 12, n. 3, p. 1647–1658, 2021.

NGUYEN, D. L. et al. Production of wood - based panel from recycled wood resource : a literature review. **European Journal of Wood and Wood Products**, n. 0123456789, 2023.

OIRAM FILHO, F. et al. Development and Validation of a Reversed Phase HPLC Method for Determination of Anacardic Acids in Cashew (Anacardium occidentale) Nut Shell Liquid. **Journal of Chromatographic Science**, v. 56, n. 4, p. 300–306, 2018.

OIRAM FILHO, F. et al. Productivity of a preparative high-performance liquid chromatography isolation of anacardic acids from cashew nut shell liquid. **Separation Science Plus**, v. 2, n. 6, p. 192–199, 2019.

PIZZI, A.; IBEH, C. C. Phenol–Formaldehydes. In: **Handbook of Thermoset Plastics**. [s.l.] Elsevier, 2014. p. 13–44.

PRASANNAKUMAR, P. et al. Influence of techniques on synthesizing cashew nut shell oil as a prospective biolubricant on its physicochemical, tribological, and thermal behaviors. **Journal of Cleaner Production**, v. 401, n. March, p. 136717, maio 2023.

REGO, R. et al. Fully quantitative carbon-13 NMR characterization of resol phenol-formaldehyde prepolymer resins. **Polymer**, v. 45, n. 1, p. 33–38, 2004a.

REGO, R. et al. Fully quantitative carbon-13 NMR characterization of resol phenol–formaldehyde prepolymer resins. **Polymer**, v. 45, n. 1, p. 33–38, jan. 2004b.

RENAN, L. et al. Progress in Organic Coatings Development of BPA-free anticorrosive epoxy coatings from agroindustrial waste. **Progress in Organic Coatings**, v.

139, n. November 2019, p. 105449, 2020.

RODRIGUES, F. H. A. et al. Comparison between physico-chemical properties of the technical Cashew Nut Shell Liquid (CNSL) and those natural extracted from solvent and pressing. **Polímeros**, v. 21, n. 2, p. 156–160, 13 maio 2011.

RUSCH, F. et al. Particleboard experimental production with bamboo, pine and mate for one product of new applications. **Maderas-Cienc Tecnol**, v. 25, n. SE-Article, p. 1–24, 2023.

SANTANA, D. A. R. et al. Pelletizing of lignocellulosic wastes as an environmentally friendly solution for the energy supply: insights on the properties of pellets from Brazilian biomasses. **Environmental Science and Pollution Research**, v. 28, n. 9, p. 11598–11617, mar. 2021.

SANTOS, J. et al. Impact of condensation degree of melamine-formaldehyde resins on their curing behavior and on the final properties of high-pressure laminates. **Proceedings of the Institution of Mechanical Engineers, Part C: Journal of Mechanical Engineering Science**, v. 235, n. 3, p. 484–496, 2021.

SERRA, D. S. et al. Archives of Environmental & Occupational Health Lung injury caused by occupational exposure to particles from the industrial combustion of cashew nut shells : a mice model. **Archives of Environmental & Occupational Health**, v. 76, n. 1, p. 1–11, 2021.

SHAHZAIB, A. et al. Superhydrophobic Mn (II) -coordinated technical cashew nut shell liquid-based bactericidal and corrosion-resistant advanced polyurethane coatings. **Materials Today Communications**, v. 35, n. April, p. 105947, 2023.

SILVERSTEIN, R. M.; BASSLER, G. C.; MORRILL, T. C. **Spectrometric Identification of Organic Compounds**. [s.l: s.n.].

SOUZA, N. DE O. et al. Cashew nut shell liquids: Antimicrobial compounds in prevention and control of the oral biofilms. **Archives of Oral Biology**, v. 133, n. July 2021, p. 0–9, 2022.

SUDPRASERT, P. et al. Synthesis and characterization of novel bio-based epoxy

polymers derived from natural phenolic compound. **Journal of Applied Polymer Science**, v. 140, n. 9, 5 mar. 2023.

TAPAS, M. B. B. R. et al. Role of cashew shell biochar on EMI shielding behaviour of carbon fibre – epoxy nanocomposites in E , F , I and J band – microwave frequencies. **Biomass Conversion and Biorefinery**, p. 375–382, 2023.

UNDP. **Sustainable Development Goals**. Available at: <https://www.undp.org/sustainable-development-goals?utm_source=EN&utm_medium=GSR&utm_content=US_UNDP_PaidSearch_Brand_English&utm_campaign=CENTRAL&c_src=CENTRAL&c_src2=GSR&gclid=CjwKCAiAheacBhB8EiwAItVO25DuoyH1lxaCvq7E9rRzGOAVENA4-QTC98fo538m7CcY_5XHRyIH0B>. Accessed on: March 3, 2023.

WILSON, L. et al. Thermal characterization of tropical biomass feedstocks. **Energy Conversion and Management**, v. 52, n. 1, p. 191–198, 2011.

YADAV, R. Development of low formaldehyde emitting particle board by nano particle reinforcement. **Journal of Applied and Natural Science**, v. 9411, p. 1187–1197, 2021.

ZHANG, S. et al. Layer-by-layer assembly of polystyrene/ag for a highly reproducible sers substrate and its use for the detection of food contaminants. **Polymers**, v. 13, n. 19, 2021.

ZHANG, Z. et al. Evaluation methods of inhibition to microorganisms in biotreatment processes : A review. **Water Cycle**, v. 4, n. February, p. 70–78, 2023.

Chapter 5

Modeling of particleboard production using SuperPro Designer

5 MODELING OF PARTICLEBOARD PRODUCTION USING SUPERPRO DESIGNER

5.1 Abstract

The conversion of agricultural waste into valuable products is a critical effort in the pursuit of a clean and sustainable environment. The aim of this study was to conduct a simulation modeling of particleboard production considering scale-up, using the SuperPro Designer software. The first stage, involving the extraction of CNSL, was modeled using a press and a mill. The second stage, consisting of the mixing and pressing of the raw material, was represented by a mixer and a heated press. Sensitivity analysis was conducted to examine the effect of scale-up on economic measures (unit cost, ROI, IRR, NPV, payback time, gross margin and revenue). The simulation results demonstrate that particleboard production is viable starting from a feed rate of 91.77 kg h^{-1}, with a production rate of 5 units per hour, a unit cost of $32.63, and a minimum investment payback period of 4 years.. Additionally, it was observed that scaling up would have a significant impact on the NPV, IRR, and ROI, resulting in a lower unit cost of particleboard panels.

5.2 Introduction

Globally, there is a growing pursuit of sustainable alternatives that can contribute to the environment. The integration of Sustainable Development Goals (SDGs) has become an encouraged practice in companies worldwide (D'ADAMO; GASTALDI; MORONE, 2022). Within this context, the circular economy emerges as a crucial alternative, providing the opportunity to reuse waste and significantly reduce environmental impact (HERRADOR et al., 2022). The promotion of the circular economy is not only aligned with the fundamental principles of sustainability but also offers practical solutions to address environmental challenges, fostering a more efficient and conscious cycle in resource management (DE OLIVEIRA; OLIVEIRA, 2023).

The cashew culture is widespread in several countries around the world, including India, Thailand, Vietnam, Indonesia, and Brazil (FAO, 2024). In Brazil, the economic exploitation of this culture is concentrated in the Northeast region. The cashew nut is widely

consumed due to its nutritional value (AKOMOLAFE; OYELEYE; OBOH, 2022), and there is a growing appreciation among consumers for the appearance and size of the nuts. Small factories have incorporated significant advancements in equipment and processes, enabling the production of whole and light-colored cashew nuts in higher proportions and with better quality.

According to the Brazilian Agricultural Research Corporation (EMBRAPA), a small factory has the capacity to process approximately 180 tons of cashew nuts per year (EMBRAPA, 2024). However, the extraction for consumption generates a considerable amount of shell, corresponding to approximately 65-70% of the total weight of the whole cashew nut (MOHOD; KHANDETOD; POWAR, 2008; (DA SILVA; DE BRITO; FERREIRA, 2023). This residue poses significant challenges in terms of environmental management and can be explored as an opportunity for the implementation of sustainable practices, such as the manufacturing of products like particleboards. The production of particleboards from cashew nutshell presents notable advantages, standing out as a simplified process that utilizes agroindustrial waste as a substitute for wood and features a biologically based resin. The resin is manufactured from the CNSL (Cashew Nutshell Liquid) found in the cashew nutshells, eliminating the need for complex processes of extraction or separation of chemical compounds (DE PAIVA et al., 2024).

Despite the presence of some studies in the literature on the reuse of cashew nutshells, such as production of bioenergy through pyrolysis (DE PAIVA et al., 2024), biochar (RAJENDRAN et al., 2024), particleboards (DE PAIVA et al., 2024) and briquette (RAMESH, 2022), the analysis of the technical and economic feasibility of large-scale production is still limited. In this context, the SuperPro Designer stands out as a suitable tool for designing a technical and economic feasibility study for particleboard production, based on laboratory data. With a comprehensive library of unit operations and equipment, such as reactors, filters, centrifuges, and dryers, the software provides support for modeling, simulating, and evaluating the project both technically and economically (AKKOYUNLU et al., 2024). Additionally, its versatility, ease of use, and ability to integrate simulation, economic evaluation, and optimization within a single platform make it particularly effective for establishing the process line, providing equipment costs, utilities, accessories, and other

essential data to achieve the study's objectives. Recent studies employ the SuperPro software for process modeling related to the production of various compounds, such as structural bioadhesive derived from glycerol (YANG; ROSENTRATER, 2019), bacterial cellulose (DE ARAÚJO E SILVA et al., 2020), biogas (HARUN et al., 2019; GAN et al., 2024), polyhydroxybutyrate polymer (AKKOYUNLU et al., 2024), biohydrogen and biomethane (DENG et al., 2024). Technology transfer from academia to industry is essential to optimize and make industrial projects viable.

In the context of evaluating the economic feasibility of industrial-scale particleboard production from cashew nutshells, a critical component involves conducting a thorough technical-economic analysis (TEA). TEA integrates technical parameters and economic factors into project analysis, offering a systemic perspective that informs decision-making regarding long-term investments (YANG; ROSENTRATER, 2019). Crucial methods such as Return on Investment (ROI), Net Present Value (NPV), and sensitivity analysis play a fundamental role in assessing the viability of the proposed study. These parameters are essential for scaling up the production process, as they assess economic feasibility, inform financial decisions, and help identify risks and project robustness. However, it is important to note that the literature currently lacks studies on the industrial-scale production of particleboard from cashew nutshells, highlighting the need for comprehensive analysis to guide future large-scale implementations.

Considering the innovative potential of producing particleboard from cashew nutshells, this study aims to investigate the economic feasibility of this production on an industrial scale using simulation with SuperPro Designer software. The study provides a solid foundation for the implementation of a sustainable production process that, once applied, can be exported to other cashew-producing countries, promoting circular economy and sustainability on a global scale.

5.3 Advancements in Particleboard Production and Economic Analysis

5.3.1 Particleboard Production from Cashew Nutshells

The studied process is based on laboratory-scale data and involves the production of particleboards using cashew nutshells and an ecofriendly phenolic resin derived from

residual CNSL. The cashew nutshells used in this project are sourced from Embrapa Agroindústria Tropical in Pacajus - CE, Brazil. These shells underwent pressing to extract the CNSL under a pressure of 5 MPa. The experimental conditions employed were adapted from a previous study of the mechanical extraction of CNSL (OIRAM FILHO et al., 2019), at room temperature. The pressed cashew nutshell (PCNS) was crushed using a Pulverisette 16 hammer mill (Fritsch, USA) and passed through a 2.0 mm mesh. PCNS composed of 70% by mass of residual shell and 30% by mass of residual CNSL.

Furthermore, sugarcane bagasse (SCB) was added to achieve the desired densities and consequently improve the mechanical properties of the particleboards (FARINASSI et al., 2015). The SCB was dried at 105 °C for 12 h. Afterwards, it was processed in a mill (Fritsch, Pulverizette 25) to reduce the particle size to 10 mm before being used in the production of particleboards.

In the production process of particleboards, the mixtures containing the residual shell, SCB, and resin load were molded and pressed. The resin load was prepared with 30% CNSL remaining from dried PCNS, benzoic acid and formaldehyde. The resin formulation was prepared at a mass ratio of 1:0.50 for CNSL and formaldehyde (37 wt.% purity, Labsynth, São Paulo, Brazil). The polymerization reaction occurs during pressing. Particleboards were manufactured to the dimensions (1.20 m x 2.20 m x 12.00 mm) with nominal densities of approximately 1000 kg m^{-3} (HD50) (DE PAIVA et al., 2024). Mass fraction of the particleboard is presented in **Figure 5.1**.

Figure 5.1 − Graphical representation of the balance of components employed in the production of particleboards.

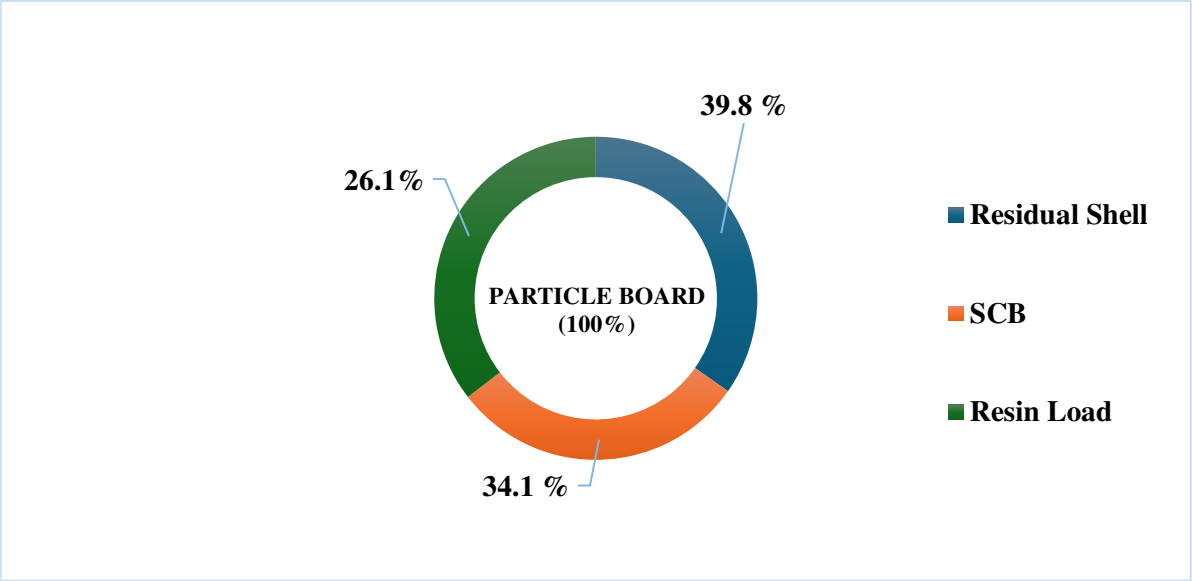

Source: Elaborated by the author

The process of producing particleboards was carried out in seven stages of heating and pressing in a steel mold using a hydraulic press (Marconi MA/098/50A/I), as described: (1) Precure: Room temperature, 0.81 MPa, 5 min; (2) curing: 180 °C, 4.05 MPa, 3 min; (3) curing: 180 °C, 3.24 MPa, 2 min; (4) curing: 180 °C, 2.43 MPa, 1 min; (5) curing: 180 °C, 1.62 MPa, 1 min; (6) curing: 180 °C, 0.81 MPa, 1 min; and (7) curing: 180 °C, 0.81 MPa, 1 min. Finally, the particleboards were prepared and kept in a controlled environment with a temperature of 25 ± 2 °C and moisture of 50 ± 5% for 24 h. Subsequently, the particleboards were cut to the needed test size according to standards and subjected to tests to evaluate their physical and mechanical properties (ASTM, 2020; ABNT, 2018).

Based on a previous study conducted by the research group, the production of particleboards was carried out on a laboratory scale, with the aim of identifying and optimizing the ideal processing conditions (DE PAIVA et al., 2024). **Figure 5.2** illustrates the laboratory process for producing the particleboards.

Figure 5.2 − Optimized laboratory process for production particleboards using cashew nutshells.

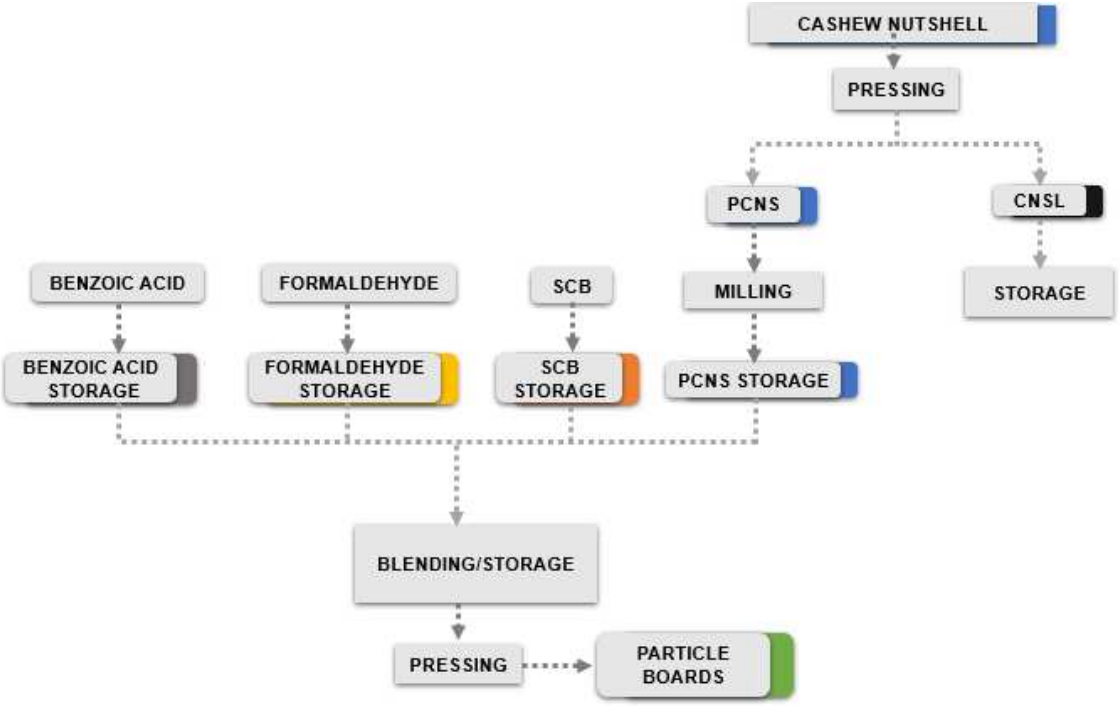

Source: Elaborated by the author

5.3.2 Modeling Particleboard Production

A production process model for particleboard panels from cashew nutshell was established using SuperPro Designer® software, version 10 (Intelligen Inc., New Jersey, USA). This software performs mass and energy balances to support the calculation of economic indicators in each simulation.

Data regarding the production conditions of particleboard panels at the laboratory scale were used based on a preliminary study (DE PAIVA et al., 2024). This includes information on temperature (180 °C), polymerization reaction time (14 min), quantity of inputs at each stage (Table 5.1), and pressure (4.05 MPa) for pressing the inputs per batch.

Table 5.1 − Raw materials on a dry basis used in the production of particleboards for analysis and optimization of the manufacturing process.

Components (input)	Mass (Kg)
Residual Shell [a]	1.93
CNSL [a]	0.83
SCB [a]	1.65
Benzoic acid	0.02
Formaldehyde	0.41

[a] Dry basis

Source: Elaborated by the author

As shown in **Figure 5.3**, the cashew nutshell undergoes a pressing process through a press (SP-101) and is subsequently ground in the knife mill (GR-101). Solid raw materials intended for the formulation of particleboards are stored in silos (SL-101, SL-102, SL-103), while formaldehyde is contained in a tank (V-102) and fed into the homogenization tank (V-103). Subsequently, the mixture is conveyed to the heated press (TP-101) through the duct (S-110). The simulation was conducted using a ratio of 1:0.5 for cashew nutshell liquid (CNSL) and formaldehyde.

Figure 5.3 − SuperPro Designer model for particleboard production process.

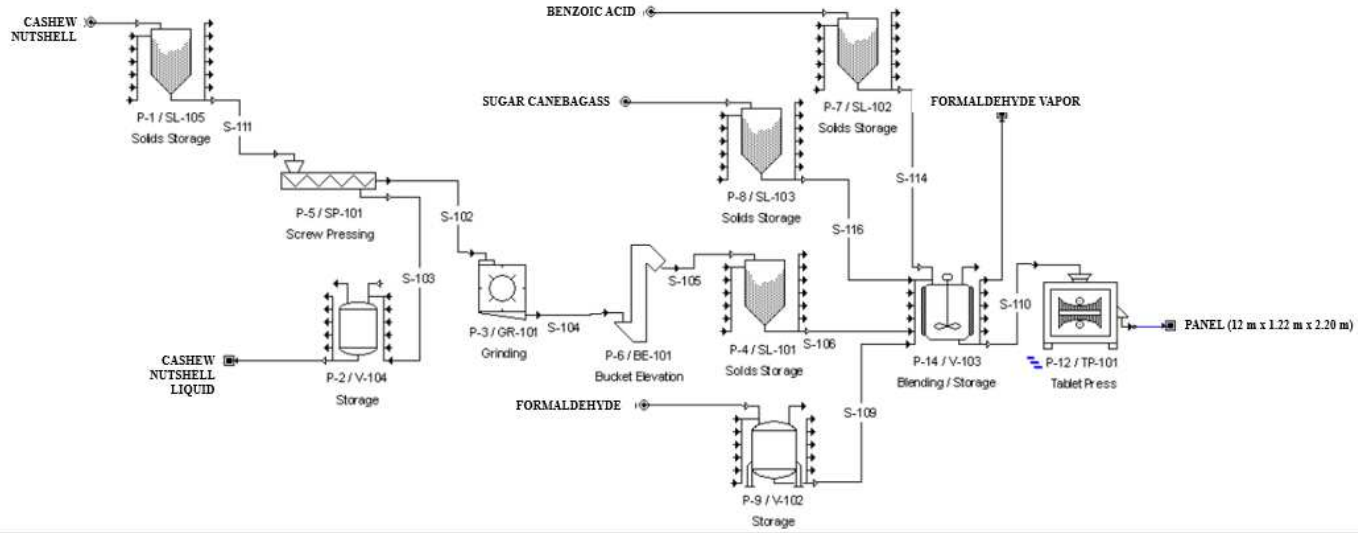

Source: Superpro Designer software

5.3.3 Economic Measures and Managerial Information Systems

The decision-making process regarding investments, especially when considering the long term, should be anchored in a managerial information system that enables the investor to anticipate opportunities or risks in the desired venture. Therefore, several economic measures were evaluated, such as unit cost, return on investment (ROI), gross margin, net present value (NPV), internal rate of return (IRR), payback time, and sensitivity analysis (CANIZALES et al., 2020; GAN et al., 2024). The Minimum Attractive Rate of the project is a requirement for calculating the Net Present Value (NPV). The simulator provides three standardized rate options: low (7% per year), medium (9.0% per year), and high (11.0% per year). In this simulation, the NPV calculation was performed using the rate corresponding to the lowest mentioned value, reflecting a lower risk associated with the project. In addition to the relevance of the investment analysis concepts, the selection of these measures is based on the results provided by the software. **Table 5.2** presents the financial metrics associated with the economic evaluation procedure.

Table 5.2 − Equations of cost indicators.

Cost Indicators	Equation	Number equation
Return on Investment	$ROI = \frac{\text{Annual Net Profit}}{\text{Total Fixed Capital Investment}} \times 100\%$	(5.1)
Net Present Value	$NPV = \sum DCF$	(5.2)
Discounted cash flow	$DCF = \sum_{1}^{n} \frac{CF_n}{(1+i)^n}$, Discounted Rate of Return, i’	(5.3)

Source: Elaborated by the author

5.3.4 Sensitivity Analysis

Sensitivity analysis was conducted to investigate the impact of varying raw material feeding costs on the overall economic model and to provide recommendations for optimizing the selling price of particleboards. The analysis considered waste feed rates ranging from 24.76 to 111.97 kg h^{-1} to evaluate a broad range of scenarios.

5.4 Results

Based on the input data related to unit operations, process yield, raw materials, etc., the software estimates equipment investment using cost correlations derived from various suppliers' internal data (YANG; ROSENTRATER, 2019). **Table 5.3** illustrates the simulation of the scale-up of the particleboard production process using pressed cashew nutshell (PCNS).

Table 5.3 − Scheduling of the particleboard production process using pressed cashew nutshell (PCNS).

Feedstock (kg h^{-1})	Feedstock (ton $batch^{-1}$)	Production Average (unit h^{-1})	Production (unit $batch^{-1}$)	Number (batches $year^{-1}$)	Batch duration (h)	Production Average (unit $year^{-1}$)	Unit cost ($)
111.97	6.57	6.13	360	455.00	58.68	163800	31.51
106.13	5.84	5.82	320	506.00	55.03	161920	31.80
99.46	5.11	5.45	280	568.00	51.38	159040	32.16
91.77	**4.38**	**5.03**	**240**	**649.00**	**47.73**	**136320**	**32.63**
82.98	3.65	4.55	200	664.00	43.99	133200	33.65
72.23	2.92	3.96	160	664.00	40.43	103840	35.26
59.55	2.19	3.26	120	665.00	36.78	79680	37.94
44.07	1.46	2.41	80	665.00	33.13	53200	43.29
24.76	0.73	1.36	40	665.00	29.48	26600	59.26

Source: Elaborated by the author

The cost of particleboard can vary significantly depending on the raw materials used and the specific properties required (NARCISO et al., 2021; WAHANE et al., 2023). Comparing scenarios with different residue feed rates (**Table 5.3**), it was observed that the lowest unit production cost of particleboard, at $31.51 per unit, was achieved when the feed rate used was 111.97 kg h^{-1}. This analysis was conducted considering particleboards with standard dimensions of 1.22 m x 2.44 m x 12 mm. Scale-up particleboard production provides significant benefits, such as increasing the number of batches per year and, consequently, higher average panel production. In comparison, commercial MDF panels, produced through

agglutination with synthetic resins and additives, have a unit cost of approximately $64.00 for the same dimensions (MUNICIPALITY, 2024). Thus, particleboard production demonstrates cost efficiency and competitiveness in the market, positioning it as a viable alternative.

Adeeb et al. concluded that using 20% recycled fiber, an estimated 20% reduction in the cost of virgin wood material and an energy saving of 7.8% in MDF production (ADEEB, EHSAN; KIM, TAE WOO; SOHN, 2018). The material cost, encompassing adhesive and wood chips for particleboard manufacturing, often represents over half of the total production cost. Agricultural biomass is estimated to be 50% cheaper than wood chips (LEE et al., 2022). Therefore, substituting wood chips with agro-industrial waste results in significant cost savings.

Table 5.4 − Summary of economic analysis for the particleboard plant

Feedstock (kg h^{-1})	**Feedstock (ton year^{-1})**	**Unit cost (U$)**	**NPV 7% (U$)**	**IRR Positive rate (U$)**	**Payback (years)**	**ROI (%)**	**Gross Margin (%)**	**Revenue (U$)**
111.97	886.82	31.51	1644806	11.69	3.27	30.56	15.93	6138957
106.13	840.57	31.8	1300384	10.73	3.44	29.1	15.15	6068498
99.46	787.75	32.16	890691	9.58	3.64	27.5	14.2	5960560
91.77	**726.85**	**32.63**	**370682**	**8.1**	**3.93**	**25.47**	**12.94**	**5837631**
82.98	657.2	33.65	-574627	5.1	4.97	20.11	10.22	4977128
72.23	572.06	35.26	-1693839	0.44	7.19	13.91	5.91	3981702
59.55	471.62	37.94	-2906755	−	14.13	7.08	-1.23	2990774
44.07	349.05	43.29	-4257565	−	−	-2.22	-15.5	1993849
24.76	196.14	59.26	-5657898	−	−	-12.2	-58.12	9969250

Source: Elaborated by the author

In **Table 5.4**, it is observed that the Net Present Value (NPV) displays negative values for a feed rate of 82.98 kg h^{-1}. However, with a minimum waste feed of 91.77 kg h^{-1}, the NPV becomes positive. The positivity of the NPV indicates the attractiveness of the investment

(YANG; ROSENTRATER, 2019), as the expected return exceeds the cost of capital, providing financial gains and enabling the recovery of the initial investment within a 4-year period. This process yielded a positive return of 25.47% on the invested amount, coupled with a total revenue of US$ 5,837,631. Furthermore, a significant positive aspect is that the process does not generate by-products, which optimizes the use of waste and contributes to the economic and environmental efficiency of the project. These financial indicators suggest a positive performance of the particleboard production investment.

As the residue feed (kg h^{-1}) increases, it is possible to observe a significant increase in the Net Present Value (NPV), the Internal Rate of Return (IRR), and the Return on Investment (ROI). This phenomenon is the result of the increased production and consequent increase in revenues, surpassing the additional costs associated with the increase in the feed rate. The increase in production generally leads to greater operational efficiency and economies of scale, which is reflected positively in the financial metrics of the project.

However, it is important to highlight that the availability of PCNS is a limiting factor in production. For example, a small factory generates approximately 139 tons of cashew nutshells per year (EMBRAPA, 2024). Considering that 49.64% (by mass) of the feed stream in the particleboard production process corresponds to cashew nutshell residue (PCSN), 360 tons of PCSN per year are required to achieve a viable particleboard production project, with a feed rate of 91.77 $kg.h^{-1}$ of raw material. Given this issue, it becomes essential to explore alternatives for acquiring waste from other cashew processing units in the region, promoting green logistics that optimize the use of local resources and meet the demand for raw materials sustainably.

A viable solution would be the installation of waste processing centers, strategically located, to collect and consolidate the residues generated by various cashew nut processing units. These centers could serve as hubs for transforming the waste into raw materials for particleboard production, optimizing transportation and resource efficiency. With this strategy, it would be possible to ensure a continuous supply of CNSL, reduce logistical costs, and increase the sustainability of the process by integrating different production units into the value chain.

5.5 Conclusion

In this study, a preliminary techno-economic analysis (TEA) was conducted to assess the economic feasibility of producing particleboard from cashew nutshell (PCNS). Nine plant scales were examined using SuperPro Designer v10 software. The lowest unit production cost recorded was $31.51 per unit of particleboard for a plant scale of 91.77 kg h-1. It was found that increasing the production scale would significantly impact the Net Present Value (NPV), Internal Rate of Return (IRR), and Return on Investment (ROI). However, the availability of PCNS in the region remains a limitation for viable particleboard production.

Considering these findings, this study is highly relevant as it presents an economically attractive and sustainable solution for utilizing agricultural residues in industrial applications, offering a competitive alternative to conventional wood-based panels. This could position companies involved in particleboard production as key players in the growing market for eco-friendly materials.

Companies that might consider investing in this proposal include those already operating in the bioeconomy, agro-industrial processing, and sustainable construction materials sectors. Manufacturers of particleboard, agro-industries involved in cashew processing, and companies focused on green construction could benefit significantly by diversifying their product portfolios and reducing costs by utilizing agro-industrial waste.

However, certain caveats must be addressed before moving forward with such an investment. The most critical limitation is the availability of PCNS, as current supply levels may not be sufficient to meet large-scale production requirements. Therefore, it would be essential to establish efficient logistics and supply chain networks, possibly through partnerships with small factories in the region, to ensure a stable and continuous feed of raw materials. Additionally, investments in infrastructure, such as waste processing centers, may be necessary to optimize the collection and transformation of residues, which could increase upfront capital costs.

Given these preliminary findings, a suggestion for future work would be to explore the logistics of receiving PCNS from small factories in the region to enhance particleboard production and ensure the viability of plant installation.

5.6 Reference

ABNT. NRB 14810-2 : Painéis de partículas de média densidade Parte 2: Requisitos e métodos de ensaio. In: **Associação Brasileira de Normas Técnicas**. Rio de Janeiro: [s.n.]. p. 71.

ADEEB, EHSAN; KIM, TAE WOO; SOHN, C. H. Cost – Benefit Analysis of Medium- Density Fiberboard Production by Adding Fiber from Recycled Medium- Density Fiberboard. v. 68, n. 17, p. 414–418, 2018.

AKKOYUNLU, B. et al. Process modelling for industrial scale p[1] B. Akkoyunlu, C. Gabarre, S. Daly, E. Casey, E. Syron, Process modelling for industrial scale polyhydroxybutyrate production using fructose, formic acid and CO2: Assessing carbon sources and economic viability, . **Bioresource Technology**, v. 393, n. November 2023, p. 130139, fev. 2024.

AKOMOLAFE, S. F.; OYELEYE, S. I.; OBOH, G. Effect of cashew (Anacardium occidentale L.) nut-supplemented diet on steroidogenic enzymes, hormonal and oxidative imbalances, and sperm parameters in cisplatin-induced reproductive toxicity in male rats. **Journal of Food Biochemistry**, v. 46, n. 7, 2 jul. 2022.

ASTM. D1037-12: Standard Test Methods for Evaluating Properties of Wood-Base Fiber and Particle Panel Materials. In: **Annual Book of ASTM Standards**. West Conshohocken: ASTM International, 2020.

CANIZALES, L. et al. SuperPro Designer®, User-Oriented Software Used for Analyzing the Techno-Economic Feasibility of Electrical Energy Generation from Sugarcane Vinasse in Colombia. **Processes**, v. 8, n. 9, p. 1180, 18 set. 2020.

D'ADAMO, I.; GASTALDI, M.; MORONE, P. Economic sustainable development goals: Assessments and perspectives in Europe. **Journal of Cleaner Production**, v. 354, n. April, p. 131730, jun. 2022.

DA SILVA, J.; DE BRITO, E. S.; FERREIRA, S. R. S. Biorefinery of Cashew By-Products: Recovery of Value-Added Compounds. **Food and Bioprocess Technology**, v. 16, n. 5, p. 944–960, 2023.

DE ARAÚJO E SILVA, R. et al. An approach for implementing ecodesign at early research stage: A case study of bacterial cellulose production. **Journal of Cleaner Production**, v. 269, p. 122245, out. 2020.

DE OLIVEIRA, C. T.; OLIVEIRA, G. G. A. What Circular economy indicators really measure? An overview of circular economy principles and sustainable development goals. **Resources, Conservation and Recycling**, v. 190, n. September 2022, p. 106850, mar. 2023.

DE PAIVA, E. M. et al. Pyrolysis of cashew nutshell residues for bioenergy and renewable chemicals: Kinetics, thermodynamics, and volatile products. **Journal of Analytical and Applied Pyrolysis**, v. 177, n. October 2023, 2024.

DE PAIVA, E. M. et al. Valorizing cashew nutshell residue for sustainable lignocellulosic panels using a bio-based phenolic resin as a circular economy solution. **Industrial Crops and Products**, v. 212, n. March, p. 118379, jun. 2024.

DENG, C. et al. Economic viability of two-stage biohydrogen and biomethane production from cassava stillage residue focusing on solids content and pretreatment. **International Journal of Hydrogen Energy**, v. 52, p. 110–121, jan. 2024.

EMBRAPA. **Empresa Brasileira de Pesquisa Agropecuária (Embrapa)**. Available at: <https://www.embrapa.br/agroindustria-tropical>. Accessed on: February 2, 2024.

FAO. **FAOSTAT : statistical Cahew nuts (crops production).** Available at: <available: https://www.fao.org/faostat/en/#data/QV>. Accessed on: February 2, 2024.

FARINASSI, R. et al. Use of sugarcane bagasse for particleboard production. **Key Engineering Materials**, v. 634, p. 163–171, 2015.

GAN, E. Y. T. et al. Examining the synergistic effects through machine learning prediction and optimisation in the anaerobic Co-digestion (ACoD) of palm oil mill effluent (POME) and decanter cake (DC) with economic analysis. **Journal of Cleaner Production**, v. 437, n. January, p. 140666, jan. 2024.

HARUN, N. et al. Simulation of Anaerobic Digestion for Biogas Production from Food Waste Using SuperPro Designer. **Materials Today: Proceedings**, v. 19, p. 1315–1320, 2019.

HERRADOR, M. et al. Circular economy and zero-carbon strategies between Japan and South Korea: A comparative study. **Science of The Total Environment**, v. 820, p. 153274, maio 2022.

LEE, S. H. et al. Particleboard from agricultural biomass and recycled wood waste: a review. **Journal of Materials Research and Technology**, v. 20, p. 4630–4658, set. 2022.

LINCOLN, A. et al. Resins and fibers from sugarcane bagasse to produce medium - density fiberboard. Biomass Conversion and Biorefinery, n. 0123456789, 2023.

MOHOD, A. G.; KHANDETOD, Y. P.; POWAR, A. G. Processed cashew shell waste as fuel supplement for heat generation. **Energy for Sustainable Development**, v. 12, n. 4, p. 73–76, 2008.

MUNICIPALITY, B. R. **Made center**. Available at:<https://madecenter.com.br/produtos/chapas-em-mdf/>. Accessed on: September 23, 2024.

NARCISO, C. R. P. et al. Potential for the Use of Coconut Husk in the Production of Medium Density Particleboard. **Waste and Biomass Valorization**, v. 12, n. 3, p. 1647–1658, 2021.

OIRAM FILHO, F. et al. Productivity of a preparative high-performance liquid chromatography isolation of anacardic acids from cashew nut shell liquid. **Separation Science Plus**, v. 2, n. 6, p. 192–199, 2019.

RAJENDRAN, S. et al. Comparative analysis of mechanical and erosion performance of cashew and sugarcane waste based biochar-reinforced polyester composites. **Cleaner Engineering and Technology**, v. 18, n. November 2023, p. 100718, fev. 2024.

RAMESH, T. T. A. K. S. T. Sustainable production of cashew nutshell briquettes : experimental assessment and optimization of factors affecting the physical and fuel characteristics. **Biomass Conversion and Biorefinery**, n. 0123456789, 2022.

WAHANE, A. et al. Evaluation of the Physical and Mechanical Properties of Composite Board by Utilizing Agricultural Waste. **Materials Today: Proceedings**, v. 84, p. 16–23, 2023.

YANG, M.; ROSENTRATER, K. A. Techno-economic analysis of the production process of structural bio-adhesive derived from glycerol. **Journal of Cleaner Production**, v. 228, n. 2019, p. 388–398, ago. 2019.

Chapter 6

Final considerations

6 FINAL CONSIDERATIONS

The implementation of circular economy in production processes brings environmental benefits, such as reducing environmental impact and mitigating greenhouse gas emissions. Reusing resources helps minimize the need for new raw materials, thus extending their lifespan. In a context of resource scarcity and concerns about climate change, circular economy is crucial to promote a more sustainable and resilient model. Additionally, this approach contributes to achieving the Sustainable Development Goals, particularly those related to Affordable and Clean Energy.

The main contribution of this multidisciplinary study to the circular economy lies in the potential valorization of cashew nutshell waste, both in its raw form (RCNS) and pressed form (PCNS), to produce bioenergy and renewable chemicals. The results indicated that the pyrolysis of RCNS and PCNS can be accurately modeled using multicomponent kinetic modeling, with the identification of different devolatilization events and determination of the kinetic triplet (Ea, A, and $f(\alpha)$). Thermodynamic analysis further supported the feasibility of converting the waste into bioenergy and renewable chemicals due to low potential energy barriers. Additionally, the Py-GC/MS analysis confirmed the potential valorization of cashew nutshell waste in the production of volatiles, showing that the production of volatile gases is temperature-dependent. An increase in pyrolysis temperature is associated with an observed increase in the relative concentration of hydrocarbons, with aliphatic hydrocarbons identified as dominant components in volatile condensable products at temperatures around 650°C. These results play an essential role in utilizing cashew nutshell waste as a low-cost raw material for pyrolysis, providing crucial data for the design and optimization of industrial pyrolyzers. This approach can not only boost the production of bioenergy and renewable chemicals but also enhance the efficiency of industrial processes.

Additionally, the study explored the utilization of cashew nutshell waste (after CNSL extraction) and an environmentally friendly phenolic resin in the particleboard industry. The results showed that manufacturing particleboards with higher density resulted in significant improvements in the mechanical properties of the boards. Techniques such as FTIR, HPLC, and NMR confirmed the resin polymerization reaction. In addition, using adhesive with

CNSL to formaldehyde mass ratios of 1:0.25 and 1:0.50 resulted in particleboards of class E1 in terms of formaldehyde emissions. The biodegradability of panels PB25, PB50 and PB75 was 30%, 21% and 20%, respectively, in 30 days. These findings underscore the potential of biomass derived from cashew nutshells, as well as the use of environmentally friendly resin as adhesive in the particleboard industry. Therefore, it is evident that the reuse of cashew nutshells has the potential to play a significant role in promoting more sustainable practices.

The preliminary techno-economic analysis (TEA) assessing the economic feasibility of producing particleboard from cashew nutshell (PCNS) indicated that a unit production cost of $31.51 per panel could be achieved at a production scale of 91.77 kg h^{-1}. Larger scales showed significant improvements in financial metrics, such as Net Present Value (NPV) and Internal Rate of Return (IRR). However, the study also identified the limited availability of PCNS in the region as a challenge for large-scale production. Despite the demonstrated economic and environmental benefits of utilizing agricultural residues, the study emphasizes the importance of efficient logistics and supply chain networks, including partnerships with local factories and investments in waste processing centers, to ensure a stable supply of raw materials and optimize production.

Future Work: Future research should investigate the catalytic pyrolysis of cashew nutshell residues, assessing its impact on activation energy and volatile product composition. Additionally, lab-scale experiments should be conducted to achieve mass and energy balance for converting cashew nutshell residues into bioenergy and renewable chemicals. Scaling up the pyrolysis process and performing techno-economic analyses using SuperPro Designer software will be essential for refining production processes. Furthermore, optimizing operational parameters for producing particleboard from cashew nutshell biomass will help eliminate formaldehyde from resin formulations. Lastly, exploring the logistics of sourcing RCNS from small factories in the region will enhance particleboard production and ensure the viability of plant installation.

APPENDIX A - DATA FOR PYROLYSIS REACTION OPTIMIZATION

Table A.1− Algebraic expressions of the most frequent reaction models used to describe the kinetics of solid-state reactions.

Model	Mechanism	$g(\alpha)$	$f(\alpha)$
		Nucleation Models	
P2	Power law	$\alpha^{1/2}$	$2\alpha^{1/2}$
P3	Power law	$\alpha^{1/3}$	$3\alpha^{2/3}$
P4	Power law	$\alpha^{1/4}$	$4\alpha^{3/4}$
P2/3	Power law	$\alpha^{3/2}$	$2/3\,\alpha^{-1/2}$
A2	Avrami-Erofeev	$\left[-\ln(1-\alpha)\right]^{1/2}$	$2(1-\alpha)\left[-\ln(1-\alpha)\right]^{1/2}$
A3	Avrami-Erofeev	$\left[-\ln(1-\alpha)\right]^{1/3}$	$3(1-\alpha)\left[-\ln(1-\alpha)\right]^{2/3}$
A4	Avrami-Erofeev	$\left[-\ln(1-\alpha)\right]^{1/4}$	$4(1-\alpha)\left[-\ln(1-\alpha)\right]^{3/4}$
		Reaction Order Models	
F1	First-Order Reaction	$-\ln(1-\alpha)$	$1-\alpha$
F2	Second-Order Reaction	$(1-\alpha)^{-1}-1$	$(1-\alpha)^{2}$
F3	Third-Order Reaction	$(1/2)\left[(1-\alpha)^{-2}-1\right]$	$(1-\alpha)^{3}$
Fn	n-Order Reaction	$\left[1-(1-a)^{1-n}\right]/(1-n)$	$(1-\alpha)^{n}$
		Geometrical Contraction Models	
R2	Contracting cylinder	$1-(1-\alpha)^{1/2}$	$2(1-\alpha)^{1/2}$
R3	Contracting sphere	$1-(1-\alpha)^{1/3}$	$3(1-\alpha)^{2/3}$
		Diffusion Models	
D1	One-dimensional diffusion	α^{2}	$1/2\,\alpha^{-1}$
D2	Two-dimensional diffusion	$(1-\alpha)\ln(1-\alpha)+\alpha$	$\left[-\ln(1-\alpha)\right]^{-1}$
D3	Three-dimensional diffusion	$\left[1-(1-\alpha)^{1/3}\right]^{2}$	$3/2(1-\alpha)^{2/3}\left[1-(1-\alpha)^{1/3}\right]^{-1}$
D4	Ginstling-Brounshtein	$1-(2/3)\alpha-(1-\alpha)^{2/3}$	$3\left[2\left((1-\alpha)^{-1/3}-1\right)\right]^{-1}$

Source: Elaborated by the author

Table A.2 − Results of the adjustable parameters of the Asym2Sig function (θ, w_1, w_2 and w_3) for each pseudo component deconvoluted from the pyrolysis behavior of raw cashew nutshells at heating rates of 5, 10 e 15 °C min^{-1}.

Biomass	T_P	P-EX	P-HC	P-CL	P-LG1	P-LG2
	5 °C min^{-1}	135.66	279.95	333.16	323.97	412.70
	10 °C min^{-1}	152.18	296.46	349.67	340.49	429.22
	15 °C min^{-1}	161.18	305.46	358.67	349.48	438.21
Raw	θ	0.02	0.20	0.11	0.02	0.02
	w_1	0.00	0.00	0.00	0.00	0.00
	w_2	26.89	34.72	11.85	15.00	14.32
	w_3	10.54	11.53	7.92	128.34	16.88

Source: Elaborated by the author

Table A.3 − Results of the adjustable parameters of the Asym2Sig function (θ, w_1, w_2 and w_3) for each pseudo component deconvoluted from the pyrolysis behavior of pressed cashew nutshells at heating rates of 5, 10 e 15 °C min^{-1}.

Biomass	T_P	P-HC1	P-HC2	P-CL	P-LG
	5 °C min^{-1}	235.56	280.15	305.21	366.62
	10 °C min^{-1}	252.08	296.67	321.73	383.14
	15 °C min^{-1}	261.07	305.66	330.72	392.14
Pressed	θ	0.19	0.09	0.13	0.04
	w_1	0.00	0.00	0.00	0.00
	w_2	23.97	10.22	4.78	24.74
	w_3	22.05	11.64	7.96	45.00

Source: Elaborated by the author

Table A.4 − Summary of five kinetic triplets that describe the pyrolysis behavior of the raw cashew nutshell, presuming five independent parallel reactions.

	P−EX	**P−HC**	**P−CL**	**P−LG1**	**P−LG2**
Starink's method					
E_a (kJ mol^{-1})	87.15	94.79	124.21	226.98	164.87
R^2	0.9993	0.9990	0.9990	0.9990	0.9991
Kinetic compensation effect					
A (min^{-1})	2.78×10^{10}	4.25×10^{8}	8.33×10^{9}	6.89×10^{16}	3.89×10^{11}
a	0.3100	0.2503	0.1919	0.1942	0.1794
b	-2.9687	-3.8627	-0.9914	-5.3181	-2.8844
R^2	0.9972	0.9955	0.9976	0.9492	0.9994
Master plot method					
$f(\alpha)$	F2: $(1-\alpha)^2$	F2: $(1-\alpha)^2$	A2: $2(1-\alpha)[-\ln(1-\alpha)]^{\frac{1}{2}}$	F9: $(1-\alpha)^9$	F1: $1-\alpha$
ε (%)	0.0869	0.1649	0.0589	0.3754	0.1504
Fractional contribution					
C_i	0.0707	0.6601	0.0801	0.1500	0.0392

Abbreviations: P−EX: pseudo-extractives; P−HC: pseudo-hemicellulose; P−CL: pseudo-cellulose; P−LG1: primary pseudo-lignin; and P−LG2: secondary pseudo-lignin.

Source: Elaborated by the author

Table A.5 − Summary of four kinetic triplets that describe the pyrolysis behavior of the pressed cashew nutshell, presuming four independent parallel reactions.

	P−HC1	**P−HC2**	**P−CL**	**P−LG**
Starink's method				
E_a (kJ mol^{-1})	91.54	106.03	117.02	156.42
R^2	0.9992	0.9990	0.9990	0.9991
Kinetic compensation effect				
A (min^{-1})	4.80×10^{8}	2.32×10^{9}	5.80×10^{9}	3.24×10^{11}
a	0.2608	0.2296	0.1999	0.1972
b	-3.8837	-2.7800	-0.9072	-4.3466
R^2	0.9968	0.9976	0.9988	0.9905
Master plot method				
$f(\alpha)$	F2: $(1-\alpha)^2$	A2: $2(1-\alpha)[-\ln(1-\alpha)]^{\frac{1}{2}}$	A3: $3(1-\alpha)[-\ln(1-\alpha)]^{\frac{2}{3}}$	F3: $(1-\alpha)^3$
ε (%)	0.0707	0.1176	0.0665	0.1362
Fractional contribution				
C_i	0.6927	0.0965	0.1339	0.0768

Abbreviations: P−HC1: primary pseudo-hemicellulose; P−HC2: secondary pseudo-hemicellulose; P−CL: pseudo-cellulose; and P−LG: pseudo-lignin.

Source: Elaborated by the author

Table A.6 − Hydrocarbons from the fast analytical pyrolysis of raw and pressed cashew nutshells at 450 °C.

450 °C					
Raw cashew nutshell			**Pressed cashew nutshell**		
Groups	**Area %**	**Name**	**Groups**	**Area %**	**Name**
Hydrocarbon	1.388407	1,3,5,7-Cyclooctatetraene	Hydrocarbon	0.974737	1,3,5,7-Cyclooctatetraene
Hydrocarbon	0.739302	1,3-Cyclohexadiene	Hydrocarbon	0.609172	1,4-Pentadiene, 3-methyl-
Hydrocarbon	0.575461	3-Hexadecene, (Z)-	Hydrocarbon	0.314947	1,3-Cyclohexadiene
Hydrocarbon	0.563829	1,4-Pentadiene, 3-methyl-	Hydrocarbon	0.229802	Undecane
Hydrocarbon	0.231016	Cyclododecene, (Z)-	Hydrocarbon	0.192702	Hexadecane
Hydrocarbon	0.115084	1,3-Cyclopentadiene	Hydrocarbon	0.184854	Cyclododecene, (Z)-
Hydrocarbon	0.104304	3-Tetradecene, (E)-	Hydrocarbon	0.098291	1,3-Cyclopentadiene
Hydrocarbon	0.091355	Undecane	Hydrocarbon	0.089762	3-Tetradecene, (E)-

Source: Elaborated by the author

Table A.7 − Hydrocarbons from the fast analytical pyrolysis of raw and pressed cashew nutshells at 550 °C.

550 °C					
Raw cashew nutshell			**Pressed cashew nutshell**		
Groups	**Area %**	**Name**	**Groups**	**Area %**	**Name**
Hydrocarbon	1.077988	1,3-Cyclopentadiene	Hydrocarbon	0.892341	1-Tridecene
Hydrocarbon	0.803521	1,3,5-Hexatriene, (Z)-	Hydrocarbon	0.750345	1,3,5-Hexatriene, (Z)-
Hydrocarbon	0.692593	Isopropylcyclobutane	Hydrocarbon	0.738131	Isopropylcyclobutane
Hydrocarbon	0.670447	1-Tridecene	Hydrocarbon	0.596921	Cyclododecene, (E)-
Hydrocarbon	0.60758	1,3-Pentadiene, 2-methyl-, (E)-	Hydrocarbon	0.514618	2-Octene, (Z)-
Hydrocarbon	0.598753	Cyclopentene, 1-methyl-	Hydrocarbon	0.471101	1-Nonene
Hydrocarbon	0.512651	C2H5CH=CHCH=CH2	Hydrocarbon	0.461367	Cyclohexene
Hydrocarbon	0.49315	Cyclopentene	Hydrocarbon	0.446301	1,3-Cyclopentadiene
Hydrocarbon	0.441589	Cyclohexene	Hydrocarbon	0.440552	Cyclopentene, 1-methyl-
Hydrocarbon	0.417504	Cyclododecene, (E)-	Hydrocarbon	0.362248	1,3-Cyclohexadiene
Hydrocarbon	0.379244	1-Nonene	Hydrocarbon	0.31921	1H-Indene, 3-methyl-
Hydrocarbon	0.373161	1,3-Cyclohexadiene	Hydrocarbon	0.315663	1,3-Nonadiene, (E)-
Hydrocarbon	0.31358	1,3-Nonadiene, (E)-	Hydrocarbon	0.315403	1,3-Pentadiene, 2-methyl-, (E)-
Hydrocarbon	0.312918	8-Hexadecyne	Hydrocarbon	0.29513	1-Decene
Hydrocarbon	0.275235	1,3-Cyclopentadiene, 1-methyl-	Hydrocarbon	0.29446	Butane, 2,2-dimethyl-
Hydrocarbon	0.250428	1-Tricosene	Hydrocarbon	0.258952	1,3-Cyclopentadiene, 1-methyl-
Hydrocarbon	0.235098	1-Decene	Hydrocarbon	0.239838	Indene
Hydrocarbon	0.226008	5-Decyne	Hydrocarbon	0.23854	5-Decyne
Hydrocarbon	0.189385	1,3,5-Hexatriene, 3-methyl-, (Z)-	Hydrocarbon	0.23326	1-Tricosene
Hydrocarbon	0.170968	9-Eicosene, (E)-	Hydrocarbon	0.186526	1-Undecene
Hydrocarbon	0.166506	Cyclopropane	Hydrocarbon	0.170895	1,3,5-Hexatriene, 3-methyl-, (Z)-
Hydrocarbon	0.151939	1-Undecene	Hydrocarbon	0.167627	1,3-Octadiene
Hydrocarbon	0.133554	1,3-Octadiene	Hydrocarbon	0.162821	Cyclopentene
Hydrocarbon	0.129758	1,4-Pentadiene	Hydrocarbon	0.162003	Cyclopropane, nonyl-
Hydrocarbon	0.127377	Cyclopropane, nonyl-	Hydrocarbon	0.153591	1,8-Nonadiene
Hydrocarbon	0.12715	1,8-Nonadiene	Hydrocarbon	0.118596	1,4-Pentadiene
Hydrocarbon	0.094217	Hexane, 2,4-dimethyl-	Hydrocarbon	0.036697	Cyclopentane, ethyl-
Hydrocarbon	0.063875	Cyclopentene,1-heptyl-	Hydrocarbon	0.029724	Cyclopropane
Hydrocarbon	0.049552	Cyclopentane, ethyl-	-	-	-

Table A.8 − Hydrocarbons from the fast analytical pyrolysis of raw and pressed cashew nutshells at 650 °C.

650 °C					
Raw cashew nutshell			**Pressed cashew nutshell**		
Groups	**Area %**	**Name**	**Groups**	**Area %**	**Name**
Hydrocarbon	6.177622	Butane	Hydrocarbon	5.321273	Butane
Hydrocarbon	5.426096	1,3-Butadiene	Hydrocarbon	4.106138	1-Hexene
Hydrocarbon	4.143419	1-Hexene	Hydrocarbon	1.715738	1,3-Cyclopentadiene
Hydrocarbon	1.625884	1,3-Cyclopentadiene	Hydrocarbon	1.378401	1,3-Pentadiene, (Z)-
Hydrocarbon	1.385633	1,3-Pentadiene, (Z)-	Hydrocarbon	1.037976	1-Butene, 3-methyl-
Hydrocarbon	1.11795	1-Butene, 3-methyl-	Hydrocarbon	1.02727	1,3,5-Hexatriene, (Z)-
Hydrocarbon	1.021174	1,3-Cyclopentadiene, 1-methyl-	Hydrocarbon	0.891227	1,3-Pentadiene, (E)-
Hydrocarbon	0.892199	1,3-Pentadiene, (E)-	Hydrocarbon	0.887046	1-Heptene
Hydrocarbon	0.846753	Cyclopentene	Hydrocarbon	0.854615	Cyclopentene
Hydrocarbon	0.720929	1-Heptene	Hydrocarbon	0.718458	C2H5CH=CHCH=CH2
Hydrocarbon	0.716448	7-Hexadecyne	Hydrocarbon	0.676904	1,15-Hexadecadiene
Hydrocarbon	0.615084	Heptane, 3-methylene-	Hydrocarbon	0.574807	1-Tetradecene
Hydrocarbon	0.610946	C2H5CH=CHCH=CH2	Hydrocarbon	0.553282	1,4-Cyclohexadiene
Hydrocarbon	0.560531	1-Tetradecene	Hydrocarbon	0.546088	2,4-Hexadiene
Hydrocarbon	0.490772	1,4-Cyclohexadiene	Hydrocarbon	0.540954	1-Nonene
Hydrocarbon	0.4871	2,4-Hexadiene	Hydrocarbon	0.486885	1,5-Hexadiene
Hydrocarbon	0.471756	Cyclododecene, (Z)-	Hydrocarbon	0.481676	1-Heptadecene
Hydrocarbon	0.411923	1-Nonene	Hydrocarbon	0.47342	Cyclododecene, (Z)-
Hydrocarbon	0.404046	1,5-Hexadiene	Hydrocarbon	0.468494	1-Decene
Hydrocarbon	0.392735	Cyclohexene	Hydrocarbon	0.442019	Cyclohexene
Hydrocarbon	0.3228	2,4-Hexadiene, (E,Z)-	Hydrocarbon	0.394163	1,3-Cyclopentadiene, 1-methyl-
Hydrocarbon	0.306029	1,3,5-Hexatriene, 3-methyl-, (Z)-	Hydrocarbon	0.342557	9-Octadecene, (E)-
Hydrocarbon	0.273574	1,3-Nonadiene, (E)-	Hydrocarbon	0.334193	1,3-Pentadiene, 2-methyl-, (E)-
Hydrocarbon	0.266306	1,3-Cycloheptadiene	Hydrocarbon	0.327263	1,3,5-Hexatriene, 3-methyl-, (Z)-
Hydrocarbon	0.264318	1-Decene	Hydrocarbon	0.311388	Indene
Hydrocarbon	0.263821	5-Decyne	Hydrocarbon	0.287767	1,3-Nonadiene, (E)-
Hydrocarbon	0.261921	1-Heptadecene	Hydrocarbon	0.281936	1-Undecene
Hydrocarbon	0.251389	Indene	Hydrocarbon	0.275228	5-Decyne
Continued...					

650 °C

Raw cashew nutshell			Pressed cashew nutshell		
Groups	**Area %**	**Name**	**Groups**	**Area %**	**Name**
Hydrocarbon	0.24893	1,3-Pentadiene, 2,3-dimethyl-	Hydrocarbon	0.272198	1,7-Octadiene
Hydrocarbon	0.235548	Vinylcyclopentane	Hydrocarbon	0.270036	1,3-Pentadiene, 2,3-dimethyl-
Hydrocarbon	0.220926	1,15-Hexadecadiene	Hydrocarbon	0.258998	1,3-Cycloheptadiene
Hydrocarbon	0.20362	1,8-Nonadiene	Hydrocarbon	0.258449	Vinylcyclopentane
Hydrocarbon	0.185929	1-Undecene	Hydrocarbon	0.25312	Cyclopropane, nonyl-
Hydrocarbon	0.185431	Cyclohexene, 3-ethenyl-	Hydrocarbon	0.216712	1-Tridecene
Hydrocarbon	0.180684	2-Methyl-1-octen-3-yne	Hydrocarbon	0.215921	Cyclohexene, 3-ethenyl-
Hydrocarbon	0.179662	Cyclohexane, ethenyl-	Hydrocarbon	0.214236	Heptane
Hydrocarbon	0.17332	6-Tridecane	Hydrocarbon	0.213999	1,8-Nonadiene
Hydrocarbon	0.171315	1-Tridecene	Hydrocarbon	0.193172	Cyclohexane, ethenyl-
Hydrocarbon	0.16537	Cyclopropane, nonyl-	Hydrocarbon	0.190807	Cyclohexane, ethylidene-
Hydrocarbon	0.161334	Cyclohexane, ethylidene-	Hydrocarbon	0.183388	1-Pentadecene
Hydrocarbon	0.147769	1,3-Cyclopentadiene, 5,5-dimethyl-	Hydrocarbon	0.178351	Cyclohexane, 1,2,4-tris(methylene)-
Hydrocarbon	0.136169	Cyclohexane, 1,2,4-tris(methylene)-	Hydrocarbon	0.178288	2-Methyl-1-octen-3-yne
Hydrocarbon	0.128274	1,3-Pentadiene, 2-methyl-, (E)-	Hydrocarbon	0.174982	4-Methyl-1,3-pentadiene
Hydrocarbon	0.096624	1,4-Hexadiene, 2-methyl-	Hydrocarbon	0.162937	6-Tridecane
Hydrocarbon	0.077965	1-Propylcyclopentene	Hydrocarbon	0.13059	1,3-Cyclopentadiene, 5,5-dimethyl-
Hydrocarbon	0.072386	1,3-Hexadiene, 3-ethyl-2-methyl-	Hydrocarbon	0.125499	Heptane, 3-methylene-
Hydrocarbon	0.071553	Octane	Hydrocarbon	0.105195	Octane
Hydrocarbon	0.069637	Cyclopentene, 1-ethenyl-3-methylene-	Hydrocarbon	0.098827	1,4-Hexadiene, 2-methyl-
Hydrocarbon	0.028928	2-Octene	Hydrocarbon	0.09743	2,4-Nonadiene, (E,E)-
Hydrocarbon	0.028268	Cyclopentene,1-heptyl-	Hydrocarbon	0.086563	1,3-Hexadiene, 3-ethyl-2-methyl-
			Hydrocarbon	0.082675	Cycloundecane, 1,1,2-trimethyl-
			Hydrocarbon	0.07601	Cetene
			Hydrocarbon	0.071319	1-Propylcyclopentene
			Hydrocarbon	0.066746	Cyclopentene, 1-ethenyl-3-methylene-
			Hydrocarbon	0.057771	Pentadecane
			Hydrocarbon	0.05191	Cyclopentene,1-heptyl-
			Hydrocarbon	0.025504	2-Octene

Source: Elaborated by the author

APPENDIX B - DATA FOR CHARACTERIZATION OF PHENOLIC RESIN

Figure B1 − Chromatographic profile (analytical) monitored at 280 nm: **(a)** natural CNSL containing (I) triene cardol, (II) diene cardol, anacardic acids (III) triene, (IV) diene and (V) monoene; **(b)** phenol-formaldehyde adhesive formulation F1; **(c)** phenol-formaldehyde adhesive formulation F2, and **(d)** phenol-formaldehyde adhesive formulation F3, containing only anacardic acids (III) triene, (IV) diene and (V) monoene.

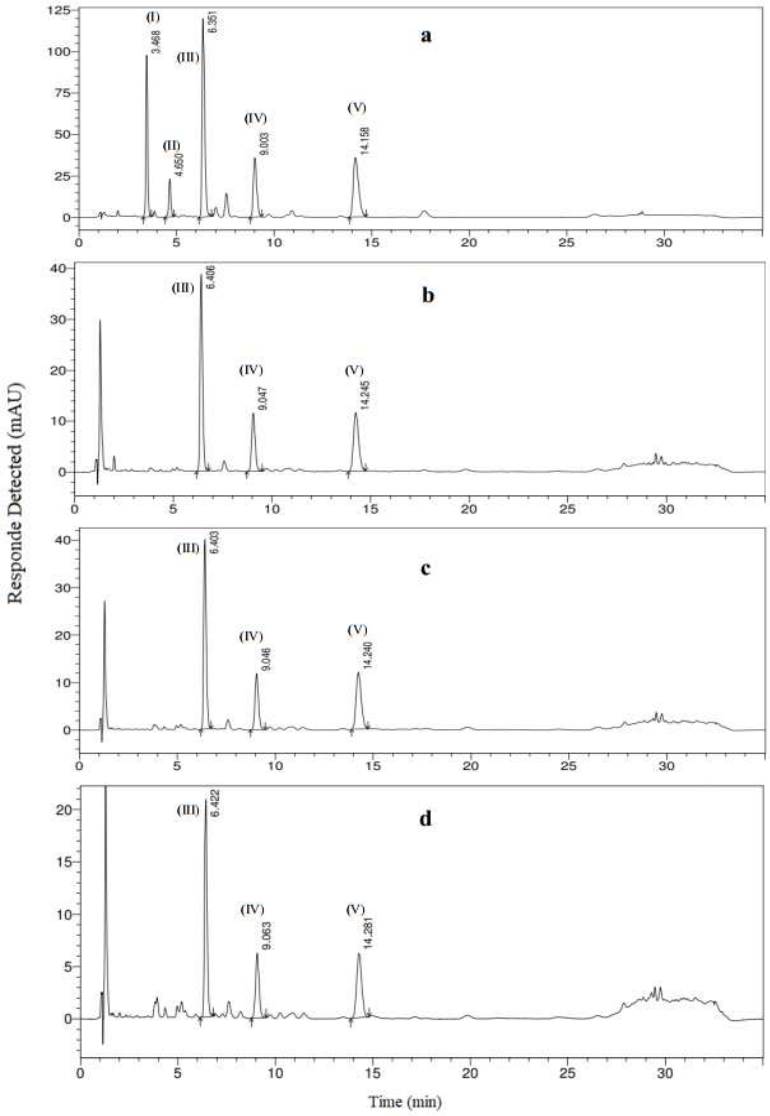

Source: Elaborated by the author

Table B1 − The chromatographic analysis includes the retention time, area (%), and height (%) measurements specifically for the CNSL and resins F1, F2, and F3.

Peak	Retention Time (min)	Area (%)	Height (%)
CNSL			
1	3.468	19.820	31.314
2	4.650	5.610	7.344
3	6.351	37.786	38.406
4	9.003	14.383	11.455
5	14.158	22.401	11.482
F1			
1	6.406	49.795	62.746
2	9.047	20.106	18.592
3	14.245	30.099	18.663
F2			
1	6.403	49.681	62.626
2	9.046	20.213	18.631
3	14.240	30.107	18.743
F3			
1	6.422	49.945	62.703
2	9.063	20.582	18.730
3	14.281	29.472	18.567

Source: Elaborated by the author